



## Executive summary

# Fractography-assisted Observations on Fatigue Thresholds in an Aerospace Aluminium Alloy



### Report no.

NLR-TP-2009-596

### Author(s)

R.J.H. Wanhill  
S.A. Barter  
T. Hattenberg  
R.A. Huls  
L.C. Ubels  
M.J. Bos

### Report classification

UNCLASSIFIED

### Date

November 2010

### Knowledge area(s)

Levensduurbewaking &  
Onderhoud van vliegtuigen

### Descriptor(s)

fatigue  
crack growth  
thresholds  
aluminium alloys  
helicopters

### Problem area

Reliable fatigue crack growth thresholds are important for fatigue crack growth analyses, especially for helicopter airframe components, since the analyses rely mainly on crack growth data in the near-threshold region. This region is often characterized by considerable data scatter, including scatter in the threshold values.

### Description

The NLR and DSTO participated in a project on helicopter fatigue

called *HeliDamTol*. This project had two main objectives. The first was to develop reliable methods of fatigue crack growth analysis for helicopter airframe components. The second was to incorporate these methods into an Operational Damage Assessment Tool (ODAT). The present report is a contribution to the first main objective.

Fatigue crack growth thresholds,  $\Delta K_{th}$ , were determined for aluminium alloy 7075-T7351 plate material used for the hinge beams

This report is a joint research activity of the NLR (Amsterdam, the Netherlands) and DSTO (Melbourne, Australia).

on the NH90 helicopter tail boom. Interpretation of the results was aided by fractographic observations of the thresholds and near-threshold crack growth regions.

**Results and conclusions**

The results show an *intrinsic* scatterband of  $\pm 0.25 \text{ MPa}\sqrt{\text{m}}$  for all values of  $\Delta K_{\text{th}}$ , and consequent variations in  $\Delta K_{\text{th}}$  of about 11 – 17 %. These variations are most probably due to variable crack front

topographies and profiles in the threshold region. However, the determined  $\Delta K_{\text{th}}$  values seem independent of normal changes in atmospheric humidity ranging from 17 – 43 % R.H. This is probably sufficient to account for the average atmospheric conditions experienced by helicopters during service.



NLR-TP-2009-596

## Fractography-assisted Observations on Fatigue Thresholds in an Aerospace Aluminium Alloy

R.J.H. Wanhill, S.A. Barter<sup>1</sup>, T. Hattenberg, R.A. Huls, L.C. Ubels and  
M.J. Bos

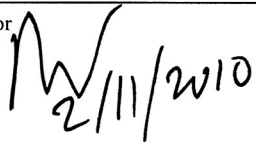
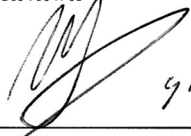

<sup>1</sup> Defence Science and Technology Organisation, Melbourne, Australia

This report is a joint research activity of the NLR (Amsterdam, the Netherlands) and DSTO (Melbourne, Australia).

The contents of this report may be cited on condition that full credit is given to NLR and the authors.  
This publication has been refereed by the Advisory Committee AEROSPACE VEHICLES.

Customer	National Aerospace Laboratory NLR; Defence Science and Technology Organisation
Contract number	-
Owner	National Aerospace Laboratory NLR; Defence Science and Technology Organisation
Division	Aerospace Vehicles (NLR), Aircraft Vehicles (DSTO)
Distribution	Unlimited
Classification of title	Unclassified
	November 2010

Approved by:

Author  2/11/2010	Reviewer  9/11/2010	Managing department 
--	--	--



## Summary

Reliable determinations of fatigue crack growth thresholds are important for fatigue crack growth analyses, especially for helicopter airframe components, since the analyses rely mainly on crack growth data in the near-threshold region. This region is often characterized by considerable data scatter, including scatter in the threshold values.

The NLR and DSTO have participated in a joint project on helicopter fatigue called *HeliDamTol*. This project has two main objectives. The first is to develop reliable methods of fatigue crack growth analysis for helicopter airframe components. The second is to incorporate these methods into an Operational Damage Assessment Tool (ODAT), which is intended to improve the operational readiness of a helicopter fleet.

The present report is a contribution to the first main objective of *HeliDamTol*. The report presents experimental determinations of fatigue crack growth thresholds in aluminium alloy 7075-T7351 plate material used for the hinge beams on the NH90 helicopter carbon-epoxy composite tail boom. Interpretation of the experimental determinations was aided by fractographic observations of the thresholds and near-threshold crack growth regions.

The thresholds were determined for the positive stress ratio range  $R = 0.1 - 0.95$ . The results may be expressed as follows:

- (1) For  $R \geq 0.58$  the measured fatigue crack growth threshold stress intensity range  $\Delta K_{th}$  is equal to the effective, or intrinsic threshold stress intensity range  $\Delta K_o$ , and is given by

$$R \geq 0.58 : \Delta K_{th} = \Delta K_o = 1.44 \pm 0.25 \text{ MPa}\sqrt{\text{m}}$$

- (2) For  $R \leq 0.58$  the measured  $\Delta K_{th}$  depends on  $R$ :

$$R \leq 0.58 : \Delta K_{th} = [(2.35 \pm 0.25) - 1.57R] \text{ MPa}\sqrt{\text{m}}$$

The results include a scatterband of  $\pm 0.25 \text{ MPa}\sqrt{\text{m}}$  for all values of  $\Delta K_{th}$ , and consequent variations in  $\Delta K_{th}$  of about 11 – 17 %. These variations are most probably due to variable crack front topographies and profiles in the threshold region, and they represent intrinsic limitations to the accuracy of  $\Delta K_{th}$  values.



On the other hand, despite evident effects of humidity on the threshold and near-threshold fracture topography and the amount of fracture surface oxidation at threshold, the determined  $\Delta K_{th}$  values seem independent of normal changes in atmospheric humidity ranging from 17 – 43 % R.H. This is probably sufficient to account for the average atmospheric conditions experienced by helicopters during service.



## Contents

<b>1</b>	<b>Introduction</b>	<b>7</b>
<b>2</b>	<b>Test programme</b>	<b>7</b>
2.1	Types of tests	7
2.2	Test plan	8
2.3	Fractography	8
<b>3</b>	<b>Threshold test results</b>	<b>9</b>
<b>4</b>	<b>Threshold and near- threshold fractography</b>	<b>10</b>
4.1	Background information and procedure	10
4.2	Survey of near-threshold crack front profiles and roughnesses	11
4.2.1	FEG-SEM stereo images	11
4.2.2	Comparisons of FEG-SEM and DFOM images	13
4.3	Detailed fractography in the threshold/near-threshold region	13
<b>5</b>	<b>Discussion</b>	<b>14</b>
<b>6</b>	<b>Conclusions</b>	<b>15</b>
<b>7</b>	<b>References</b>	<b>16</b>
	<b>Appendix A: Temperature and humidity records during testing</b> .....	<b>1</b>

**Stereofractographs anaglyph viewer in envelope on inside back cover**

## Nomenclature and acronyms

$R = S_{\min}/S_{\max} = K_{\min}/K_{\max}$	Stress or stress intensity factor ratio for a fatigue load cycle
$R > R_c$	Stress or stress intensity factor ratios with no crack closure
$R_L$	Linear roughness parameter
$K_{\max}, K_{\min}$	Maximum and minimum stress intensity factors
$\Delta K = K_{\max} - K_{\min}$	Stress intensity factor range
$K_{\max,th}, K_{\min,th}$	Maximum and minimum stress intensity factors at the fatigue crack growth threshold
$\Delta K_{th} = K_{\max,th} - K_{\min,th}$	Fatigue crack growth threshold stress intensity factor range
$K_{\max,o}$	Maximum stress intensity factor for $\Delta K_{th}$ when $R = 0$
$K_{op}$	Crack opening stress intensity factor
$\Delta K_o = K_{\max,o} - K_{op}$	Effective, or intrinsic, fatigue crack growth threshold stress intensity factor range
$a$	Crack length
$da/dN$	Fatigue crack growth rate
$N$	Number of cycles
$\sigma_{ts}$	Tensile strength
$\sigma_y$	Yield strength (generally at 0.2% offset)
AESP	AEroSPace
ASTM	American Society for Testing and Materials
CT	Compact Tension (specimen)
D.C.	Direct Current
DFOM	Deep Focus Optical Microscope
FEG-SEM	Field Emission Gun Scanning Electron Microscope
ISIS	NLR automated system for D.C. potential drop measurement of crack growth
ODAT	Operational Damage Assessment Tool
L	Longitudinal
T	Transverse (long-transverse)
S	Short-transverse
L-T	Crack plane orientation (L = loading direction, T = crack growth direction)
T-L	Crack plane orientation (T = loading direction, L = crack growth direction)



## 1 Introduction

Reliable determinations of fatigue crack growth thresholds are important for fatigue crack growth analyses, especially for helicopter airframe components (Irving *et al.* 2003; Vaughan and Chang 2003; Wanhill and Bos 2004). This is because these analyses rely mainly on crack growth data in the near-threshold region. This region is often characterized by considerable data scatter, including scatter in the threshold values.

The NLR and DSTO have participated in a joint project on helicopter fatigue called *HeliDamTol*. This project has two main objectives. The first is to develop reliable methods of fatigue crack growth analysis for helicopter airframe components. The second is to incorporate these methods into an Operational Damage Assessment Tool (ODAT), which is intended to improve the operational readiness of a helicopter fleet.

This report is a contribution to the first main objective of *HeliDamTol*. The report presents experimental determinations of fatigue crack growth thresholds in aluminium alloy 7075-T7351 plate material used for the hinge beams on the NH90 helicopter carbon-epoxy composite tail boom. The tail boom folds forward to reduce parking and storage space.

Interpretation of the experimental determinations was aided by fractographic observations of the thresholds and near-threshold crack growth regions.

## 2 Test programme

### 2.1 Material and specimens

Production quality aluminium alloy 7075-T7351 plate material was obtained from Fokker AESP in the form of two pieces  $900(L) \times 62(T) \times 40(S)$  mm. This material had the nominal mechanical properties  $\sigma_y = 435$  MPa and  $\sigma_{ts} = 505$  MPa.

10 mm thick Compact tension (CT) specimens were machined from the plate such that loading would be in the longitudinal (L) direction and crack growth in the long-transverse (T) direction. The crack plane orientation is then referred to as L-T. The specimens were provided with drilled holes for the electrical leads of a D.C. potential drop automated crack growth measurement system (ISIS), see figure 1.

### 2.1 Types of tests

Two types of tests were used to determine the fatigue thresholds. These are illustrated schematically in figure 2:

- (1) Constant R tests: The applied loads are reduced during fatigue crack growth such that the stress ratio,  $R$ , remains constant while the cyclic stress intensity factor range,  $\Delta K$ , gradually decreases to the threshold value,  $\Delta K_{th}$ .
- (2) Constant  $K_{max}$  tests: The applied loads are changed during fatigue crack growth such that the maximum stress intensity factor,  $K_{max}$ , remains constant while the minimum stress intensity factor,  $K_{min}$ , gradually increases until  $\Delta K$  reaches  $\Delta K_{th}$ .

Constant R tests are useful for obtaining  $\Delta K_{th}$  values over a wide range of R, from  $R = 0$  to  $R \geq 0.8$ . In the present programme values of  $R = 0.1, 0.4, 0.7$  and  $0.8$  were selected. Constant  $K_{max}$  tests are useful for obtaining  $\Delta K_{th}$  values in the range  $R = 0.7$  to  $R \geq 0.9$ . This range is particularly of interest for helicopter airframe components (Wanhill and Bos 2004).  $K_{max}$  values of 5, 15 and 25  $\text{MPa}\sqrt{\text{m}}$  were selected.

All tests were done following ASTM Standard E 647, using an MTS 810 electrohydraulic machine equipped with a 10kN load cell and customized specimen grips. The specimens were electrically insulated from the grips by the use of SiC ceramic loading pins. The fatigue stress waveform was sinusoidal, with a cycle frequency of 40Hz. ISIS measurements of crack lengths were made automatically every 0.1 mm of crack growth until approaching the thresholds, when measurements were made every 10,000 cycles. Each ISIS measurement required a hold time of 5 s at maximum load. Optical (travelling microscope) measurements of crack lengths were made as intermittent checks on the ISIS measurements. This kind of check is essential for each test.

The environment surrounding the specimens was laboratory air. A dummy specimen was required to eliminate the effects of ambient temperature fluctuations on the D.C. potential drop measurements. Also, after the first tests, with  $R = 0.1$ , examination of the near-threshold fatigue fracture surfaces, see section 4, indicated that the environment influenced the fatigue fracture topography. This unexpected and previously unreported result led to continuous measurements of the air temperature and relative humidity during the remaining tests<sup>1</sup>.

## 2.2 Test plan

Table 1 lists the specimens used for the  $\Delta K_{th}$  determinations and ISIS calibration. Each  $\Delta K_{th}$  specimen was used for three tests. The two-digit specimen code refers to locations and positions in the original plate material: the first digit gives a location at which three specimens were machined from the plate thickness; the second digit refers to the top (1), middle (2) or bottom (3) specimen at each location.

Table 1 Specimen allocations for threshold test determinations

Specimen code	Type of test
1-2	$K_{max} = 5 \text{ MPa}\sqrt{\text{m}}$ $R = 0.1$
1-3	
2-1	
2-2	D.C. potential drop calibration $R = 0.7$
3-1	
6-2	$K_{max} = 15 \text{ MPa}\sqrt{\text{m}}$ $R = 0.8$
6-3	
8-1	$K_{max} = 25 \text{ MPa}\sqrt{\text{m}}$

## 2.3 Fractography

Following ASTM E 647, the fracture surfaces of the  $\Delta K_{th}$  specimens were examined optically at low magnifications to measure the final crack front lengths and curvatures. These measurements were used to correct the ISIS crack length data and the nominal calculated stress intensity factors, if necessary.

Detailed fractography was done using a Philips Field Emission Gun Scanning Electron Microscope (FEG-SEM) and DSTO-customized Deep Focus Optical Microscope (DFOM).

<sup>1</sup> The measurement of ambient air temperature and humidity is not mentioned in ASTM E 647.

### 3 Threshold test results

The ISIS crack length *versus* cycles data were corrected for offsets; an apparent influence of making optical measurements, when the tests had to be temporarily stopped; and data dropouts. Then the data were processed to obtain crack growth rate,  $da/dN$ , *versus*  $\Delta K$  data. The methods to do the corrections and processing have been incorporated into a MATLAB Graphical User Interface developed by the NLR (Huls 2007).

It was found that the constant R threshold tests were reliable. However, 5 of the 9 constant  $K_{max}$  tests were invalid: one each for  $K_{max}$  values of 5 and 15  $MPa\sqrt{m}$ , for reasons unknown; and all three for  $K_{max} = 25 MPa\sqrt{m}$ . The SiC ceramic loading pins were found to be severely cracked after the third  $K_{max} = 25 MPa\sqrt{m}$  test, and it is possible that they started to crack already during the first test (which was on the same specimen, as mentioned in subsection 2.3).

Figures 3 – 8 show the corrected  $da/dN$  *versus*  $\Delta K$  data for each value of R and  $K_{max}$ . Plotted in this way the data show the considerable scatter in crack growth rates over the entire range of  $\Delta K$ , especially as  $da/dN$  decreases below  $10^{-9}$  m/cycle.

The data shown in figures 3 – 8 were used to derive  $\Delta K_{th}$  values according to ASTM E 647. For each test a vertical-line best fit was made to the lowest set of data points below, or downwardly approaching,  $10^{-10}$  m/cycle. The best fit  $\Delta K$  values at  $10^{-10}$  m/cycle were taken to be the  $\Delta K_{th}$  values. Table 2 gives these values and also the corresponding  $K_{max,th}$  values.

Table 2 7075-T7351 L-T fatigue crack growth thresholds

Type of test	R	$\Delta K_{th}$ (MPa $\sqrt{m}$ )	$K_{max,th}$ (MPa $\sqrt{m}$ )
Constant R	0.1	2.07	2.30
		2.34	2.60
		1.96	2.12
	0.4	1.55	2.58
		1.45	2.42
		1.59	2.65
	0.7	1.45	4.83
		1.69	5.63
		1.19	3.97
	0.8	1.32	6.60
		1.55	7.75
		1.41	7.05
$K_{max} = 5 MPa\sqrt{m}$	0.70 (test 2)	1.42	5.00
	0.69 (test 3)	1.55	5.00
$K_{max} = 15 MPa\sqrt{m}$	0.92 (test 1)	1.22	15.0
	0.92 (test 3)	1.21	15.0

Figures 9 – 11 present the values from table 2 in a specific sequence:  $K_{max,th}$  *versus* R; the two-parameter  $\Delta K_{th}$  *versus*  $K_{max,th}$  diagram; and finally  $\Delta K_{th}$  as a function of R. These figures will now be discussed:

Figure 9: A plot of  $K_{\max,th}$  versus  $R$  enables determination of  $K_{\max,o}$  and  $R_c$ , as shown in the figure. The best fit value of  $K_{\max,o}$  is  $2.5 \text{ MPa}\sqrt{\text{m}}$ , and  $R_c = 0.58$ . Also, the horizontal part of the plot, from  $R = 0$  to  $R = 0.58$ , indicates that  $K_{\max,o}$  will be constant for negative  $R$  (Döker 2005).

Figure 10: A plot of  $\Delta K_{th}$  versus  $K_{\max,th}$ , indicating the best fit value of  $K_{\max,o}$ , gives a scatterband for  $\Delta K_o$ , as shown. The value of  $\Delta K_o$  is  $1.44 \pm 0.25 \text{ MPa}\sqrt{\text{m}}$ .

Figure 11: The best fit value of  $K_{\max,o}$ , the value of  $R_c$ , and the scatterband for  $\Delta K_o$  are added to a plot of  $\Delta K_{th}$  versus  $R$ . This enables estimating the scatterband for  $\Delta K_{th}$  as a function of  $R$ . The result is as follows:

- $R \geq 0.58$  :  $\Delta K_{th} = \Delta K_o = 1.44 \pm 0.25 \text{ MPa}\sqrt{\text{m}}$
- $R \leq 0.58$  :  $\Delta K_{th} = [(2.35 \pm 0.25) - 1.57R] \text{ MPa}\sqrt{\text{m}}$

Obtaining the fatigue crack growth thresholds via this sequence of plots means that scatter in all the  $\Delta K_{th}$  values is considered when making the final  $\Delta K_{th}$  versus  $R$  plot. This is more representative than simply fitting a curve to the  $\Delta K_{th}$  versus  $R$  data (Döker 2005). This final result has a scatterband of  $\pm 0.25 \text{ MPa}\sqrt{\text{m}}$ . This is the same as the 7075-T7351 threshold scatterband obtained by Marci (2000).

Figure 12 compares the  $\Delta K_{th}$  versus  $R$  and  $\Delta K_{th}$  versus  $K_{\max,th}$  values from the present investigation and from Marci (2000). Bearing in mind that the 7075-T7351 aluminium alloy came from different batches, the specimen orientations were different, and the tests were done using different equipment in different laboratories, the agreement is very good. The effective, or intrinsic, fatigue crack growth threshold stress intensity factor ranges,  $\Delta K_o = K_{\max,o} - K_{op}$ , are slightly different:

- Marci :  $1.0 \leq \Delta K_o \leq 1.5 \text{ MPa}\sqrt{\text{m}}$
- NLR :  $1.19 \leq \Delta K_o \leq 1.69 \text{ MPa}\sqrt{\text{m}}$

## 4 Threshold and near- threshold fractography

### 4.1 Background information and procedure

Rather surprisingly, there has been limited investigation of the near-threshold fatigue fracture topography of aluminium alloys. The following is known, or suggested, about overaged 7000 series alloys like 7075-T7351 (Vasudévan and Suresh 1982; Suresh *et al.* 1984):

- (1) Atmospheric humidity influences the oxidation of the near-threshold fracture surface. Increased humidity increases the oxide thickness.
- (2) At low  $R$  values oxidation *may* play a dominant role in influencing the near-threshold fatigue crack growth behaviour. Increased oxidation enhances fatigue crack closure and could arrest the fatigue cracks. In other words, enhanced fracture surface oxidation might lead to higher values of  $\Delta K_{th}$ , though this was not explicitly stated by Vasudévan and Suresh.

- (3) At high R values other factors besides oxidation *may* play a role, namely the fracture surface roughness and crack front profile.

In terms of fractographic observation there is a difference in scale. Fracture surface oxidation and any variations in oxide thickness are properly observable only at medium-to-high SEM magnifications, generally beyond the capability of optical microscopy. However, fracture surface roughnesses and crack front profiles are most readily observed and compared at lower magnifications.

Owing to this difference in observational scale, we shall first survey the fracture surface roughnesses and near-threshold crack front profiles, using both the DFOM and FEG-SEM. This survey is followed by more localised, and hence more detailed, examination of the threshold and near-threshold region, relying mainly on FEG-SEM images for interpretation.

## 4.2 Survey of near-threshold crack front profiles and roughnesses

### 4.2.1 FEG-SEM stereo images

Figures 13 – 31 give examples of the threshold and near-threshold fatigue crack front profiles and roughnesses. The stereo images were prepared for viewing using the anaglyph viewer in the envelope attached to the inside back cover of this report.

Table 3 classifies the threshold and near-threshold fatigue fracture features per test condition, including the local relative humidity (R.H.), temperature, and fracture surface roughness ( $R_L$ ) at threshold. The following trends were observed:

- At low to intermediate stress ratios ( $R = 0.1 - 0.4$ ) the fracture topography consisted mainly of flat “scallops” (locally curved crack fronts) separated by narrow ridges. The scallops in figures 13 – 15 were clearly marked by alternating light and dark bands having the contours of the fatigue crack fronts. Observation of these bands for the specimen tested at  $R = 0.1$  led to recording the humidity and temperature for the remaining tests, see Appendix A. Though much less evident, the alternation of light and dark bands can also be seen in figures 19, 20 and 24.
- At high stress ratios ( $R = 0.67 - 0.8$ ) the scallops tended to be fewer, ill-defined and separated by wide and rough ridges, giving an overall increase in fracture surface roughness. However, one test where the threshold was reached at higher humidities (2-2: III) was better characterized by flat scallops separated by narrow ridges.
- At very high stress ratios ( $R = 0.92 - 0.95$ ) the fracture topographies consisted of mixtures of flat facets and rough ridges.
- The fracture surface roughnesses showed considerable variation, but there was a tendency for the roughness to increase with increasing stress ratio.

Table 3 Classification of 7075-T7351 L-T threshold and near-threshold fatigue fracture features

<b>R</b>	<b>Specimen code</b>	<b>Thresholds and figures</b>	<b>Threshold R.H. (%)</b>	<b>Threshold Temp. (°C)</b>	<b>R<sub>L</sub></b>	<b>Fatigue fracture features</b>
0.1	1-3	I : fig. 13 II : fig. 14 III : fig. 15	– – –	– – –	1.10 1.09 1.10	• scalloped flat fracture separated by narrow ridges; light and dark bands contouring the crack fronts prior to threshold
0.4	3-1	I : fig. 16 II : fig. 17 III : fig. 18	29 - 30 38 - 39 26 - 27	24 * 20	1.21 1.05 1.20	• scalloped flat fracture separated by narrow ridges; faint light and dark bands contouring the crack fronts prior to threshold
0.67 - 0.70	1-2	I : fig. 19 II : fig. 20 III : fig. 21	17 - 18 23 - 24 25 - 26	22 23 23	1.21 1.18 1.14	• scalloped fracture separated by wide and rough ridges; light and dark bands contouring the crack fronts prior to threshold
0.7	2-2	I : fig. 22 II : fig. 23 III : fig. 24	29 - 30 42 - 43 38 - 39	21 21 20	1.20 1.15 1.10	• I, II: wide and rough ridges separating some scalloped fracture • III: scalloped flat fracture separated by narrow ridges: light and dark bands prior to threshold
0.8	6-3	I : fig. 25 II : fig. 26 III : fig. 27	33 - 34 26 - 27 23 - 24	22 22 22	1.25 1.20 1.25	• wide and rough ridges separating some scalloped fracture
0.92	6-2	I : fig. 28 II : fig. 29 III : fig. 30	21 - 22 28 - 29 31 - 32	25 25 25	1.27 1.18 1.15	• mixtures of flat facets and rough ridges
0.95	8-1	I : fig. 31	30	26	1.31	• mixtures of flat facets and rough ridges

\* Data dropout near end of test

#### 4.2.2 Comparisons of FEG-SEM and DFOM images

Figures 32 – 38 compare FEG-SEM and DFOM overviews of some of the thresholds, covering the range  $R = 0.1 - 0.92$  and for various local R.H. values, see table 4. In the first instance the FEG-SEM and DFOM images look very different. In fact, it requires considerable expertise to match the same features observed by these techniques. Perhaps the most obvious correlations, apart from the transitions from third thresholds to overload fracture, are provided by the flat scallops. These tend to be highly reflective in the DFOM images, see figures 32, 33 and 35. Also, table 4 suggests that there is a correlation between the occurrence of flat scallops and local relative humidities approaching 40 %.

Table 4 Threshold fracture surfaces selected for FEG-SEM and DFOM comparisons

R	Specimen code	Thresholds and figures	Threshold R.H. (%)	Fatigue fracture features
0.1	1-3	III : fig. 32	–	mainly flat scallops
0.4	3-1	II : fig. 33	38 - 39	mainly flat scallops
0.7	2-2	I : fig. 34 III : fig. 35	29 - 30 38 - 39	mainly wide rough ridges mainly flat scallops
0.8	6-3	II : fig. 36	26 - 27	mainly wide rough ridges
0.92	6-2	I : fig. 37 III : fig. 38	21 - 22 31 - 32	flat facets and rough ridges flat facets and rough ridges

#### 4.3 Detailed fractography in the threshold/near-threshold region

As mentioned in subsection 4.2.1, the FEG-SEM images in figures 13 – 15, and to a lesser extent figures 19, 20 and 24, show alternations of light and dark bands which have the contours of the fatigue crack fronts. Figure 39 gives a perspective view of a typical dark band between two light ones on a flat scallop. This view shows that (a) the dark band has an even flatter topography and (b) the fracture surface details are partially obscured by an overlying featureless layer.

Interpretation of the FEG-SEM image dark band phenomenon has been aided by detailed examination of the thresholds by both FEG-SEM and DFOM imaging. Figures 40 – 43 give examples from which the following conclusions are drawn:

- (1) The FEG-SEM dark bands correspond to highly reflective and almost featureless bands in DFOM images, see figures 40 and 42.
- (2) These bands occurred only at relative humidities approaching 40 %, compare figures 41 and 42.
- (3) These almost featureless bands are the result of a brittle layer overlying the fatigue fracture surfaces, see figure 43.
- (4) The most obvious explanation for these bands is that they are due to fracture surface oxidation that requires a local relative humidity approaching 40 %, and certainly more than 30 %. This explanation is semi-quantitatively consistent with the earlier work of Vasudévan and Suresh (1982) and Suresh *et al.* (1984) mentioned in subsection 4.1.

They observed enhanced near-threshold fracture surface oxidation for overaged 7000 series alloys tested in air of 95 % R.H.

## 5 Discussion

As stated in the introduction to this report, the present investigation is a contribution to the first main objective of the *HeliDamTol* programme: namely, the development of reliable methods of fatigue crack growth analysis for helicopter airframe components.

Of primary importance to this objective is the determination of fatigue crack growth thresholds,  $\Delta K_{th}$ . Figures 11 and 12 show the final results of the present investigation, including the very good agreement with Marci's data (Marci 2000). Our results may be quantitatively expressed as follows:

- $R \geq 0.58$  :  $\Delta K_{th} = \Delta K_o = 1.44 \pm 0.25 \text{ MPa}\sqrt{\text{m}}$
- $R \leq 0.58$  :  $\Delta K_{th} = [(2.35 \pm 0.25) - 1.57R] \text{ MPa}\sqrt{\text{m}}$

The scatterband is  $\pm 0.25 \text{ MPa}\sqrt{\text{m}}$ , which is the same as that obtained by Marci. He stated that a scatterband of  $\pm 0.2 \text{ MPa}\sqrt{\text{m}}$  is "a realistic aim for the experimental determination of  $\Delta K_{th}$ ." However, this seems slightly optimistic.

The scatterbands signify variations in  $\Delta K_{th}$  of about 11 – 17 %, the latter value being for  $R \geq 0.58$ . These variations are significant, certainly in the context of modelling fatigue crack growth, and the question naturally arises why there are such significant variations.

In our opinion, a reasonable answer to this question is given by the fractography survey in subsection 4.2. At and near the fatigue crack thresholds the individual crack front topographies and profiles showed considerable variations, especially for higher R. These variations would probably have affected the local crack driving forces (stress intensity factor ranges) both geometrically and through variations in roughness-induced fatigue crack closure. This explanation agrees with the suggestions of Vasudévan and Suresh (1982) and Suresh *et al.* (1984).

However, our results do not fit with the suggestion by Vasudévan and Suresh (1982) about the effect of atmospheric humidity on near-threshold fatigue crack growth, namely that at low R values oxide build-up could arrest cracks. (As stated in subsection 4.1, this type of crack arrest would be expected to cause higher  $\Delta K_{th}$  values.) Figure 44 shows that there were no consistent correlations between the local variations in atmospheric humidity, ranging from 17 – 43 % R.H., and  $\Delta K_{th}$ . This is despite the evident effects of humidity on (a) the threshold and near-threshold fracture topography, see subsection 4.2, and (b) the amount of fracture surface oxidation at threshold, see subsection 4.3.

A likely reason for this discrepancy, if it should be called that, is the relative severity of the air environments. Vasudévan and Suresh (1982) tested overaged 7000 series alloys in air of 95 % R.H., considerably above the maximum local relative humidity (43 % R.H.) at threshold in our tests. Certainly, it is known that severe test environments (sump tank water and synthetic seawater) result in increased  $\Delta K_{th}$  values owing to oxide build-up (Wanhill and Schra 1990).



In the light of the foregoing remarks, we arrive at the following main conclusions:

- (1) For positive R all values of  $\Delta K_{th}$  will be subject to variations of at least  $\pm 0.25 \text{ MPa}\sqrt{\text{m}}$ . This has to be considered as the limiting accuracy for fatigue crack growth modelling.
- (2) The presently determined  $\Delta K_{th}$  values and variations of  $\Delta K_{th}$  cover normal changes in atmospheric humidity ranging from 17 – 43 % R.H. This range is probably sufficient to account for the average atmospheric conditions experienced by helicopters during service.

## 6 Conclusions

Fatigue crack growth thresholds,  $\Delta K_{th}$ , were determined for the aluminium alloy plate material 7075-T7351, as used for the NH90 helicopter hinge beams. The parameter  $\Delta K_{th}$  is of primary importance for modelling fatigue crack growth in the airframes of helicopters and other aerospace vehicles.

The thresholds were determined for the positive stress ratio range  $R = 0.1 - 0.95$ . The results may be expressed as follows:

- (1) For  $R \geq 0.58$  the measured fatigue crack growth threshold stress intensity range  $\Delta K_{th}$  is equal to the effective, or intrinsic threshold stress intensity range  $\Delta K_o$ , and is given by

$$R \geq 0.58 : \Delta K_{th} = \Delta K_o = 1.44 \pm 0.25 \text{ MPa}\sqrt{\text{m}}$$

- (2) For  $R \leq 0.58$  the measured  $\Delta K_{th}$  depends on R:

$$R \leq 0.58 : \Delta K_{th} = [(2.35 \pm 0.25) - 1.57R] \text{ MPa}\sqrt{\text{m}}$$

The results include a scatterband of  $\pm 0.25 \text{ MPa}\sqrt{\text{m}}$  for all values of  $\Delta K_{th}$ , and consequent variations in  $\Delta K_{th}$  of about 11 – 17 %. These variations are most probably due to variable crack front topographies and profiles in the threshold region, and they represent intrinsic limitations to the accuracy of  $\Delta K_{th}$  values.

On the other hand, despite evident effects of humidity on the threshold and near-threshold fracture topography and the amount of fracture surface oxidation at threshold, the determined  $\Delta K_{th}$  values seem independent of normal changes in atmospheric humidity ranging from 17 – 43 % R.H. This is probably sufficient to account for the average atmospheric conditions experienced by helicopters during service.

## 7 References

Döker, H., 2005, Personal Communication from the DLR, Porz-Wahnheide (Cologne), to M.J. Bos and R.J.H. Wanhill.

Huls, R.A., 2007, Processing of crack growth data with application to aluminium alloy 7075-T7351, Contract Report NLR-CR-2007-396, National Aerospace Laboratory NLR, Amsterdam, the Netherlands.

Irving, P.E., Lin, J., Bristow, J.W., 2003, Damage tolerance in helicopters. Report on the Round Robin challenge, American Helicopter Society 59th Annual Forum, Phoenix, AZ, May 2003, MIRA Digital Publishing, St. Louis, MO, USA.

Marci, G., 2000, Fatigue crack growth threshold concept and test results for Al- and Ti-alloys, Fatigue Crack Growth Thresholds, Endurance Limits, and Design, ASTM STP 1372 (Editors J.C. Newman, Jr. and R.S. Piascik), pp. 81-95, American Society for Testing and Materials, West Conshohocken, PA, USA.

Suresh, S., Vasudévan, A.K., Bretz, P.E., 1984, Mechanisms of slow fatigue crack growth in high strength aluminum alloys: role of microstructure and environment, Metallurgical Transactions A, Vol. 15A, pp. 369-379.

Vasudévan, A.K., Suresh, S., 1982, Influence of corrosion deposits on near-threshold fatigue crack growth behavior in 2XXX and 7XXX series aluminum alloys, Metallurgical Transactions A, Vol. 13A, pp. 2271-2280.

Vaughan, R.E., Chang, J.H., 2003, Life predictions for high cycle dynamic components using damage tolerance and small threshold cracks, American Helicopter Society 59th Annual Forum, Phoenix, AZ, MIRA Digital Publishing, St. Louis, MO, USA.

Wanhill, R.J.H., Bos, M.J., 2004, Literature study of damage tolerance in helicopters, Contract Report NLR-CR-2004-464, National Aerospace Laboratory NLR, Amsterdam, the Netherlands.

Wanhill, R.J.H., Schra, L., 1990, Corrosion fatigue crack arrest in aluminium alloys, Quantitative Methods in Fractography, ASTM STP 1085 (Editors B.M. Strauss and S.K. Putatunda), pp. 144-165, American Society for Testing and Materials, Philadelphia, PA, USA.

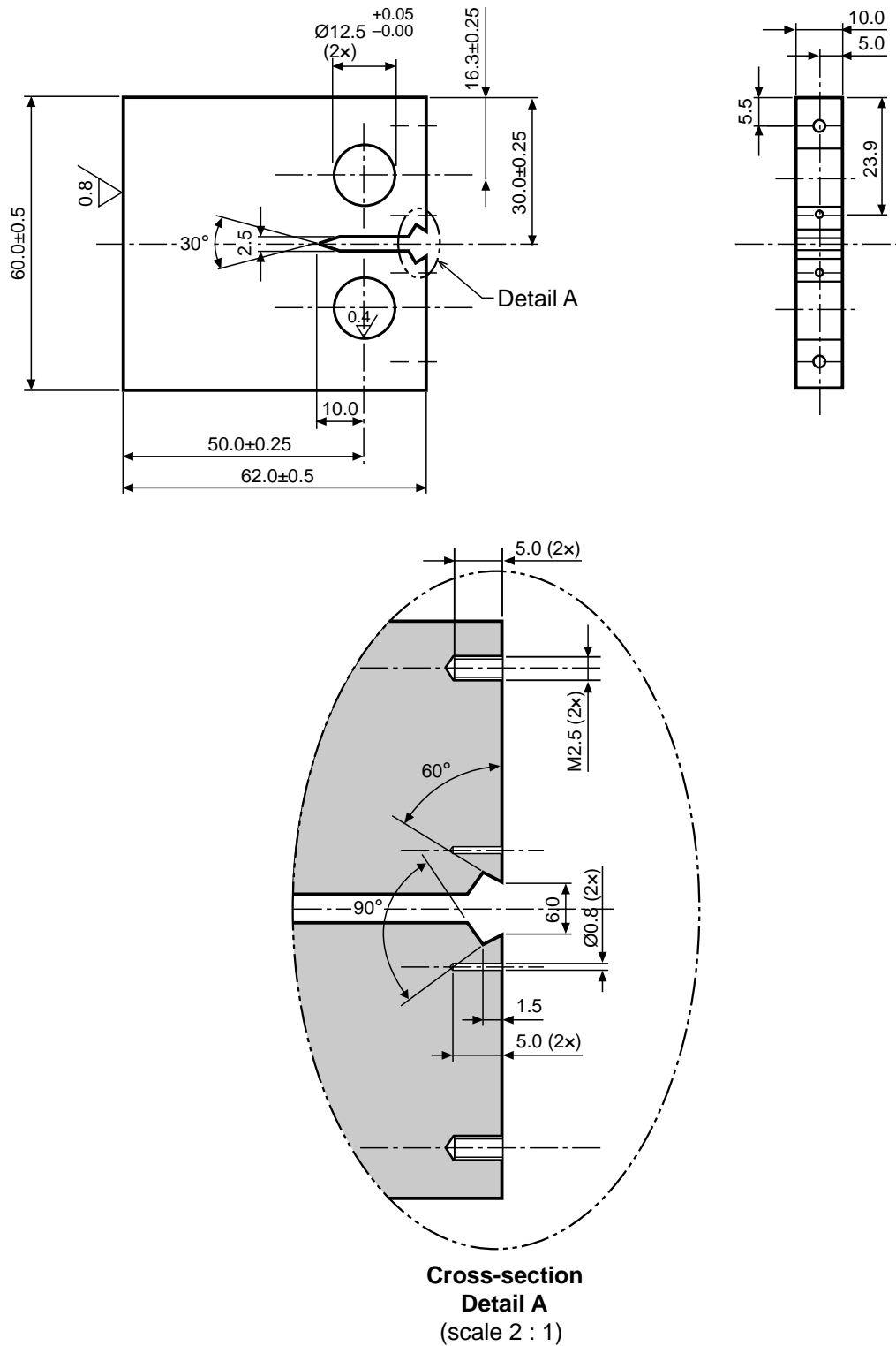


Fig. 1 Compact Tension (CT) specimen dimensions (mm). Detail A shows the locations of the leads for the DC. potential drop measurement system and the integrally machined knife edges for clip gauge measurements of crack opening displacements

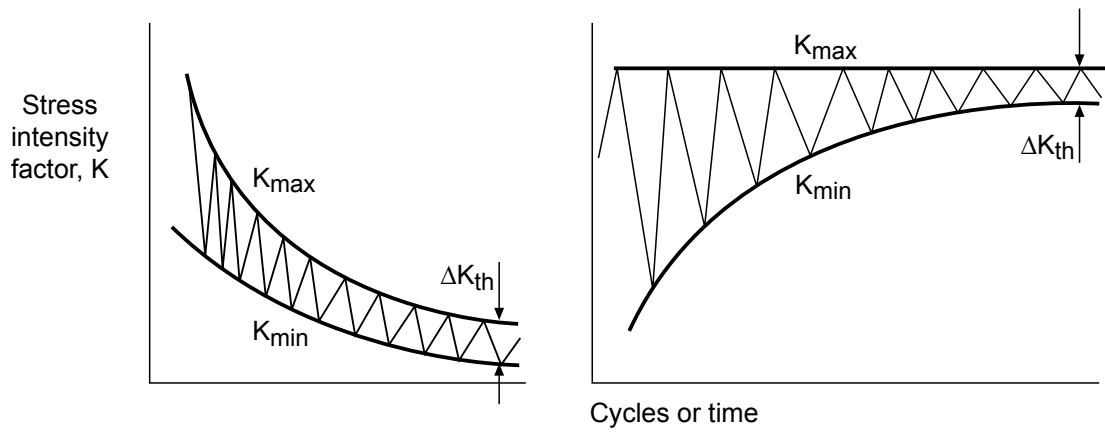


Fig. 2 Constant  $R$  (left) and constant  $K_{max}$  test methods to determine  $\Delta K_{th}$ ;  $R$  is the stress ratio,  $S_{min}/S_{max} = K_{min}/K_{max}$ , of a loading cycle

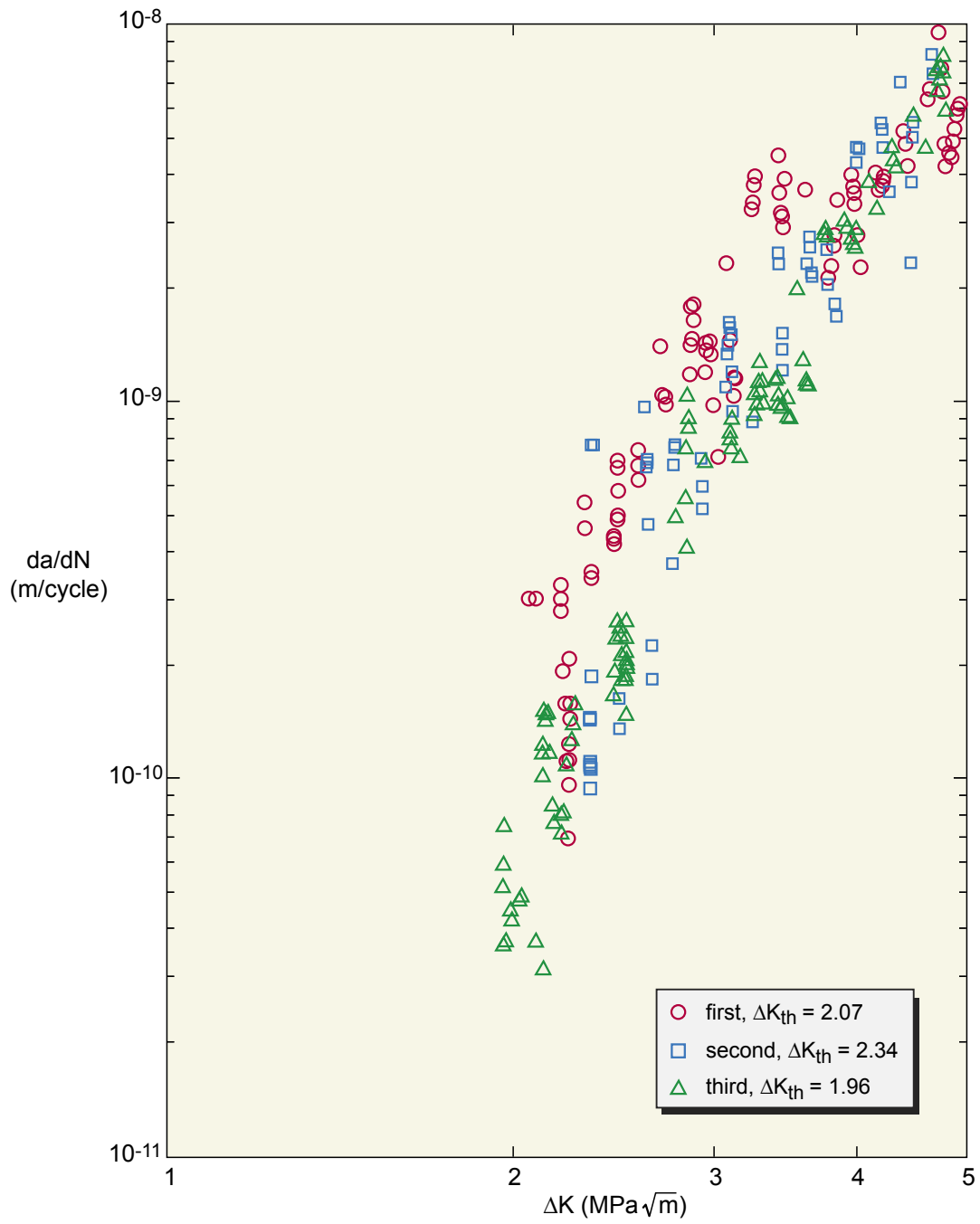


Fig. 3 Corrected crack growth rate results for  $R = 0.1$

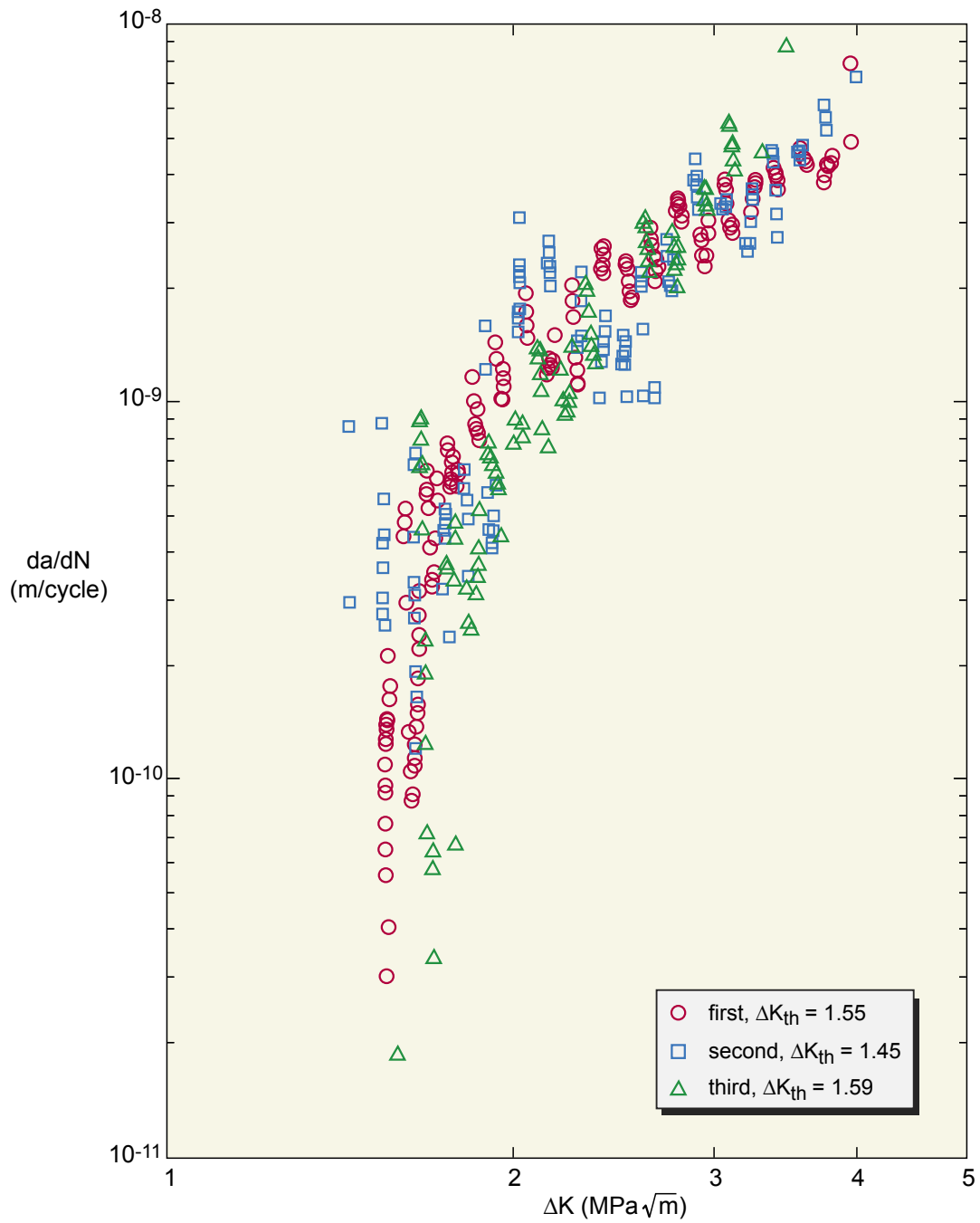


Fig. 4 Corrected crack growth rate results for  $R = 0.4$

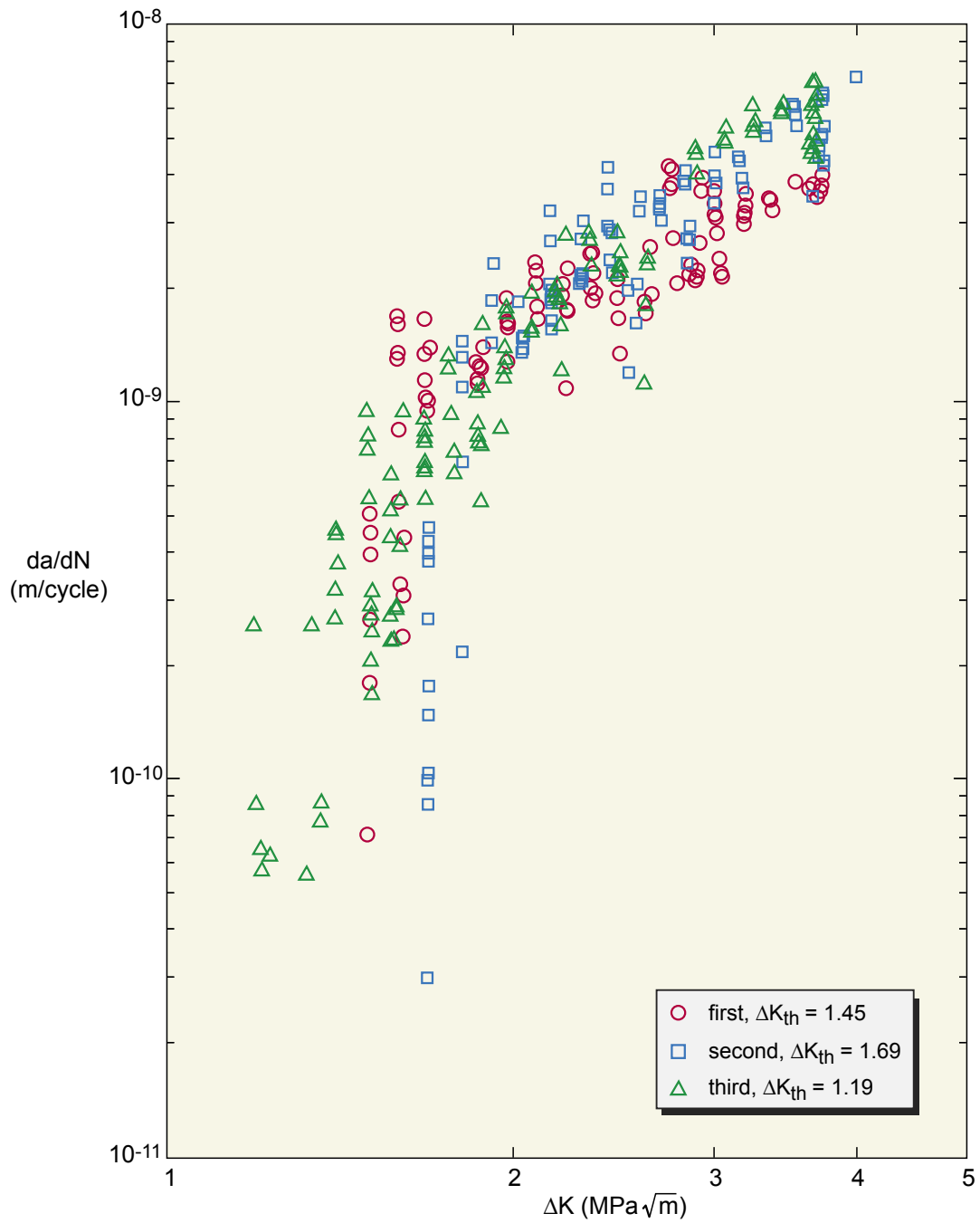


Fig. 5 Corrected crack growth rate results for  $R = 0.7$

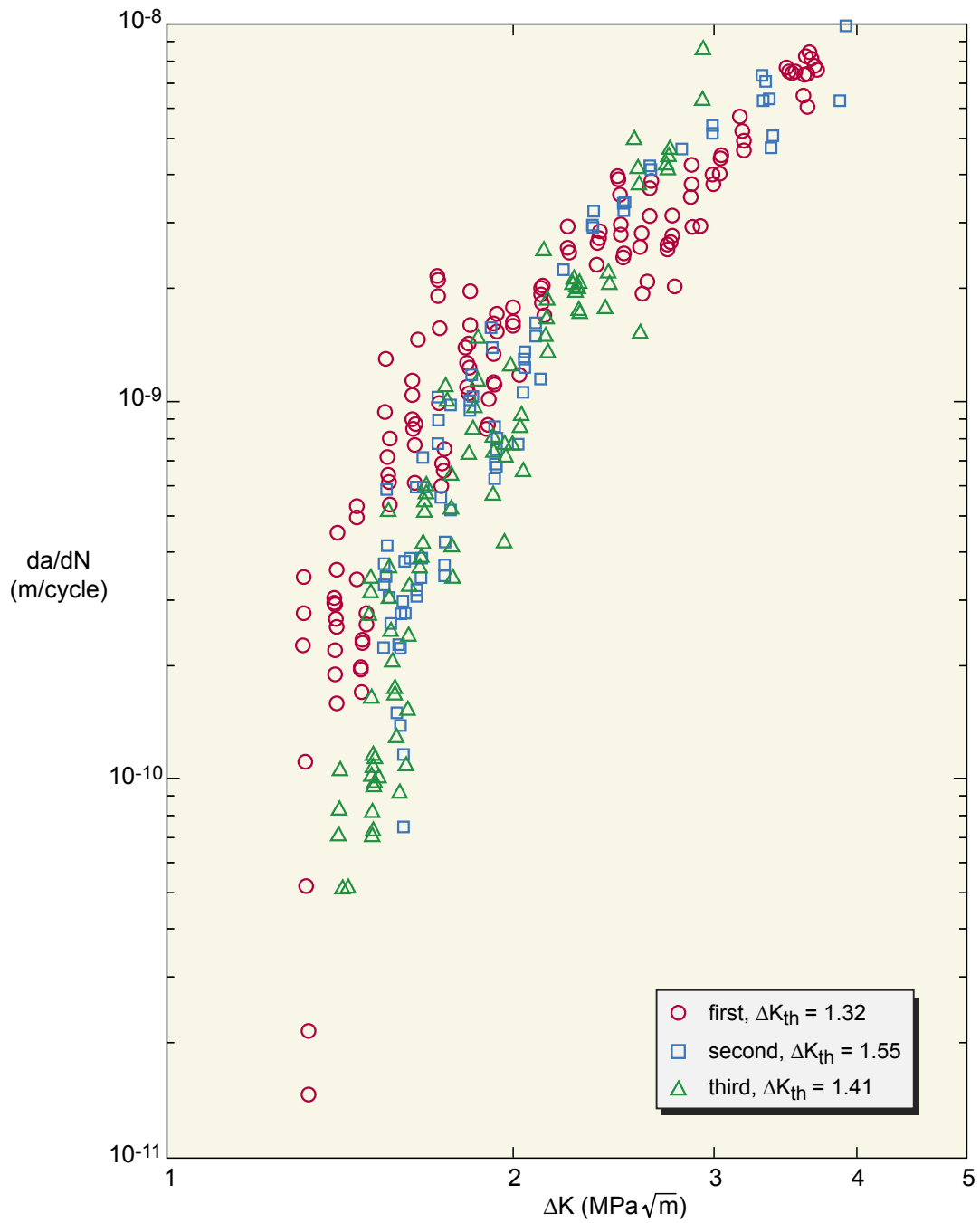


Fig. 6 Corrected crack growth rate results for  $R = 0.8$



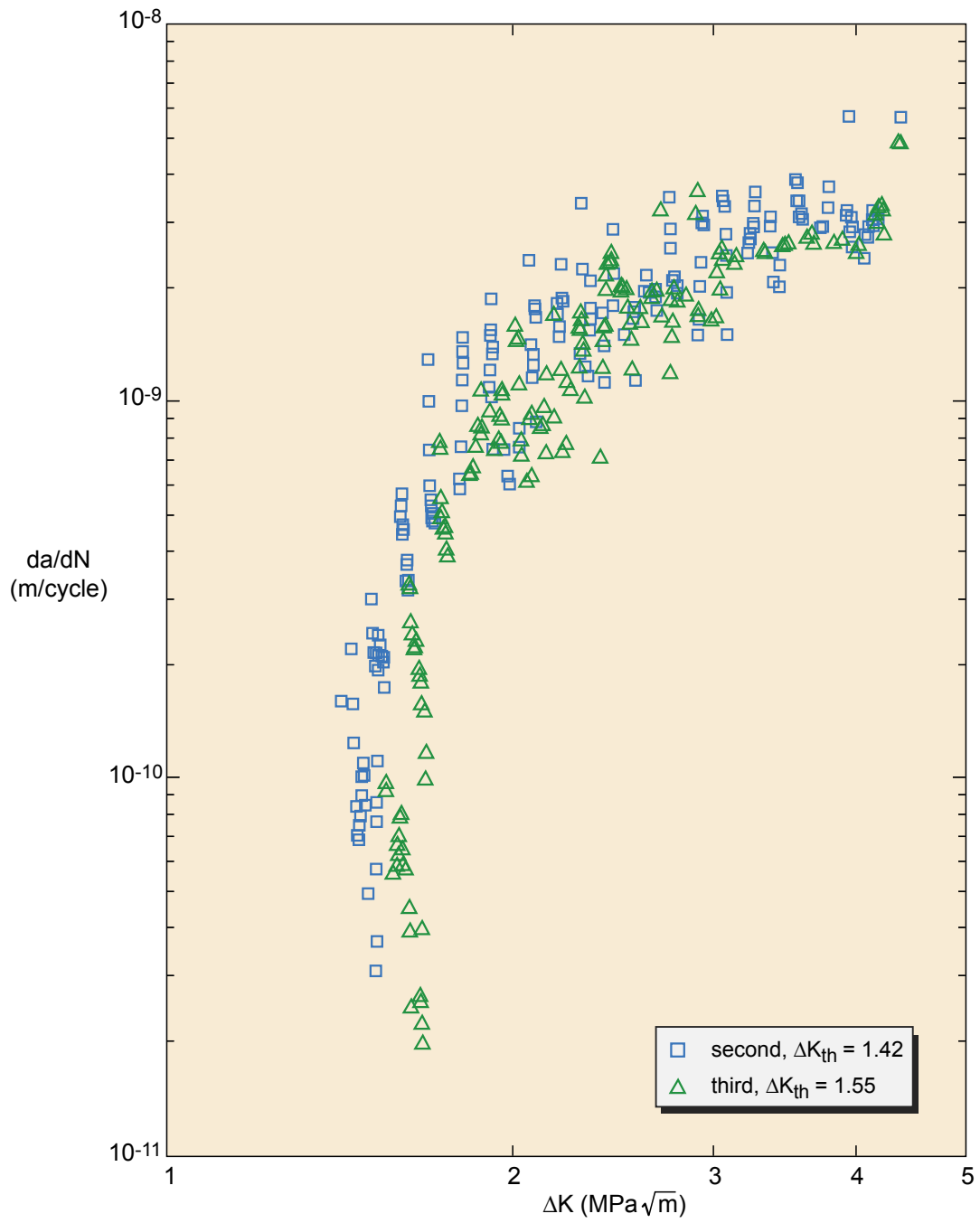


Fig. 7 Corrected crack growth rate results for  $K_{max} = 5 \text{ MPa}\sqrt{\text{m}}$

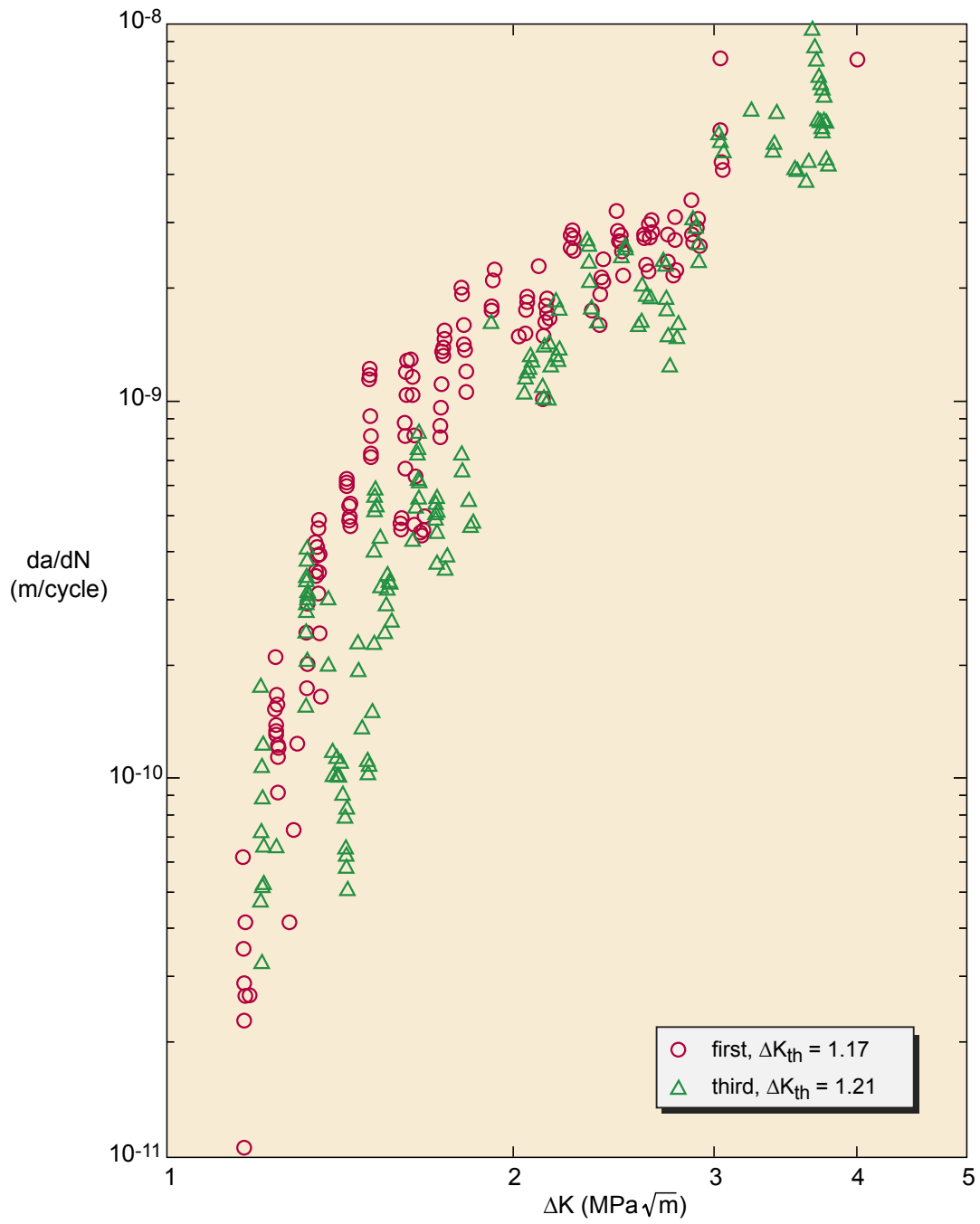


Fig. 8 Corrected crack growth rate results for  $K_{max} = 15 MPa\sqrt{m}$

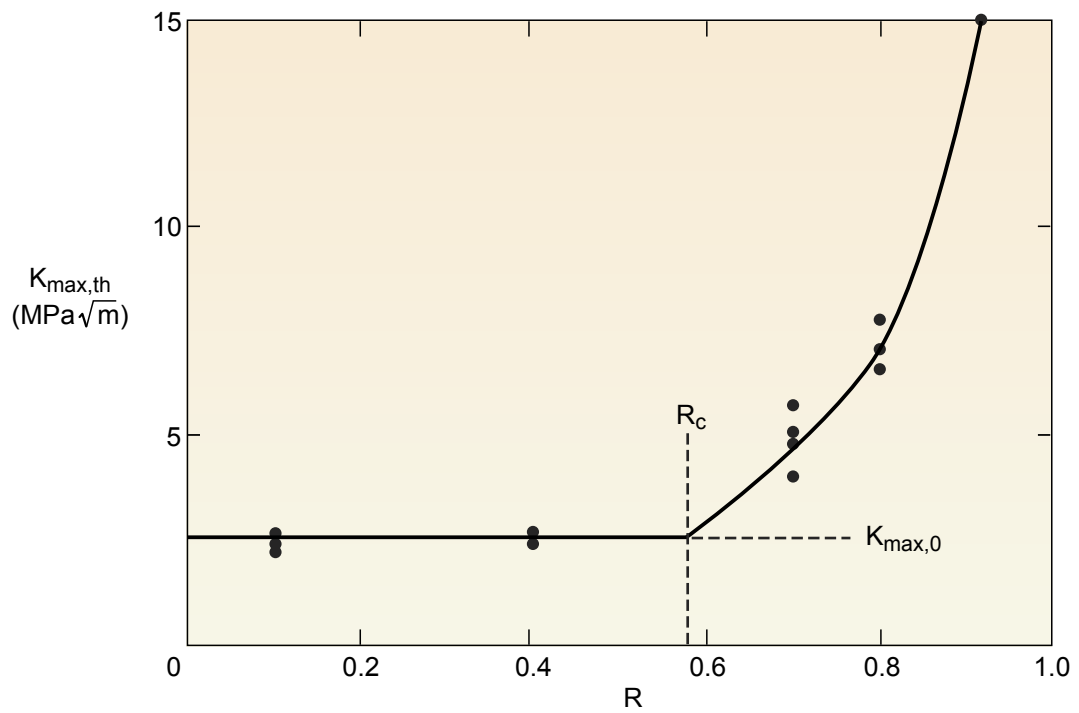


Fig. 9  $K_{max,th}$  versus R: data from table 2

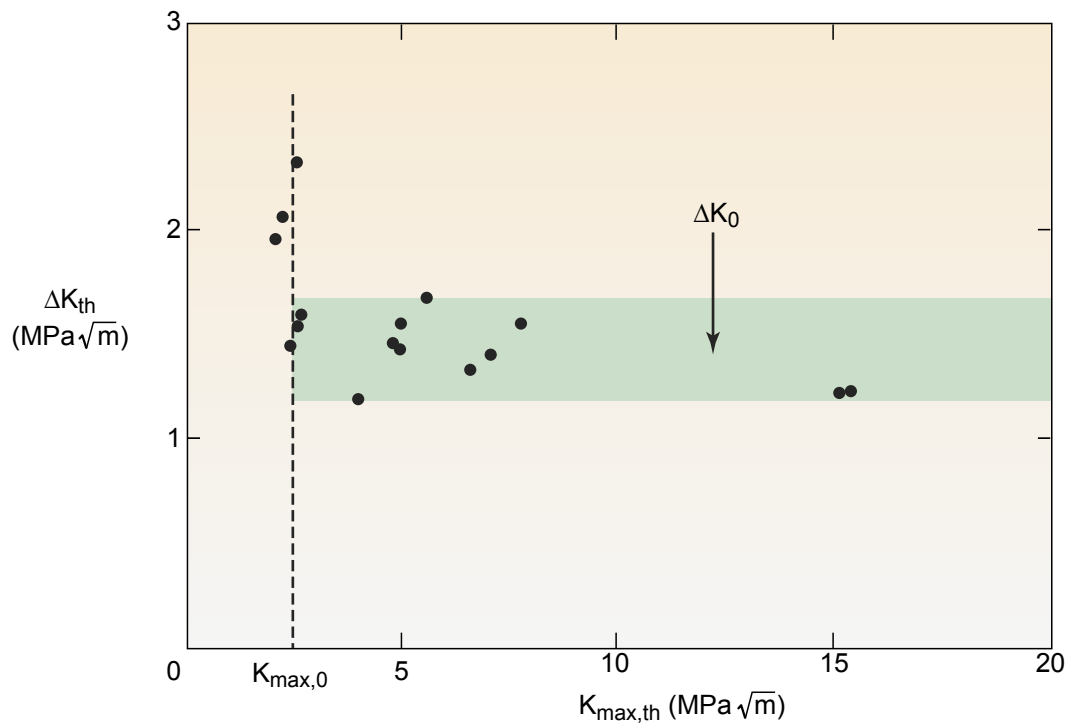


Fig. 10 Two parameter  $\Delta K_{th}$  versus  $K_{max,th}$  diagram: data from table 2

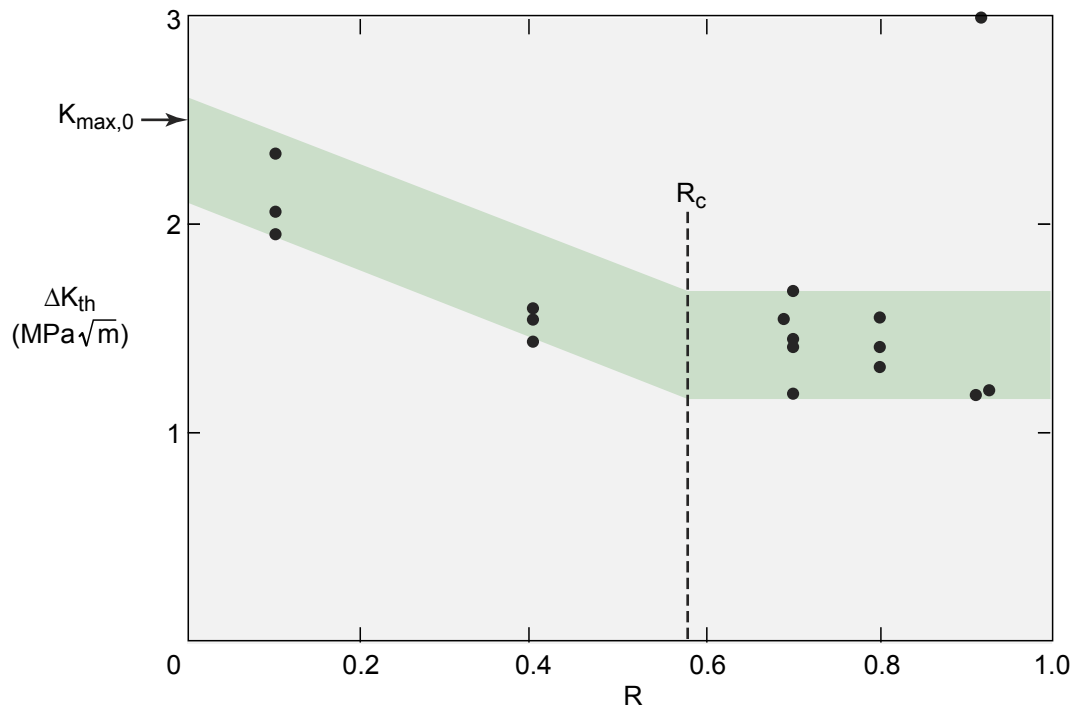


Fig. 11  $\Delta K_{th}$  versus  $R$ : data from table 2

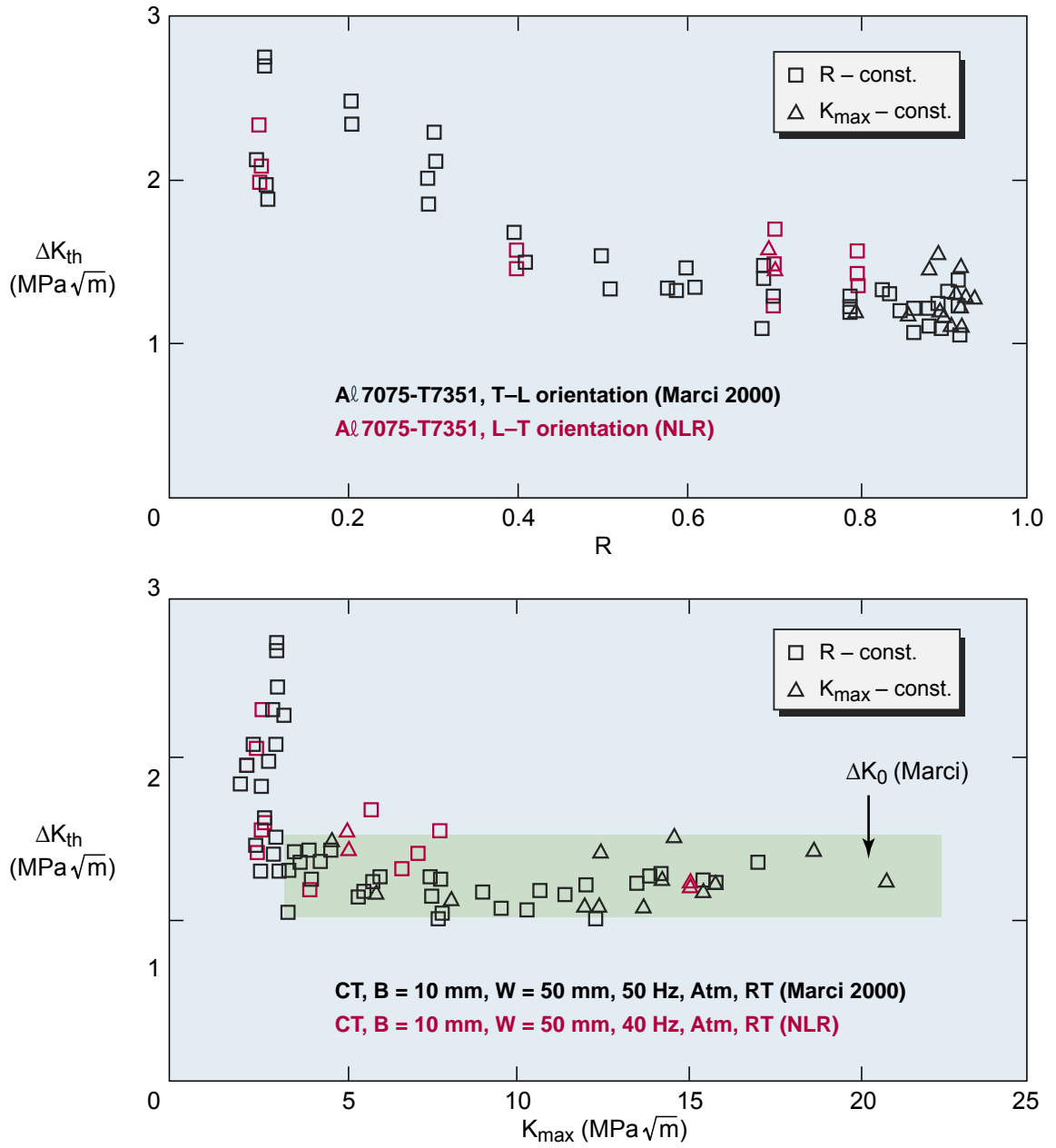
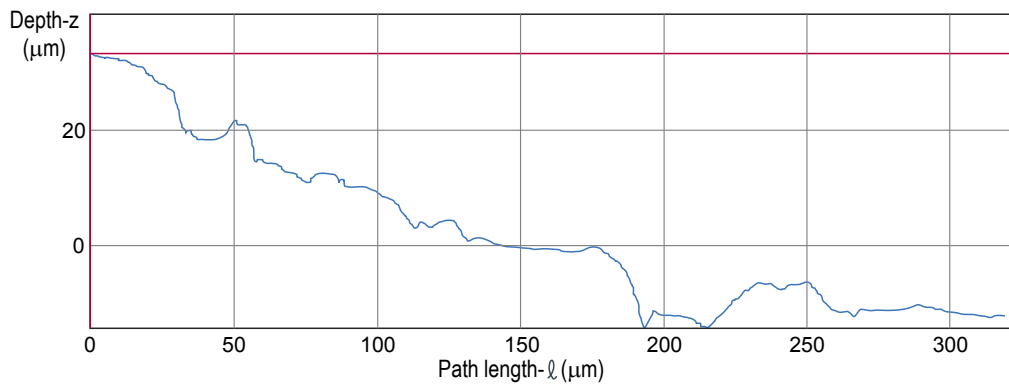


Fig. 12 Comparison of the NLR's and Marci's threshold data



RL = 1.10

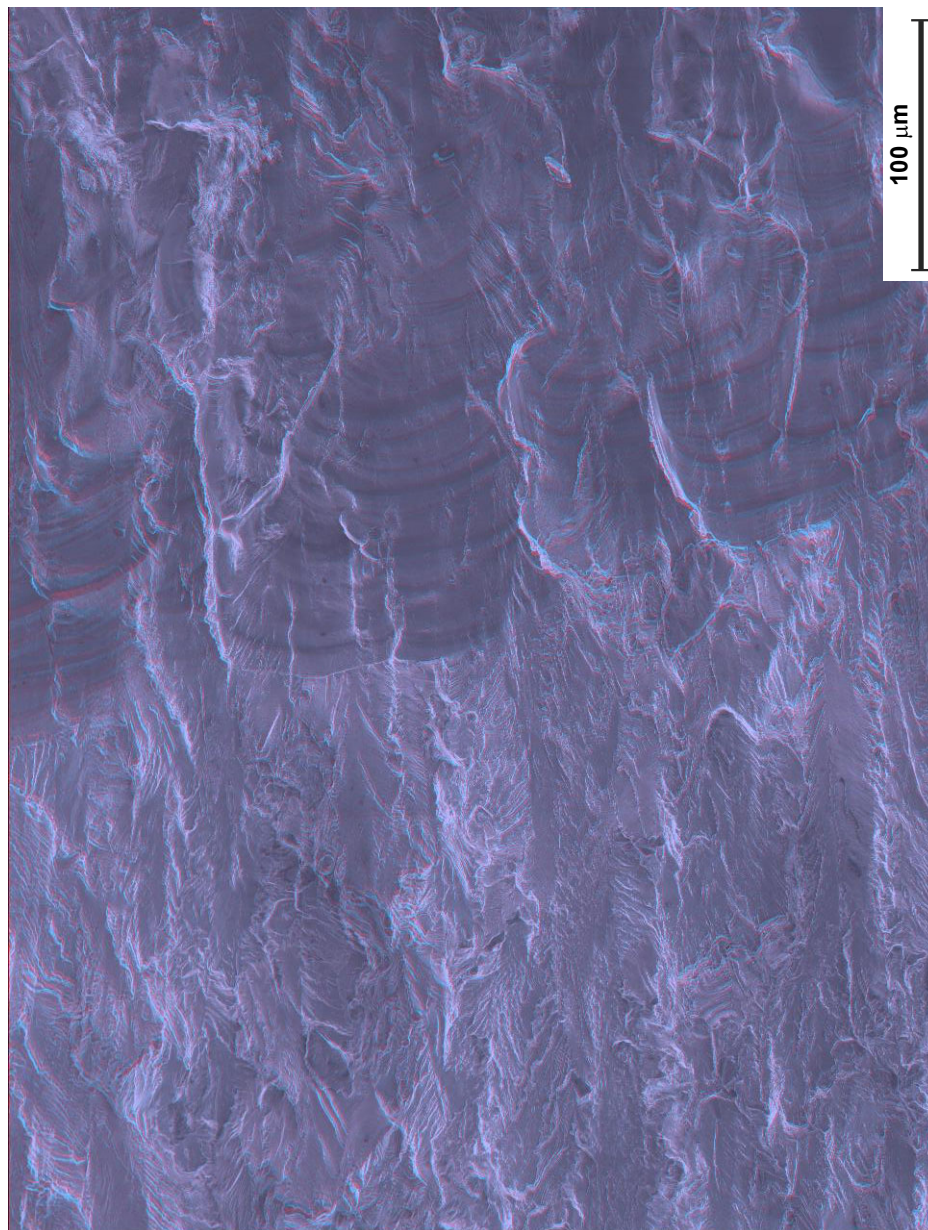
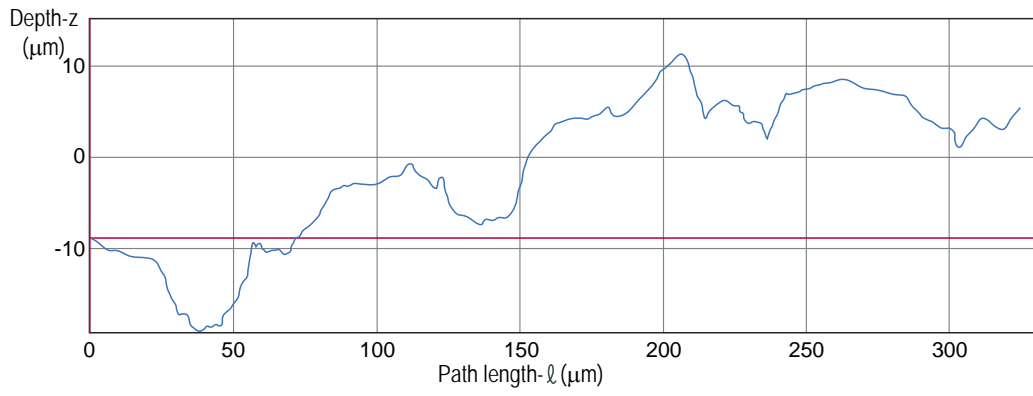


Fig. 13 Overview of first threshold for specimen 1–3,  $R = 0.1$ : mainly flat scallops



RL = 1.09

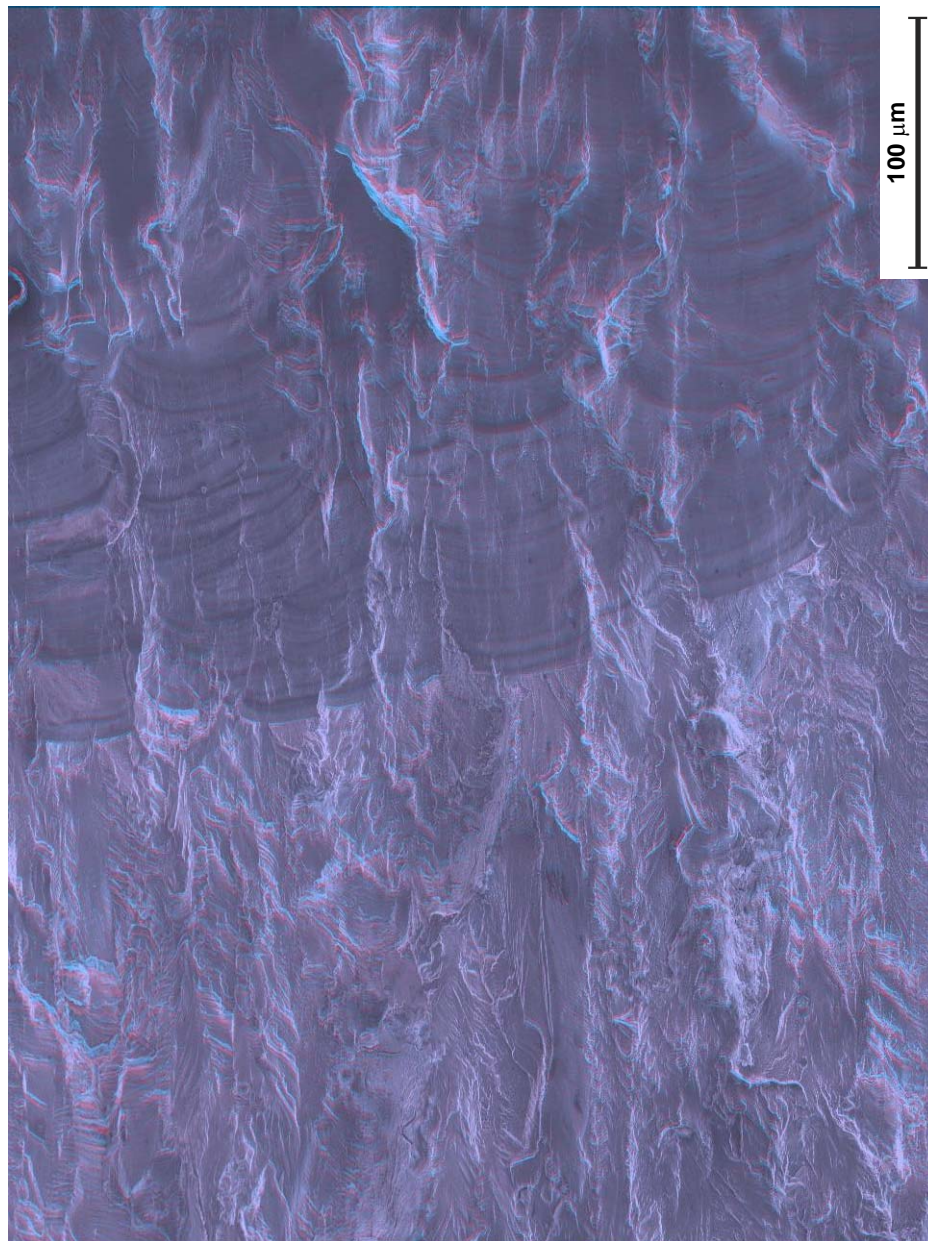
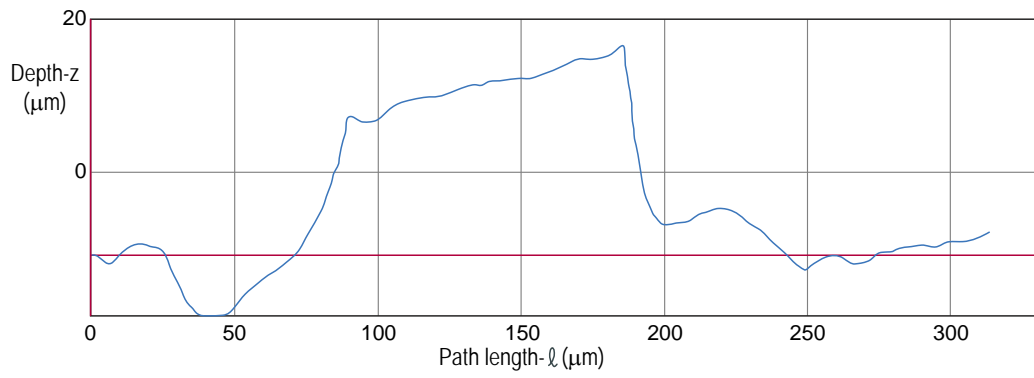


Fig. 14 Overview of second threshold for specimen 1–3,  $R = 0.1$ : mainly flat scallops



RL = 1.10

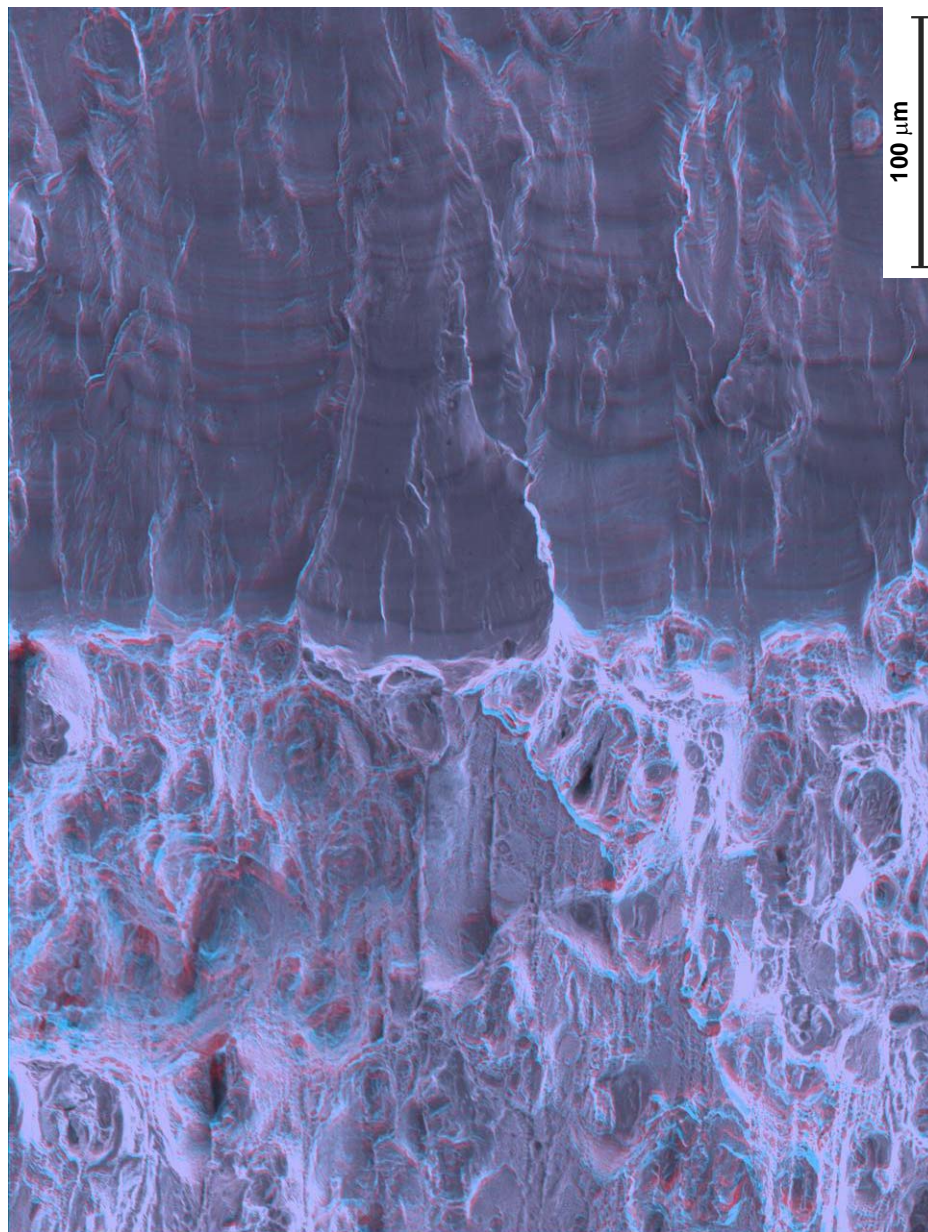
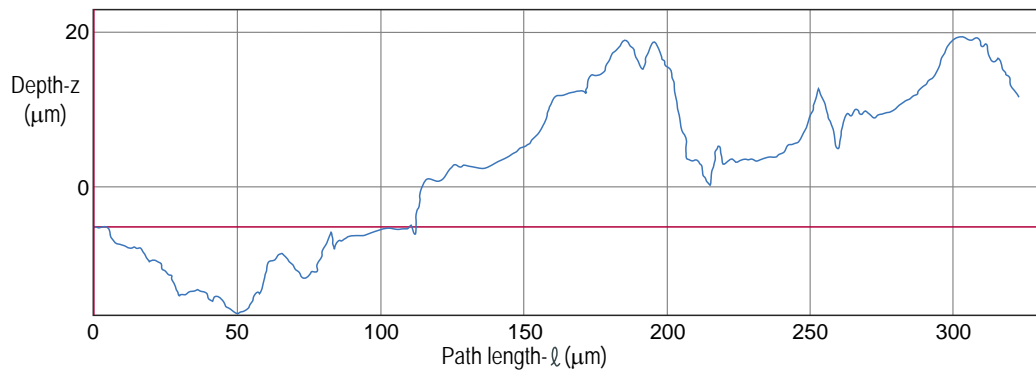


Fig. 15 Overview of third threshold for specimen 1–3,  $R = 0.1$ : mainly flat scallops





RL = 1.21

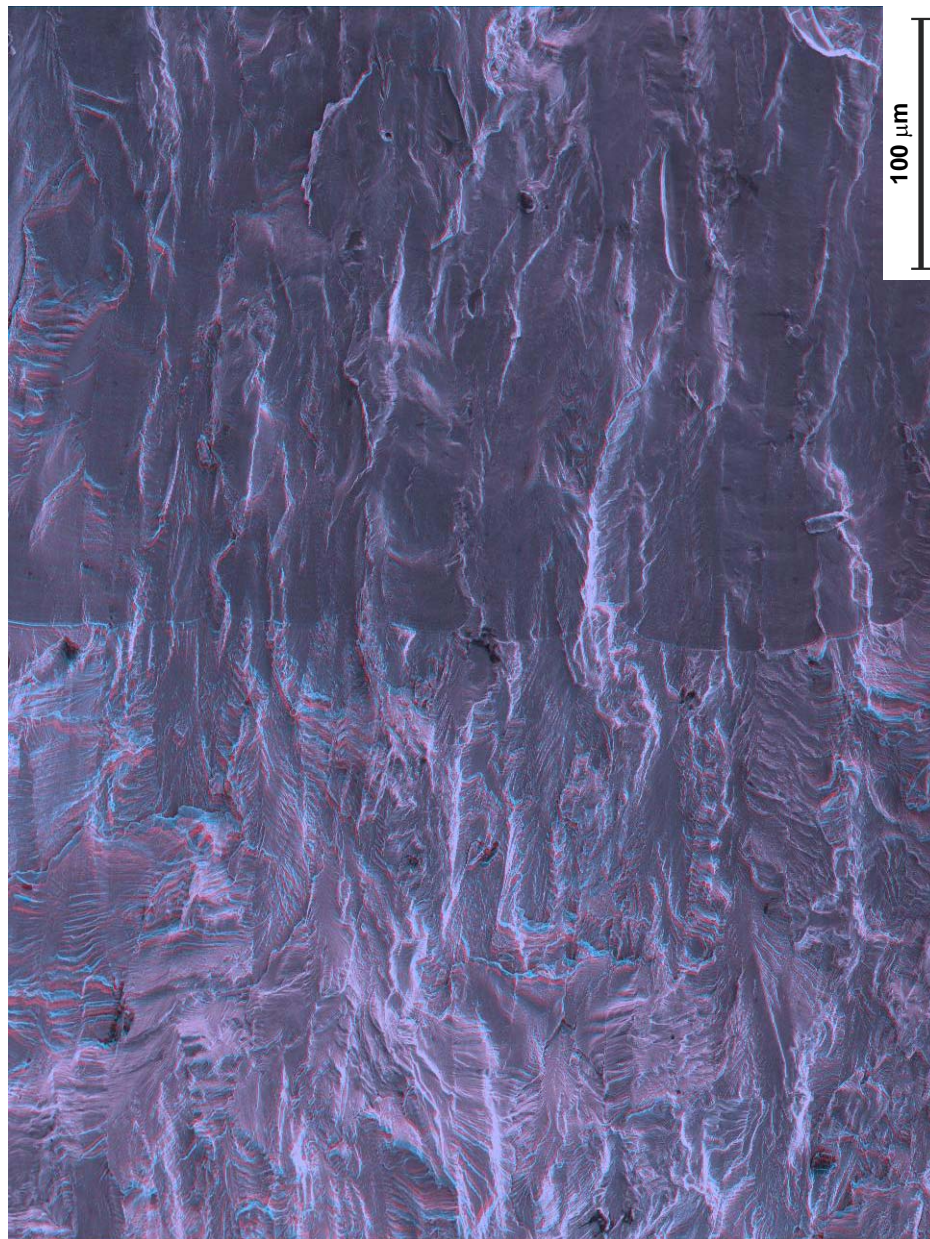
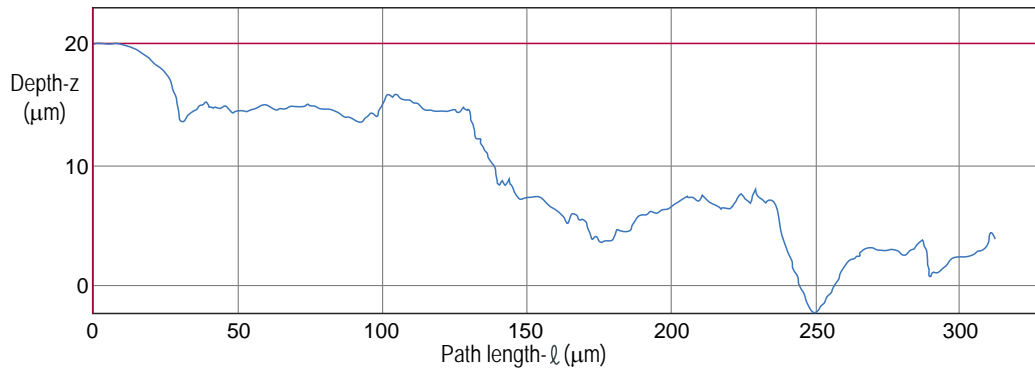


Fig. 16 Overview of first threshold for specimen 3-1,  $R = 0.4$ : mainly flat scallops



RL = 1.05

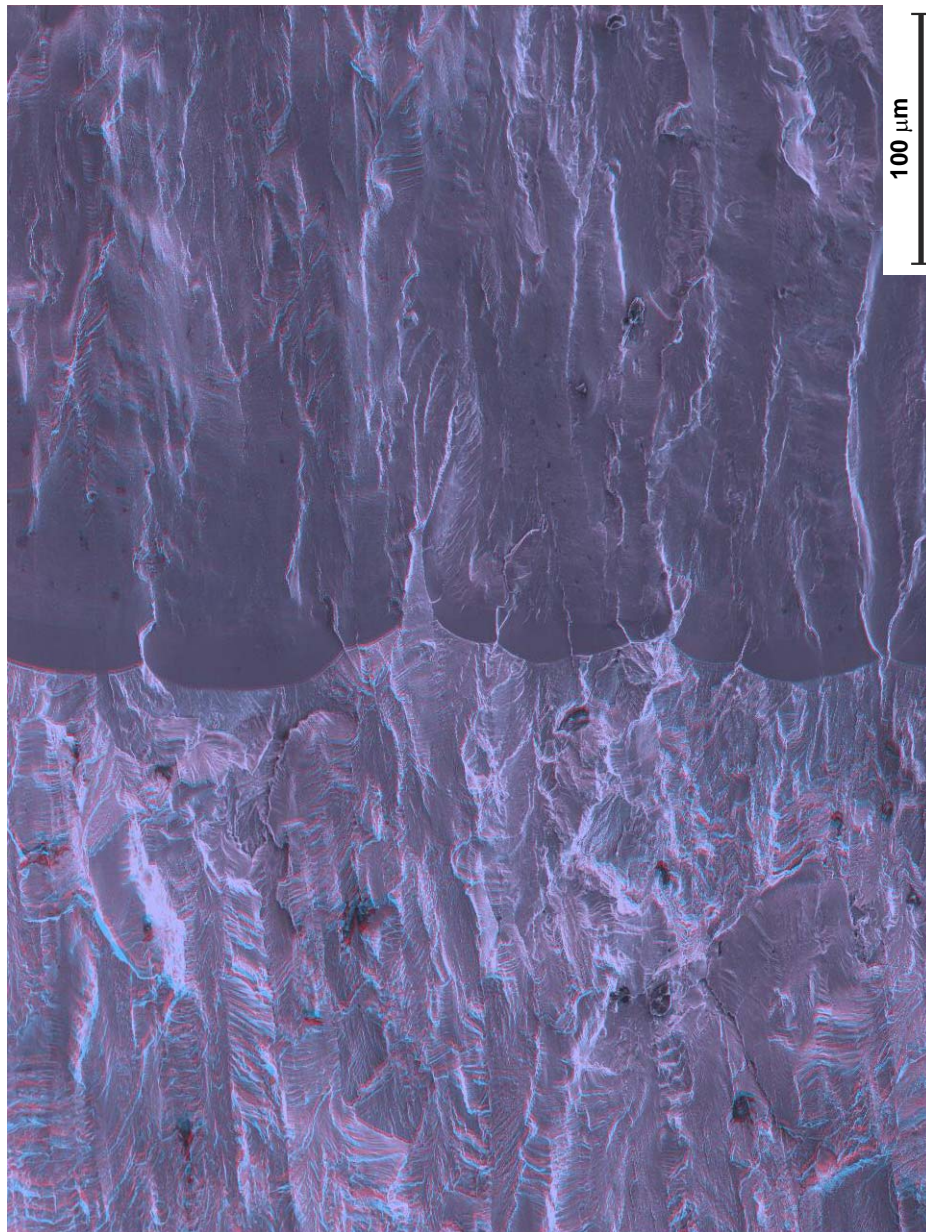
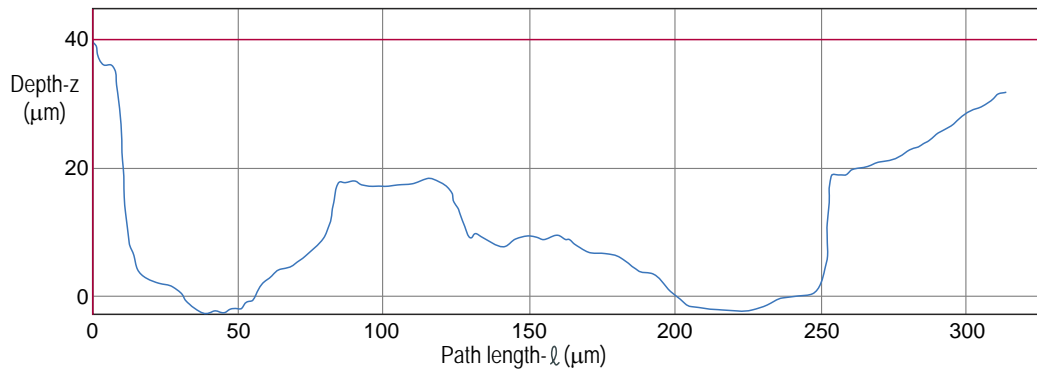


Fig. 17 Overview of second threshold for specimen 3-1,  $R = 0.4$ : mainly flat scallops



RL = 1.20

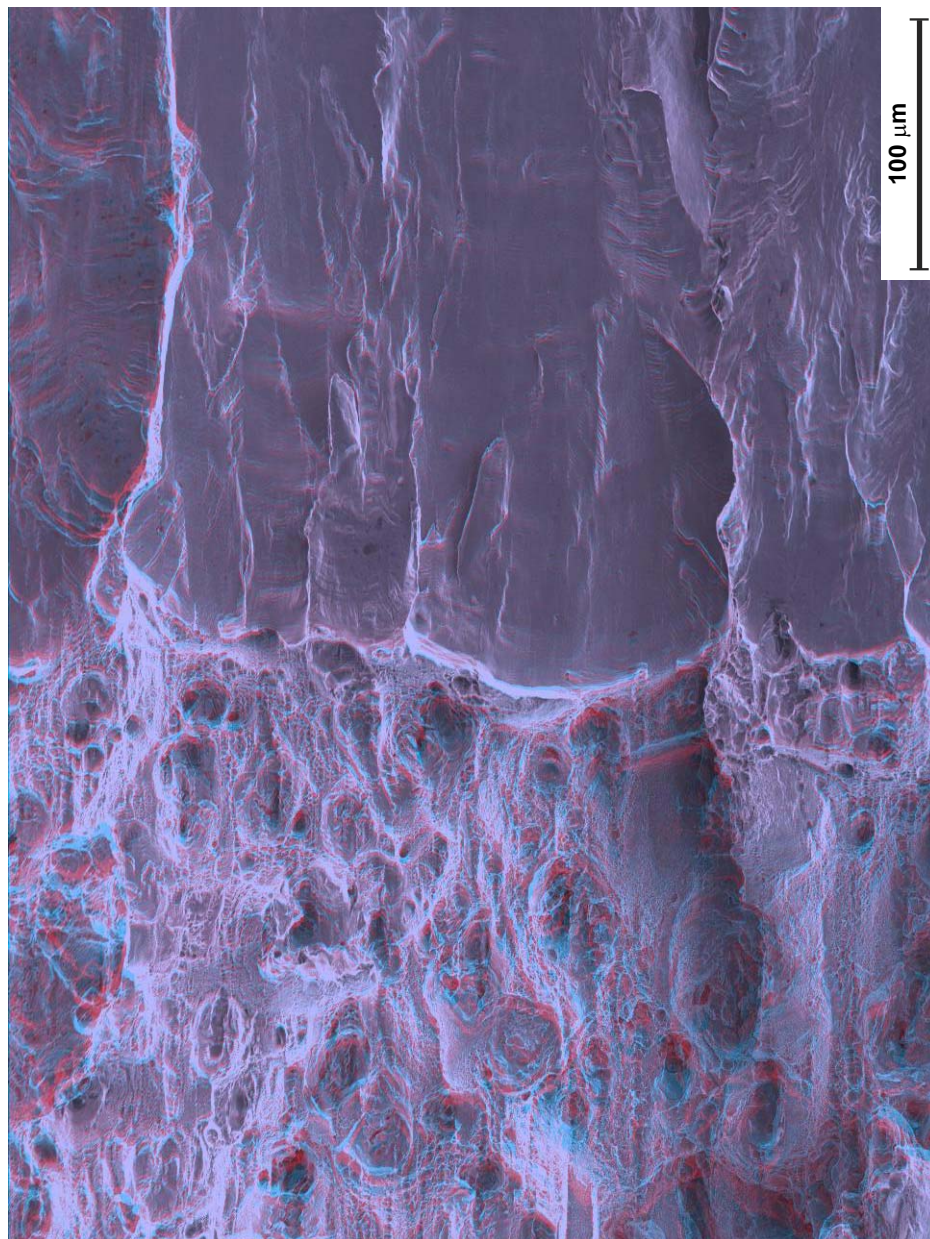
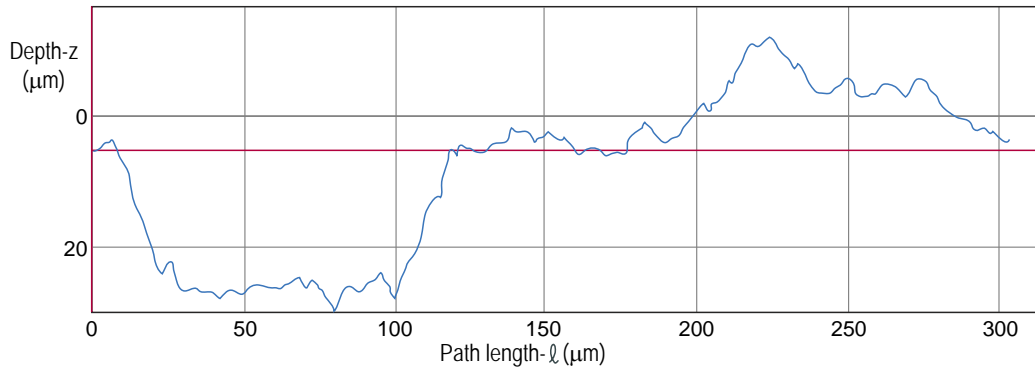


Fig. 18 Overview of third threshold for specimen 3-1,  $R = 0.4$ : mainly flat scallops



RL = 1.21

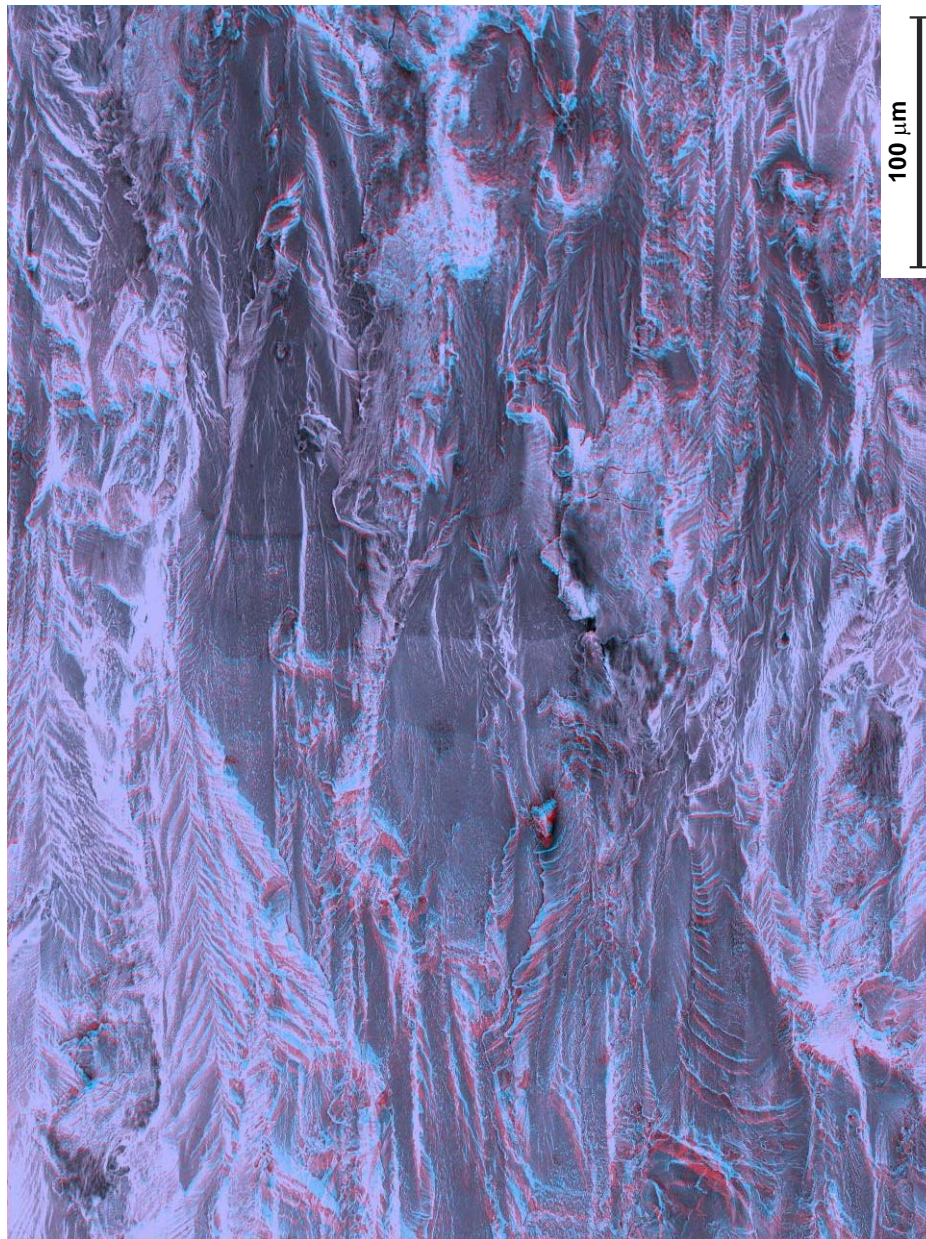
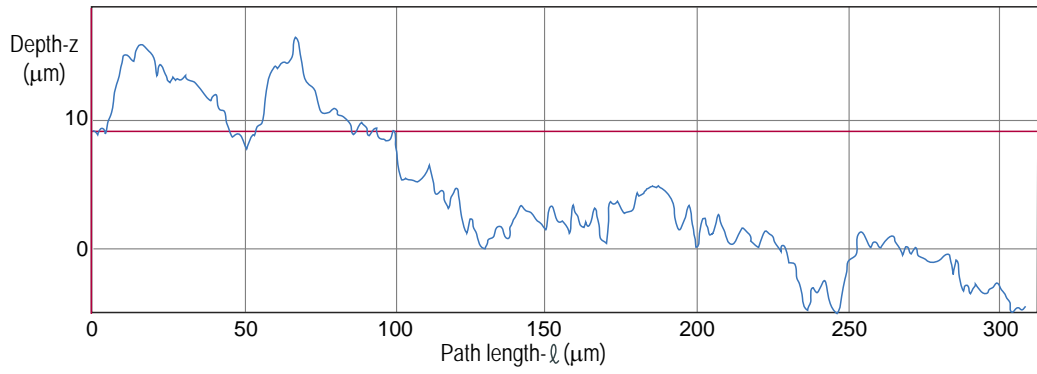


Fig. 19 Overview of first threshold for specimen 1-2,  $R = 0.67$ : scallops and wide rough ridges



RL = 1.21

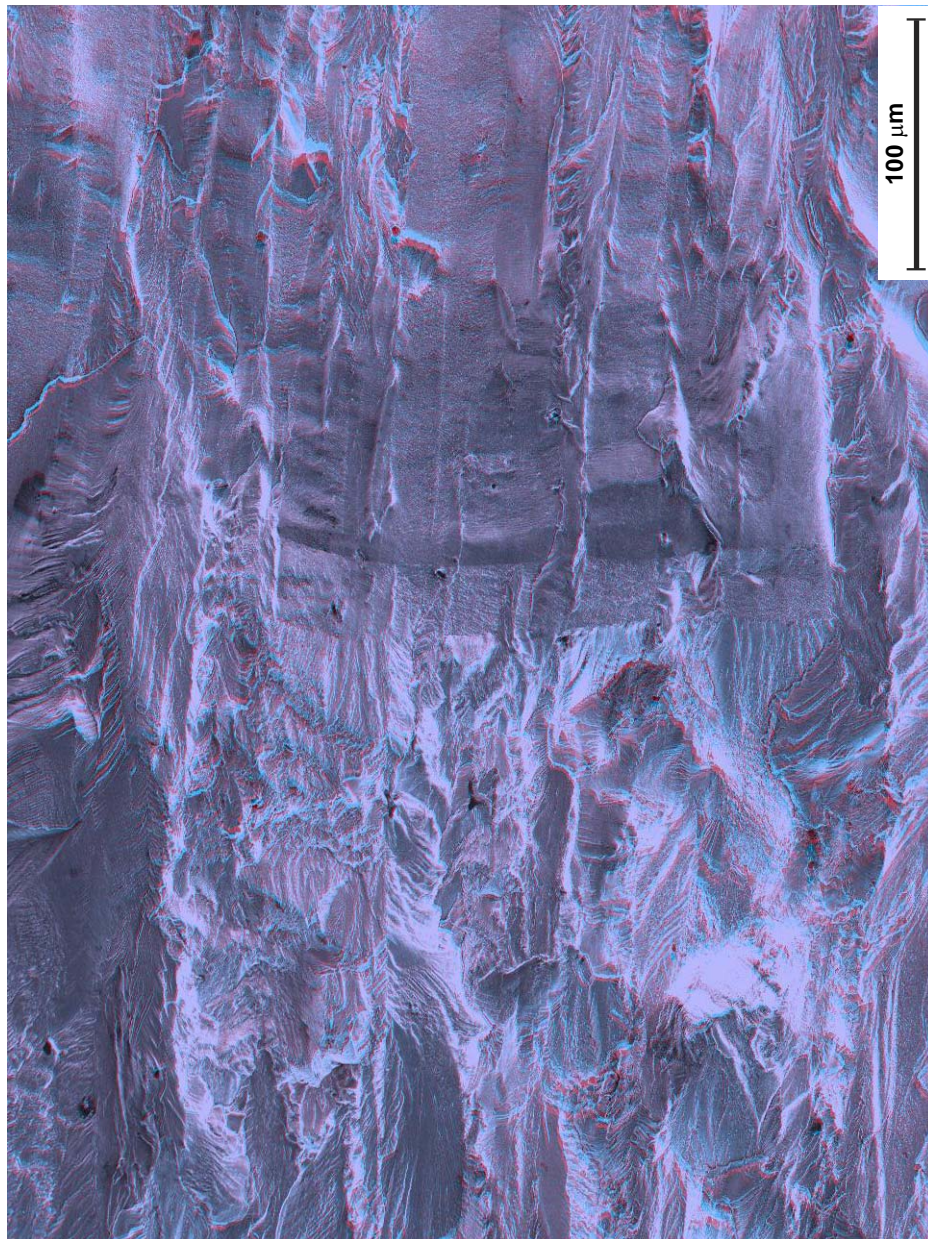


Fig. 20 Overview of second threshold for specimen 1-2,  $R = 0.70$ : scallops and many ridges

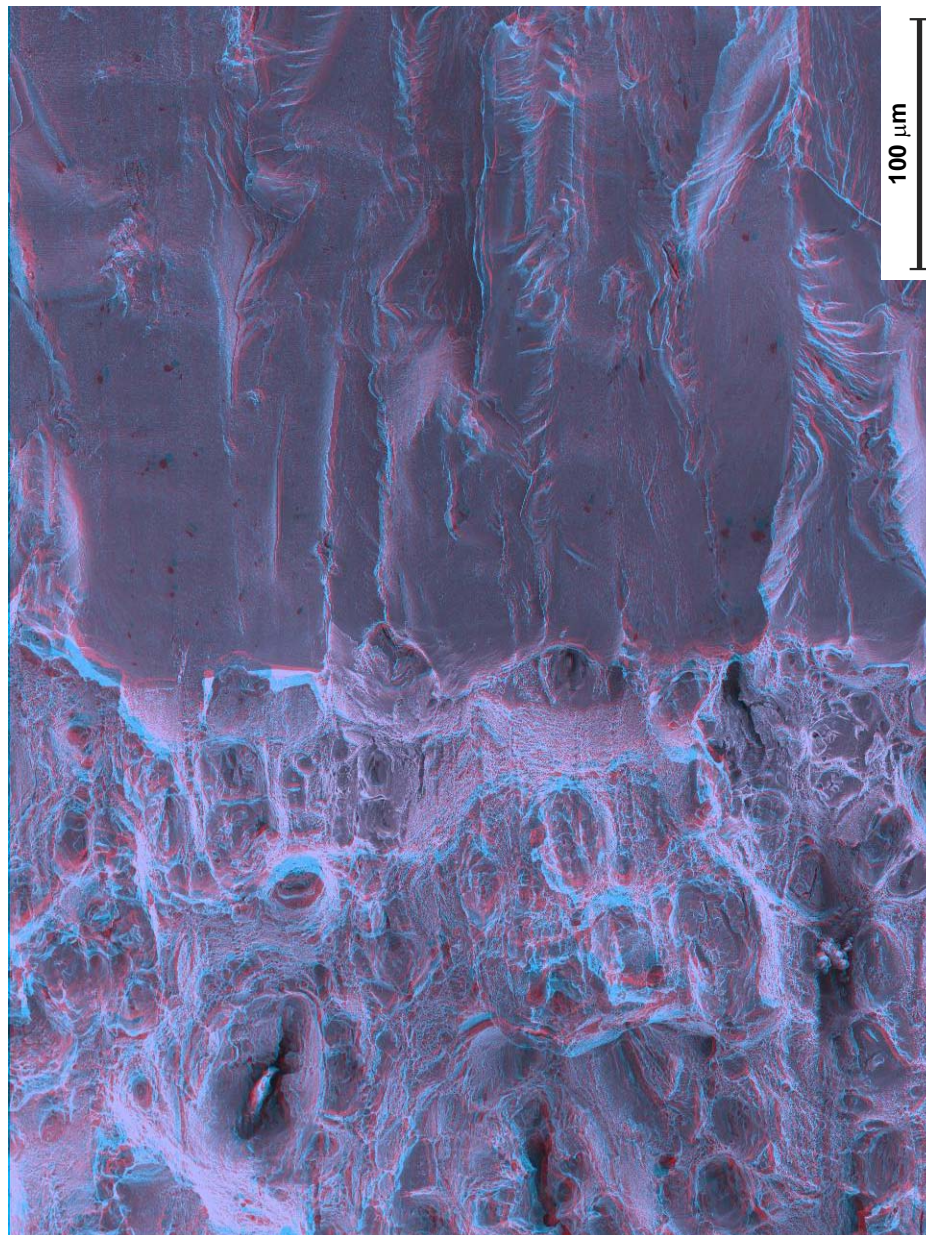
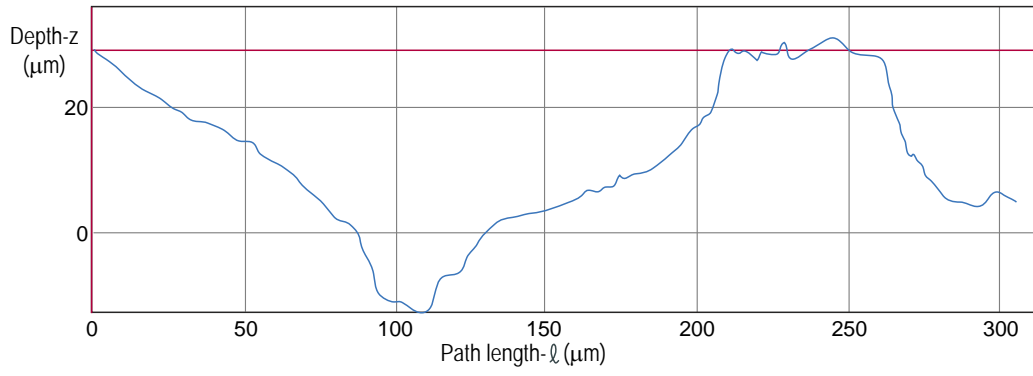
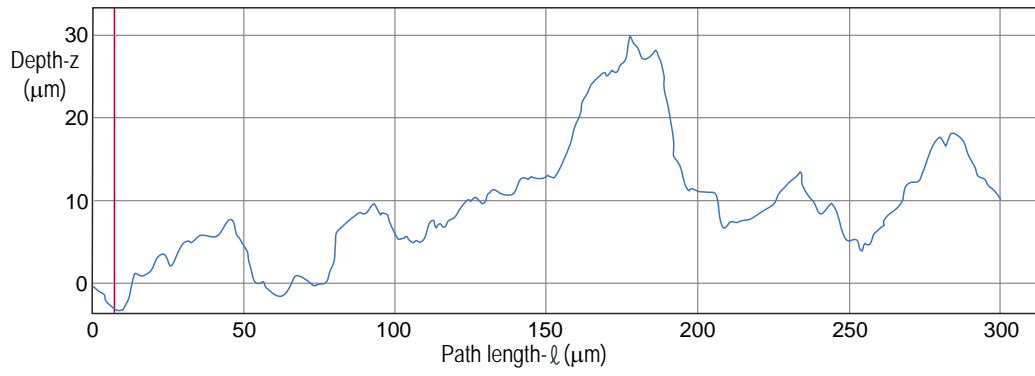


Fig. 21 Overview of third threshold for specimen 1-2,  $R = 0.69$ : mainly flat scallops



RL = 1.20

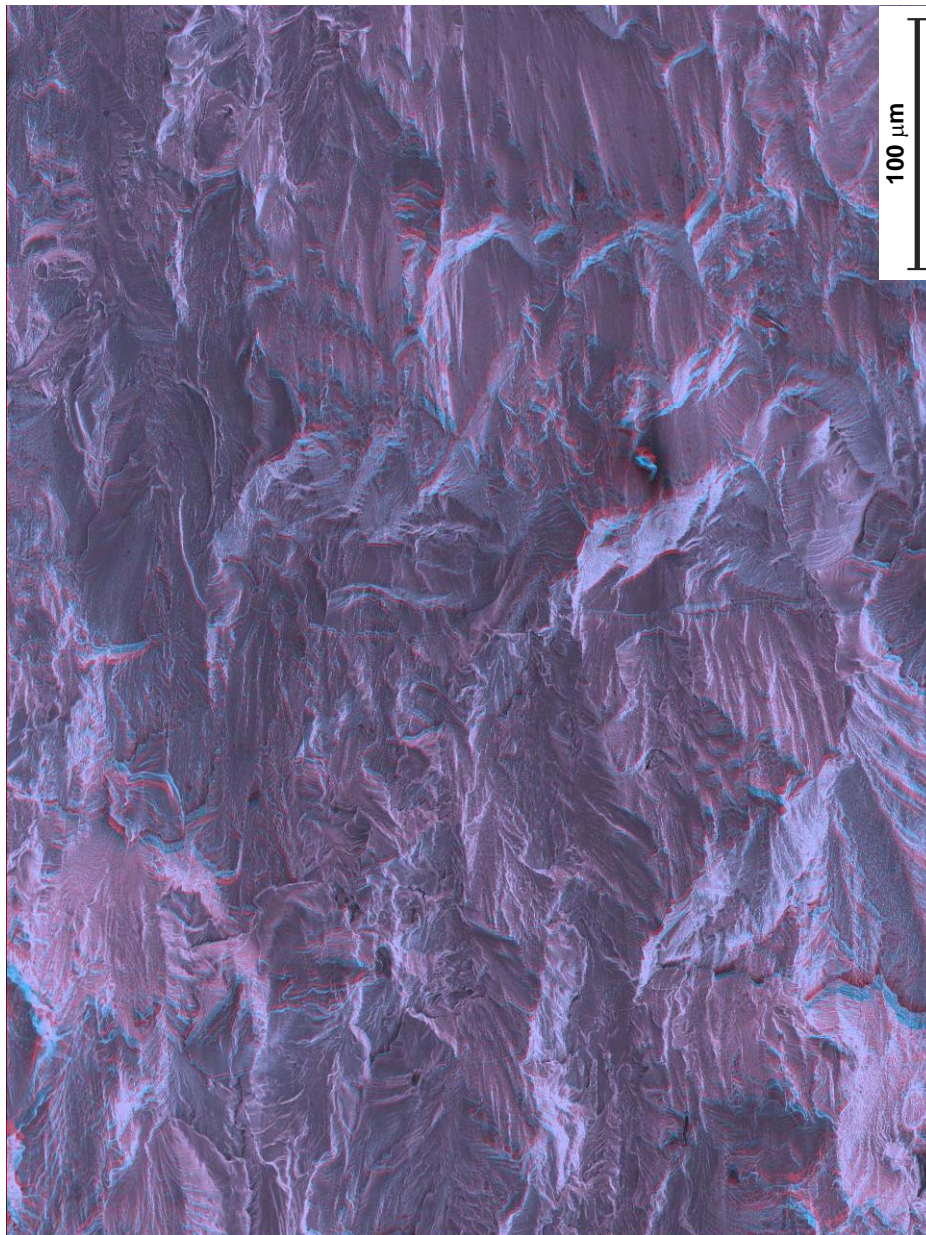
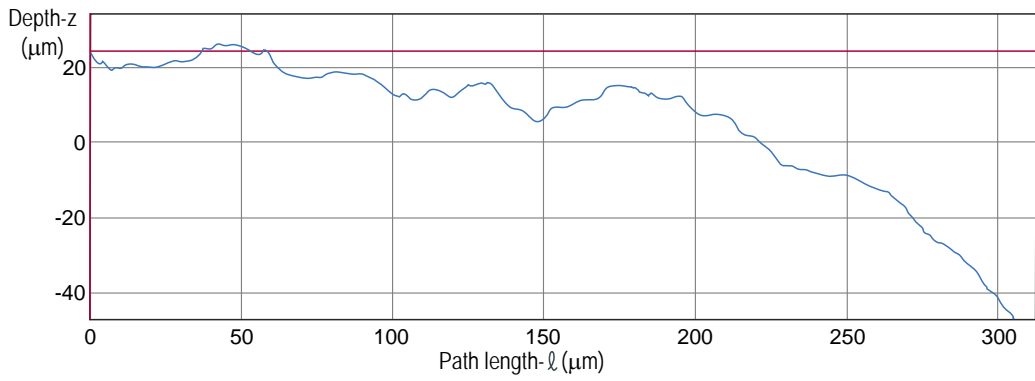


Fig. 22 Overview of third threshold for specimen 2-2,  $R = 0.7$ : wide rough ridges and few scallops



RL = 1.15

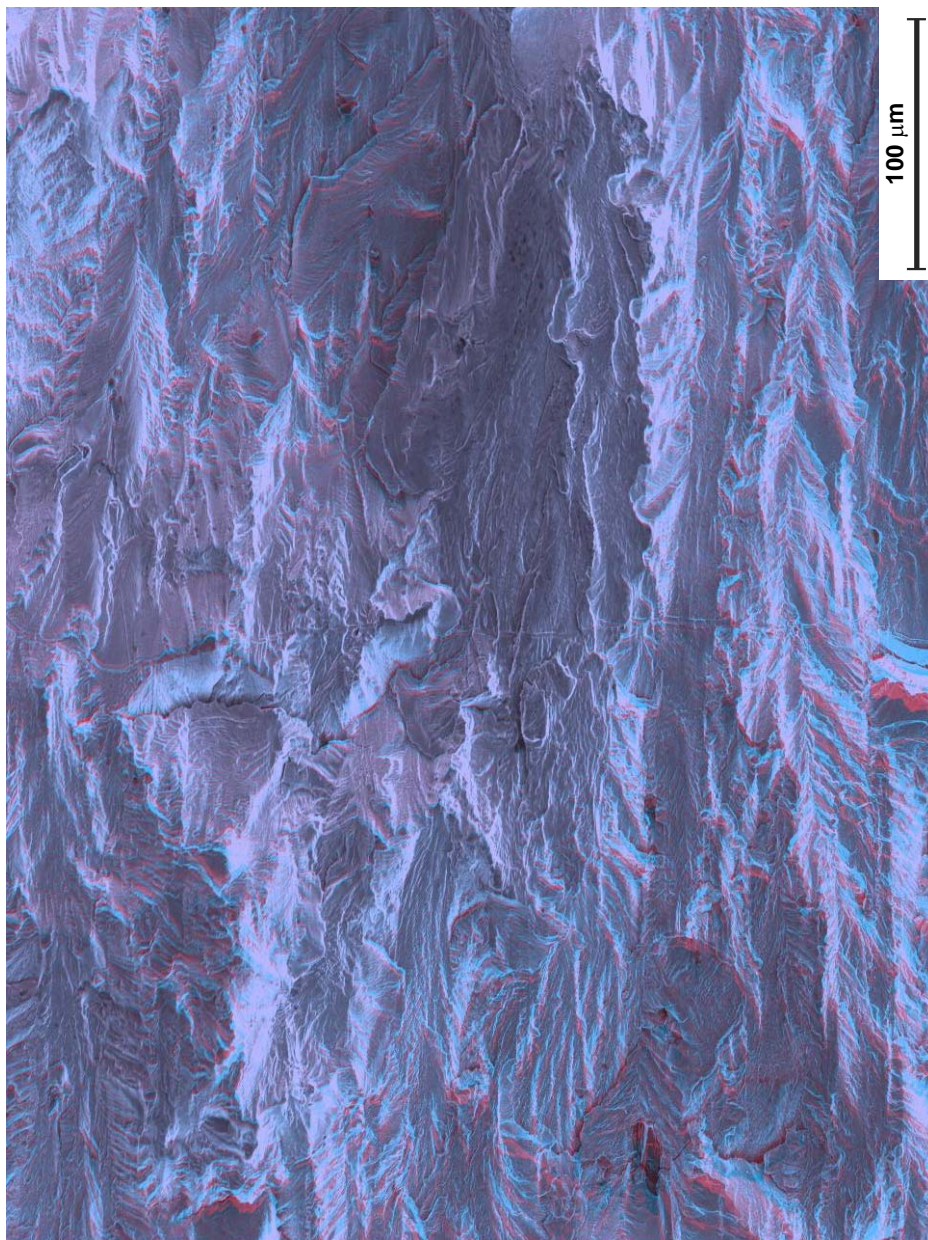
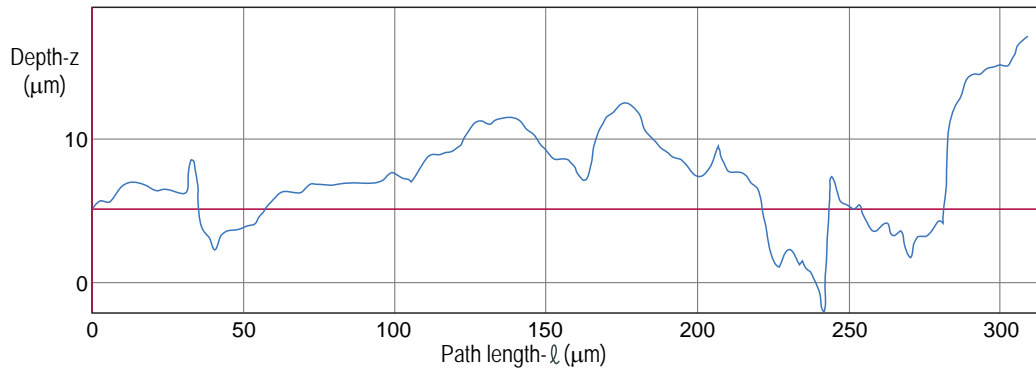


Fig. 23 Overview of third threshold for specimen 2-2,  $R = 0.7$ : wide rough ridges and few scallops





RL = 1.10

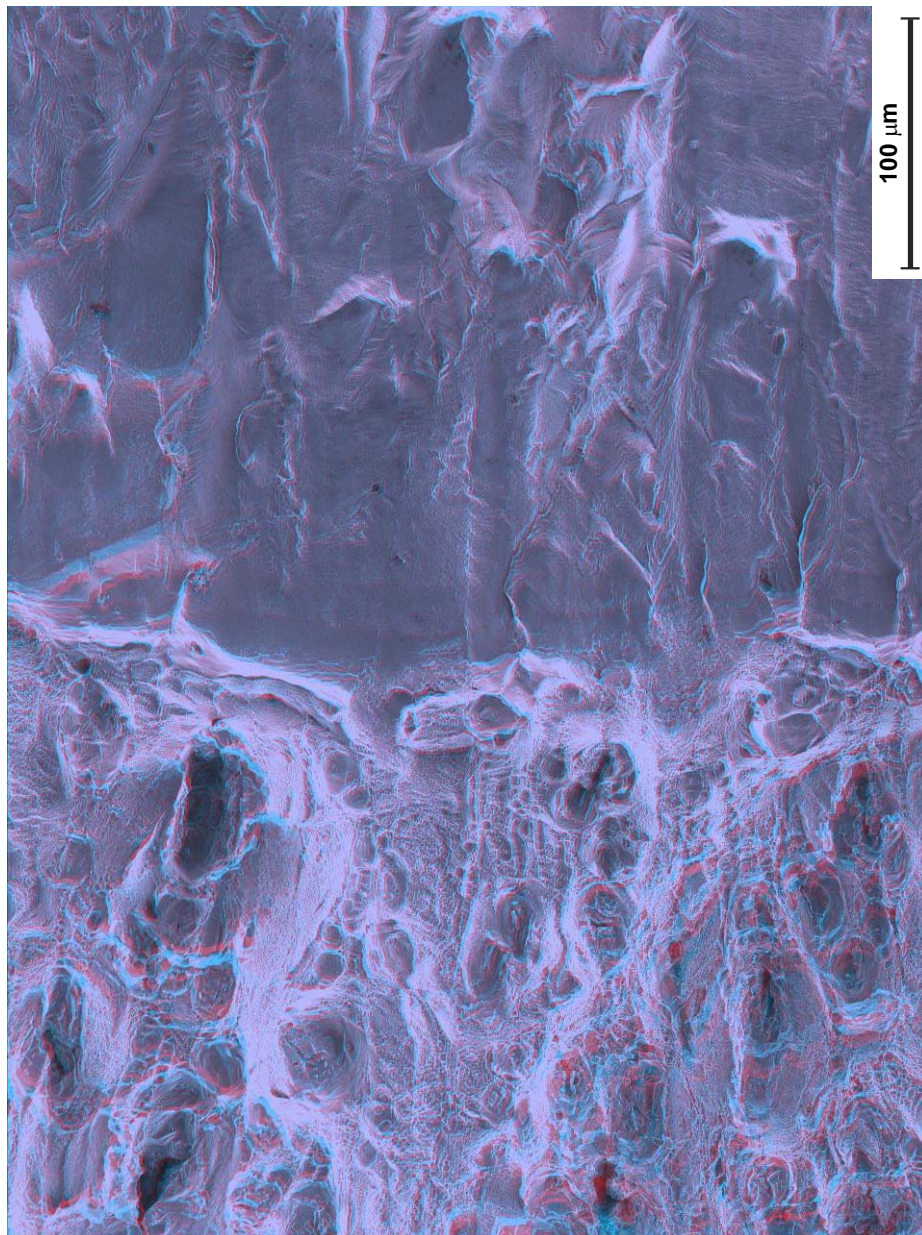


Fig. 24 Overview of third threshold for specimen 2-2,  $R = 0.7$ : mainly scallops

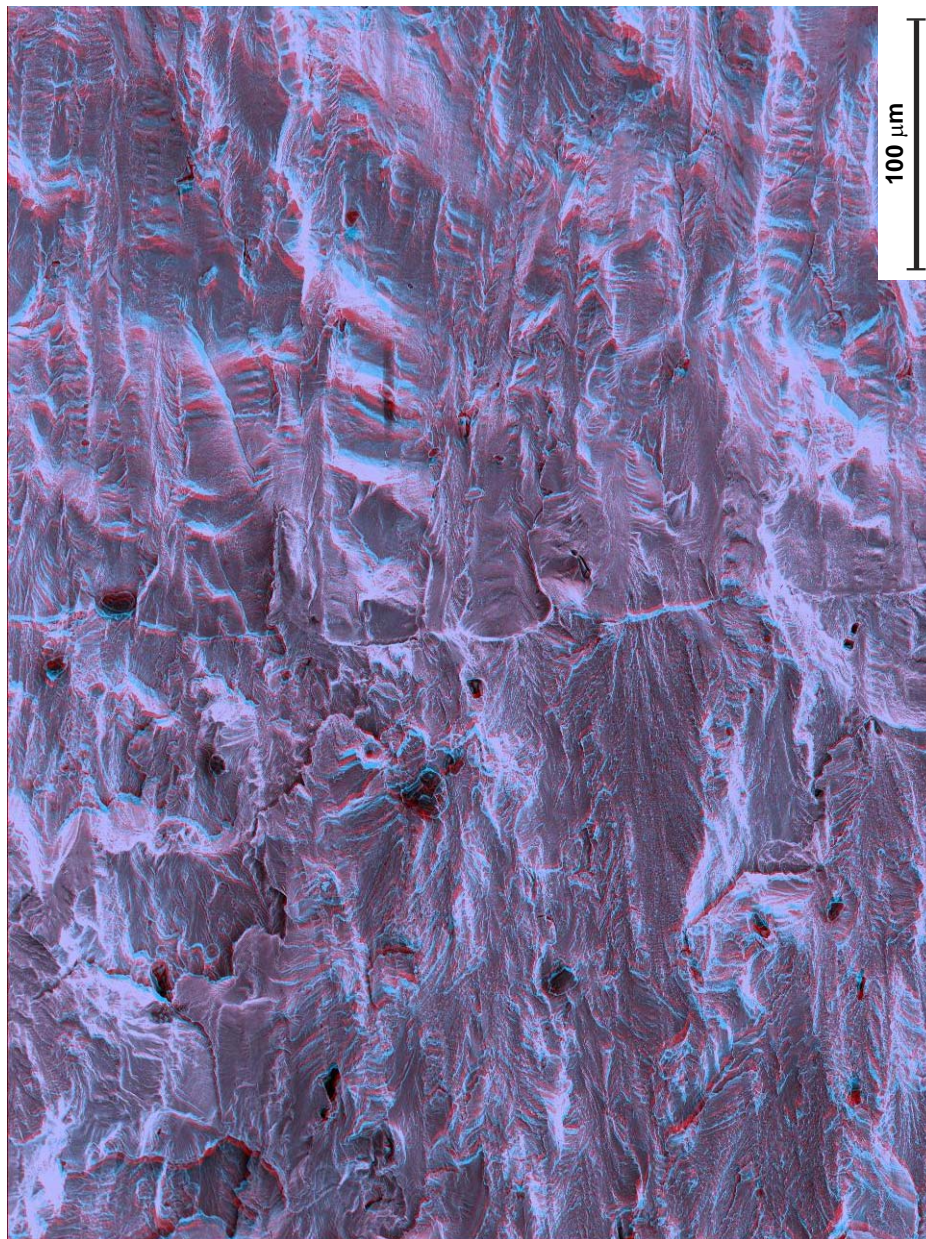
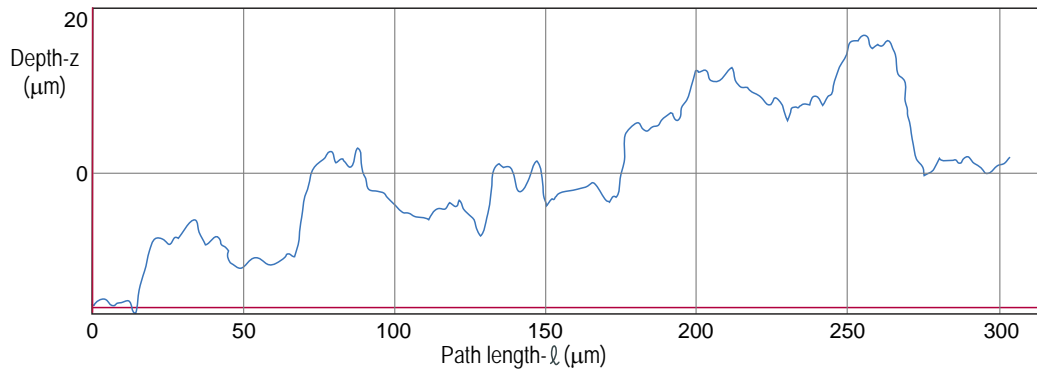
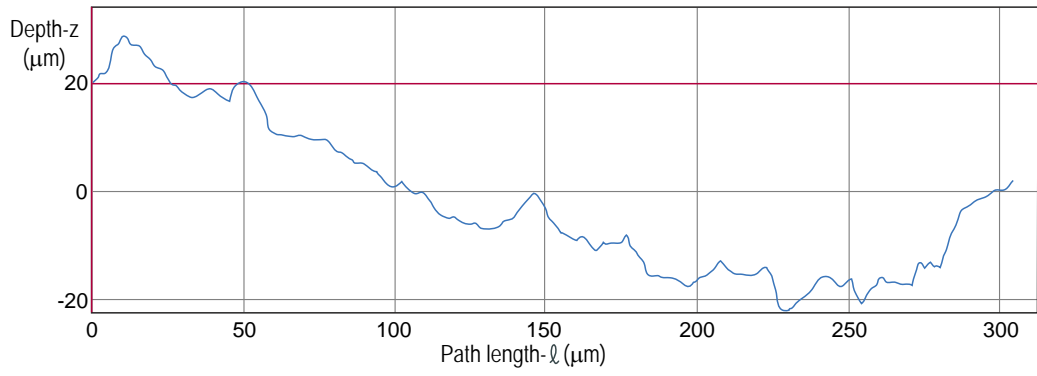


Fig. 25 Overview of third threshold for specimen 6-3,  $R = 0.8$ : wide rough ridges and few scallops



RL = 1.20

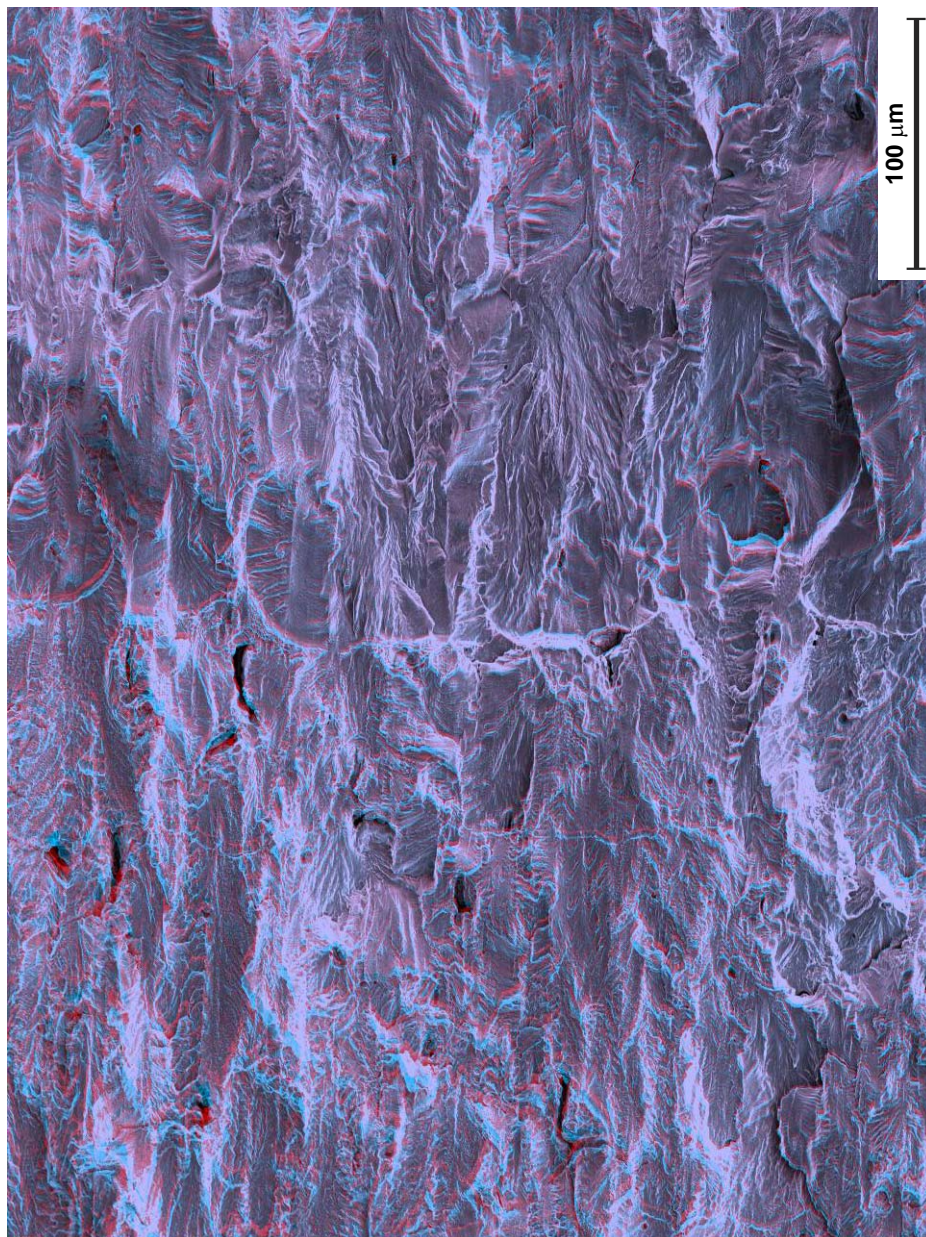


Fig. 26 Overview of second threshold for specimen 6-3,  $R = 0.8$ : wide rough ridges and few scallops

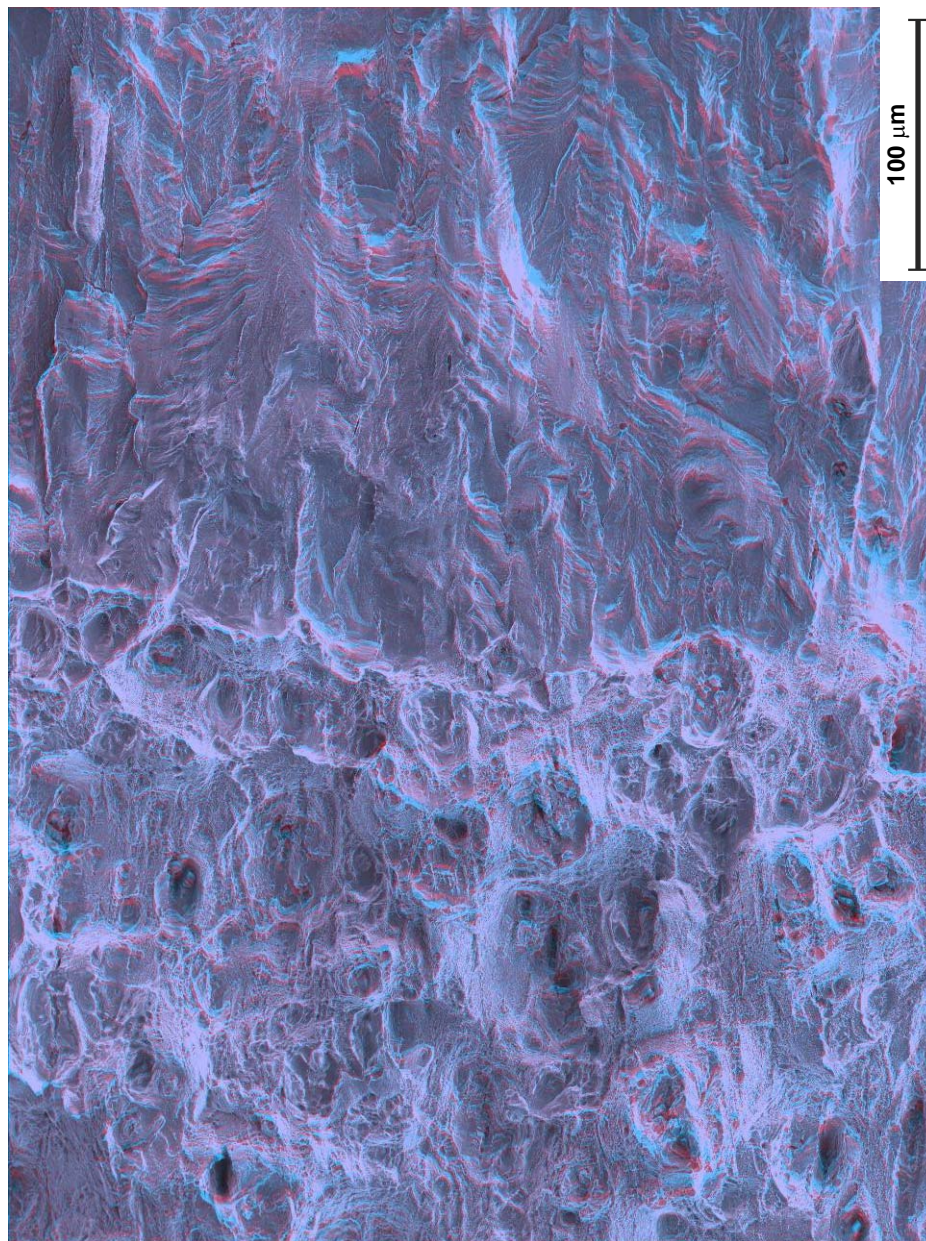
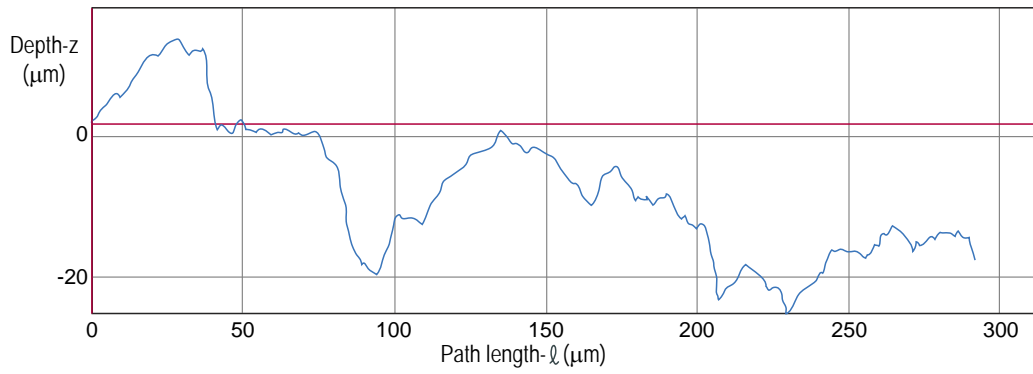


Fig. 27 Overview of third threshold for specimen 6-3,  $R = 0.8$ : wide rough ridges and few scallops

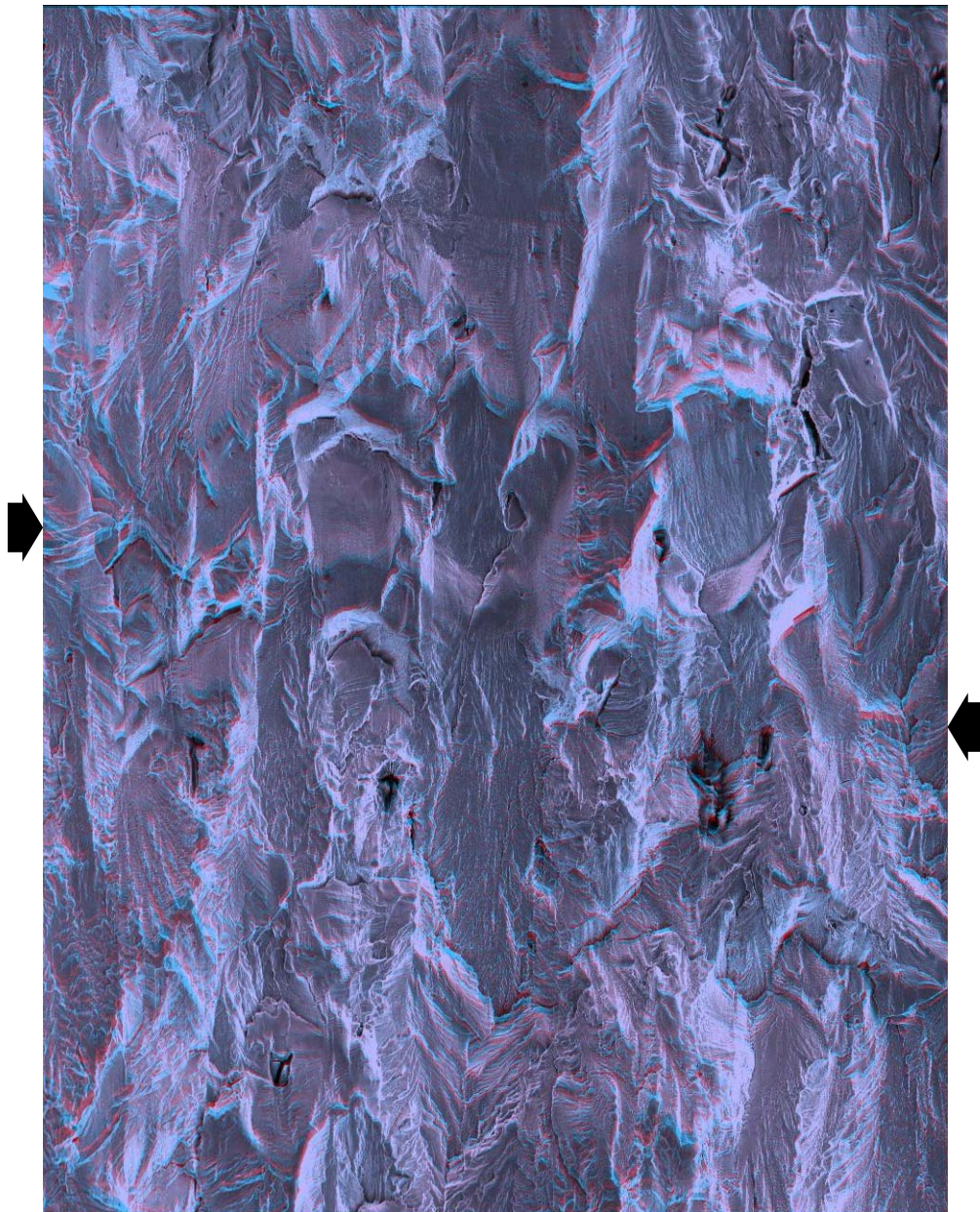
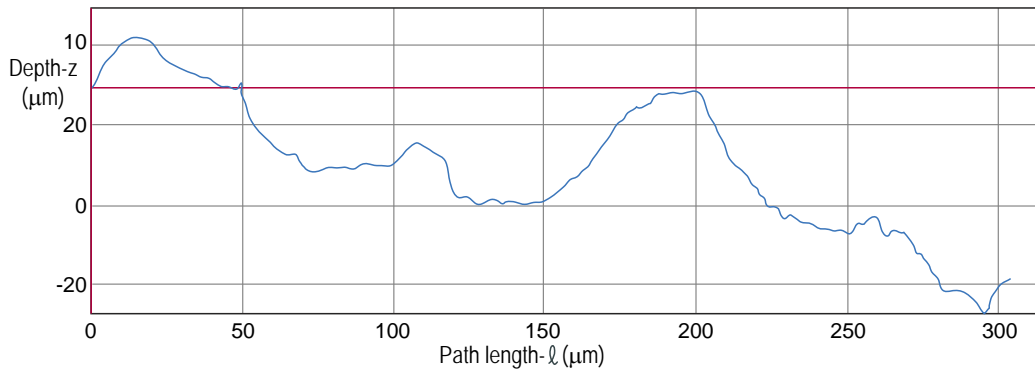


Fig. 28 Overview of first threshold for specimen 6-2,  $R = 0.92$ : flat facets and rough ridges. The arrows point to the threshold crack front

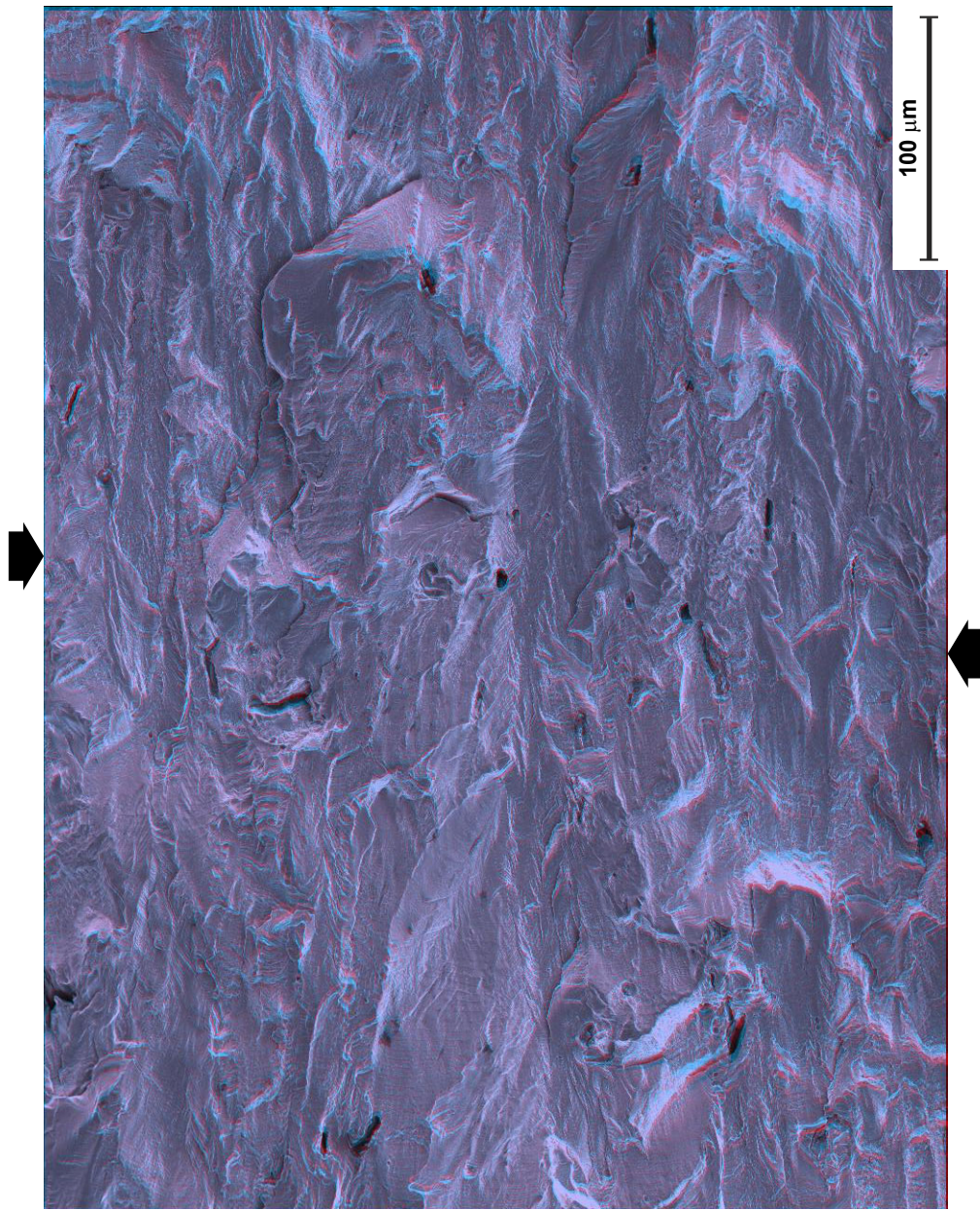
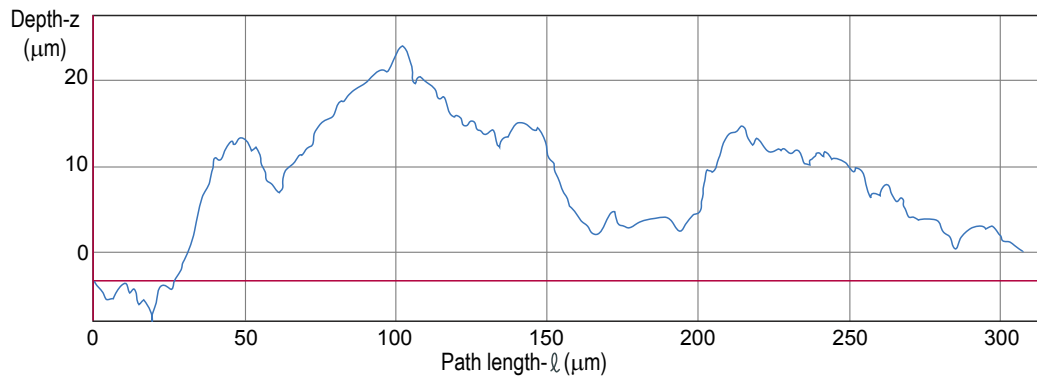


Fig. 29 Overview of second threshold for specimen 6-2,  $R = 0.92$ : flat facets and rough ridges. The arrows point to the threshold crack front

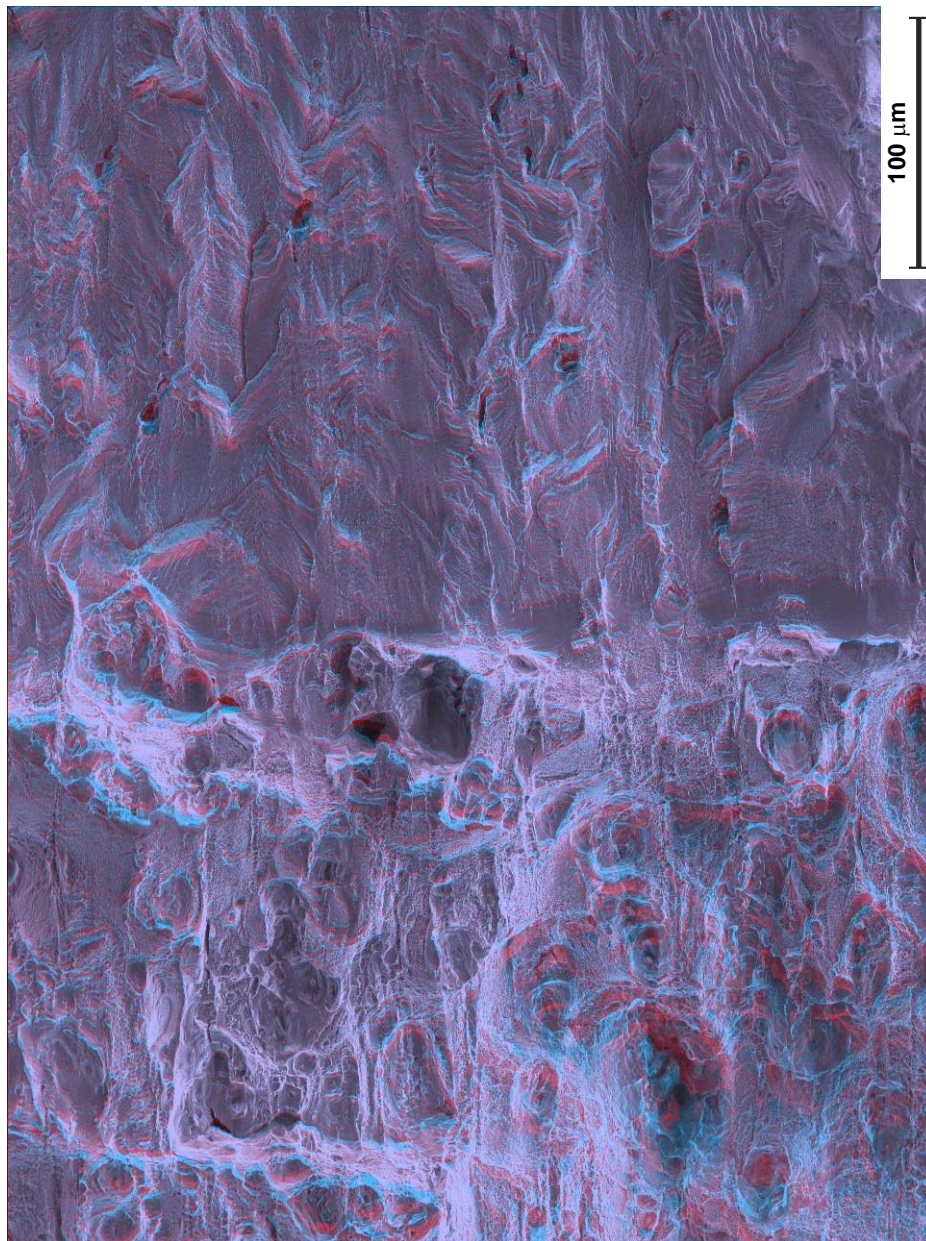
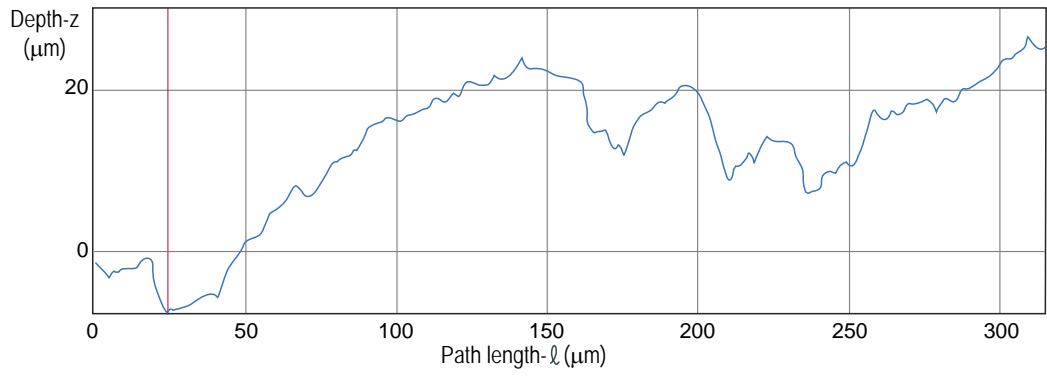


Fig. 30 Overview of third threshold for specimen 6-2,  $R = 0.92$ : flat facets and rough ridges.

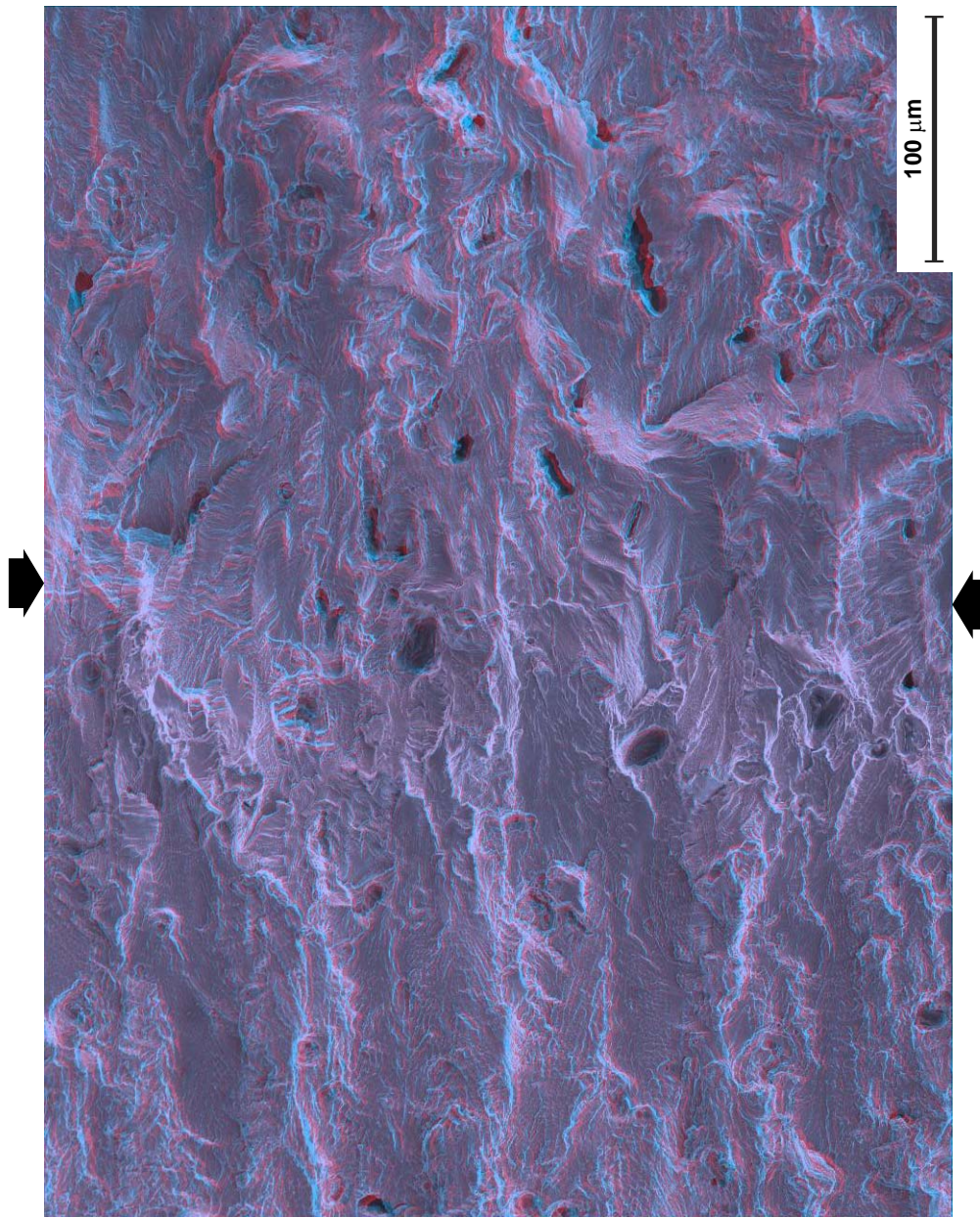
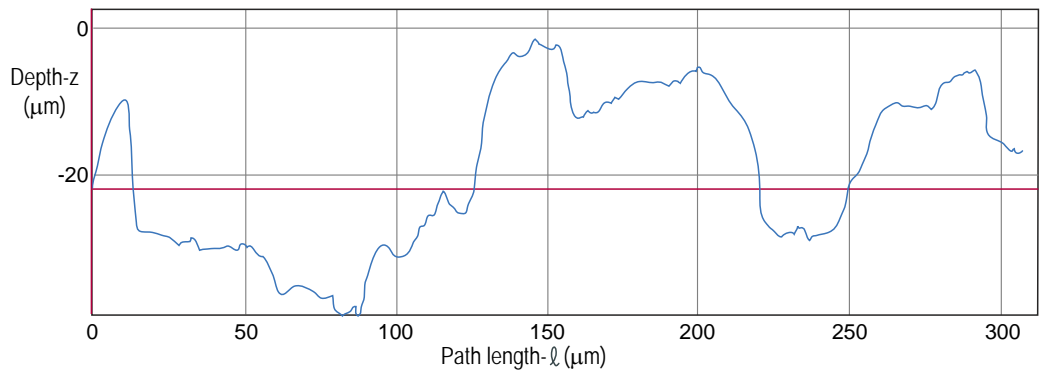


Fig. 31 Overview of first threshold for specimen 8-1,  $R = 0.95$ : flat facets and rough ridges.  
The arrows point to the threshold crack front



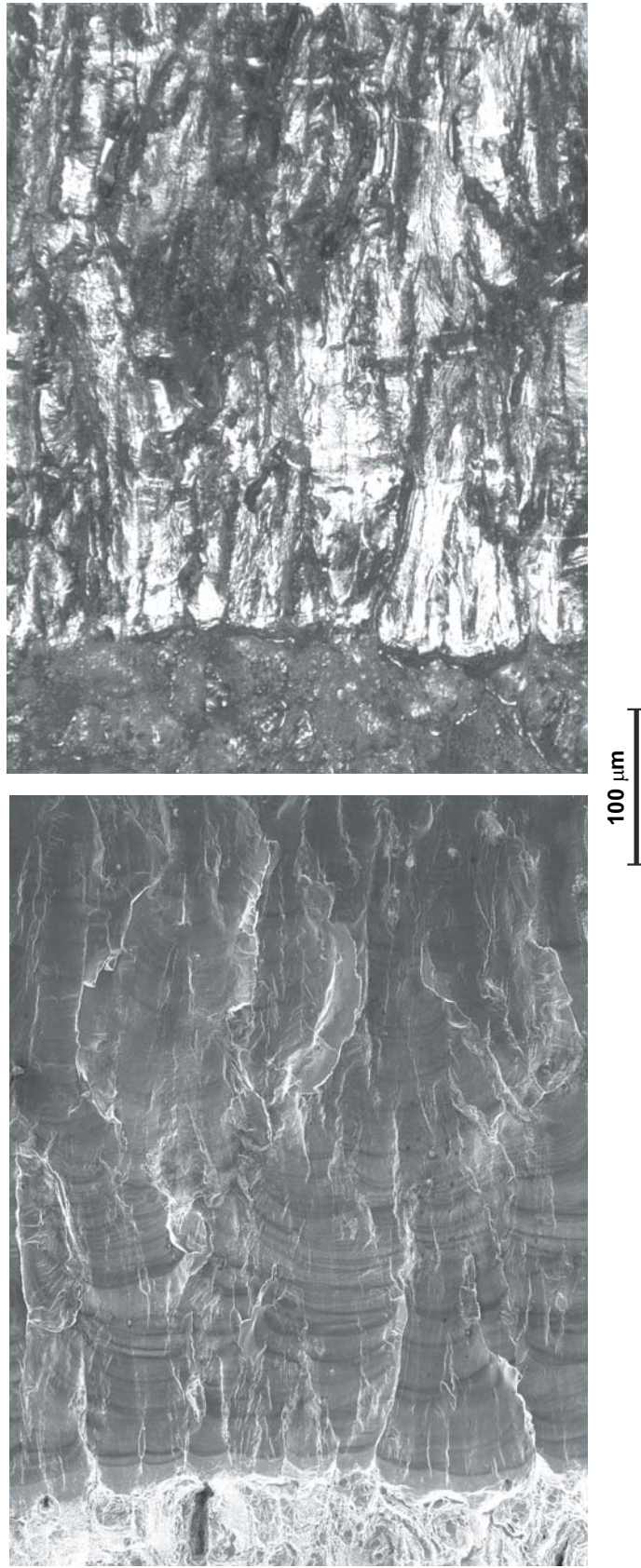


Fig. 32 Comparison of FEG-SEM and DFOM overviews of third threshold for specimen 1–3,  $R = 0.1$ : mainly flat scallops

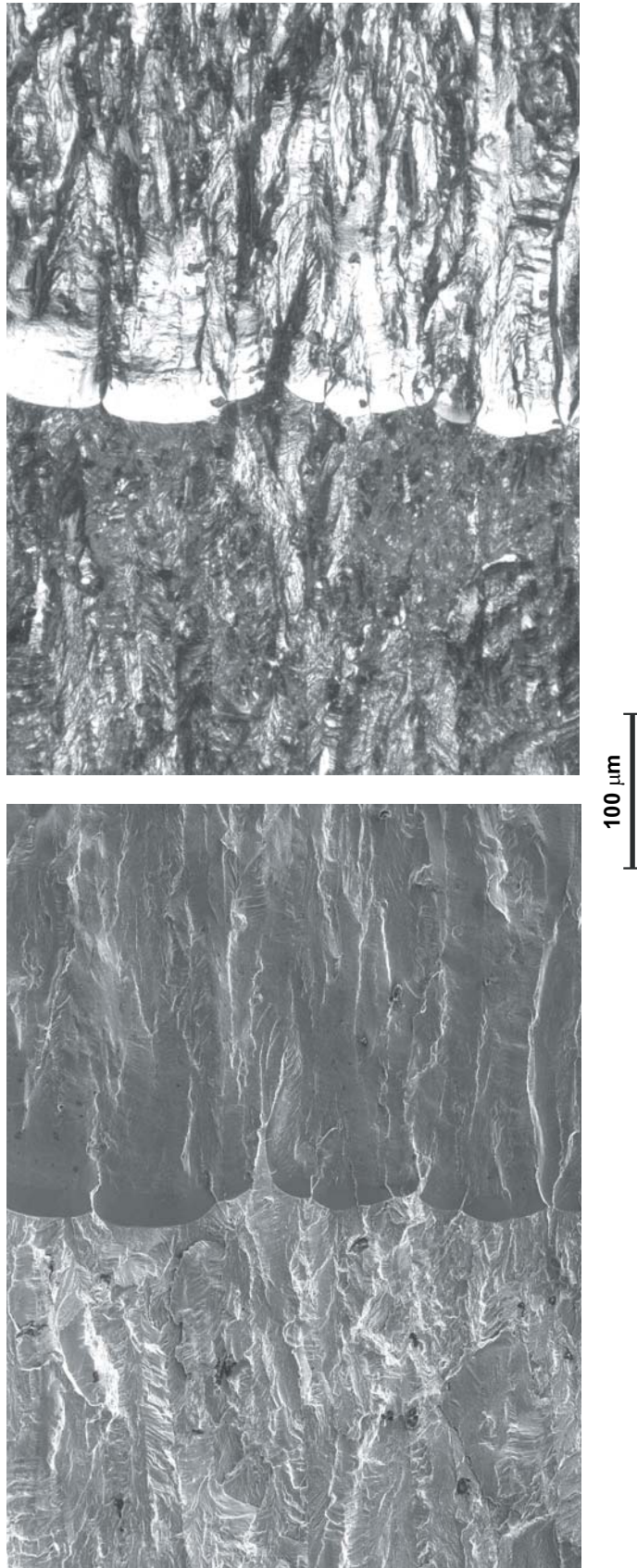


Fig. 33 Comparison of FEG-SEM and DFOM overviews of second threshold for specimen 3-1,  $R = 0.4$ : mainly flat scallops

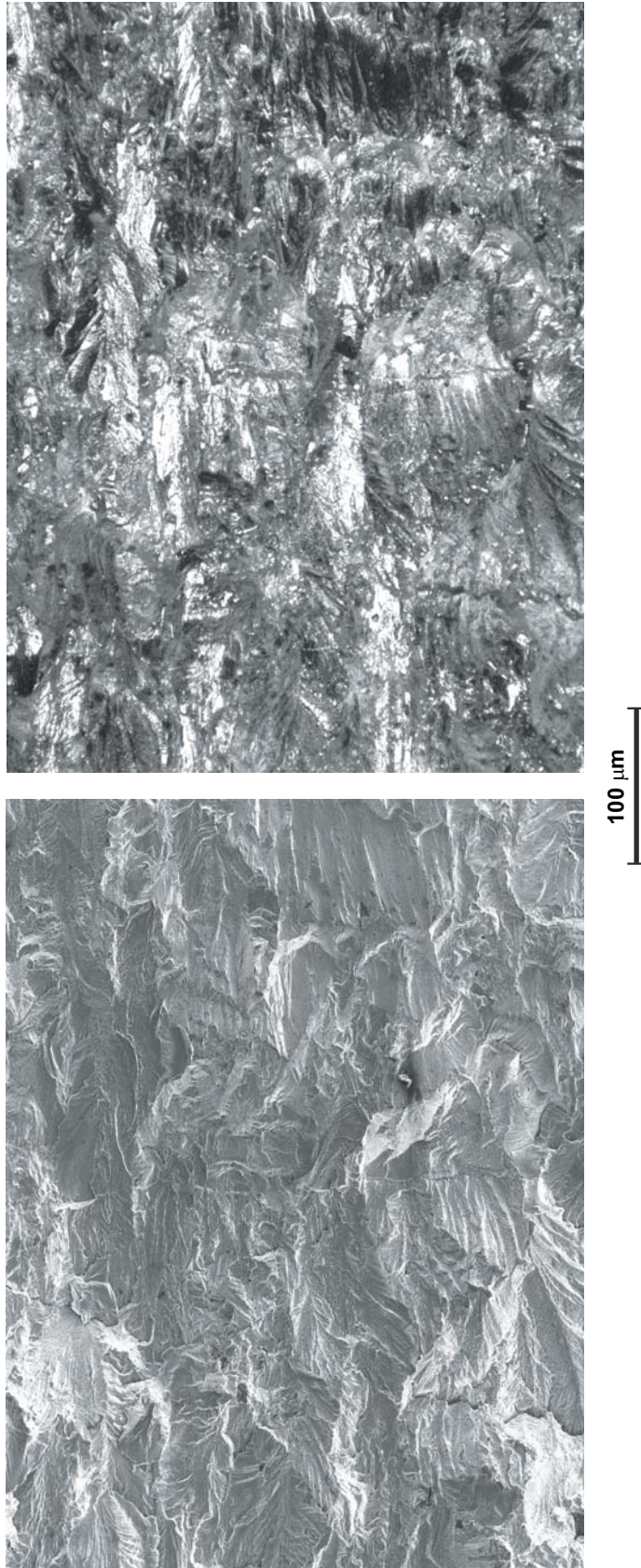


Fig. 34 Comparison of FEG-SEM and DFOM overviews of first threshold for specimen 2-2,  $R = 0.7$ : wide rough ridges and few s callops

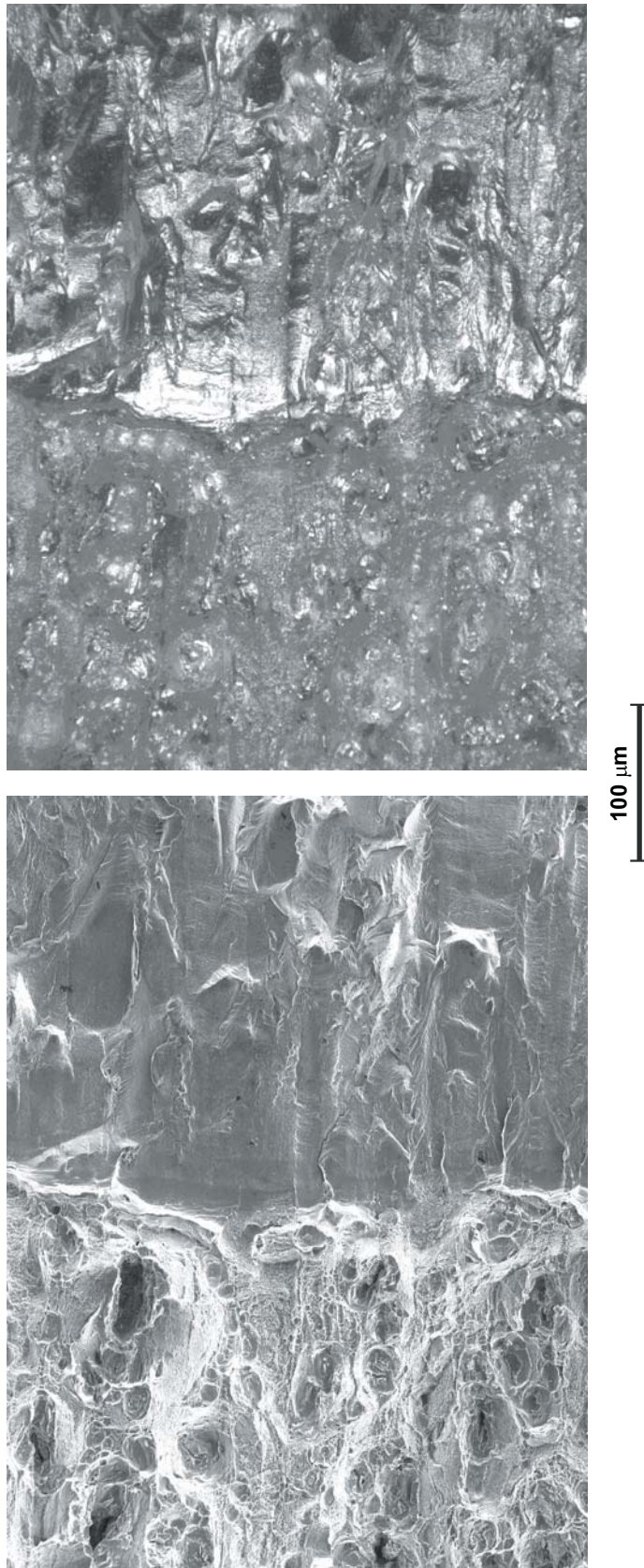


Fig. 35 Comparison of FEG-SEM and DFOM overviews of third threshold for specimen 2-2,  $R = 0.7$ : mainly flat scallops

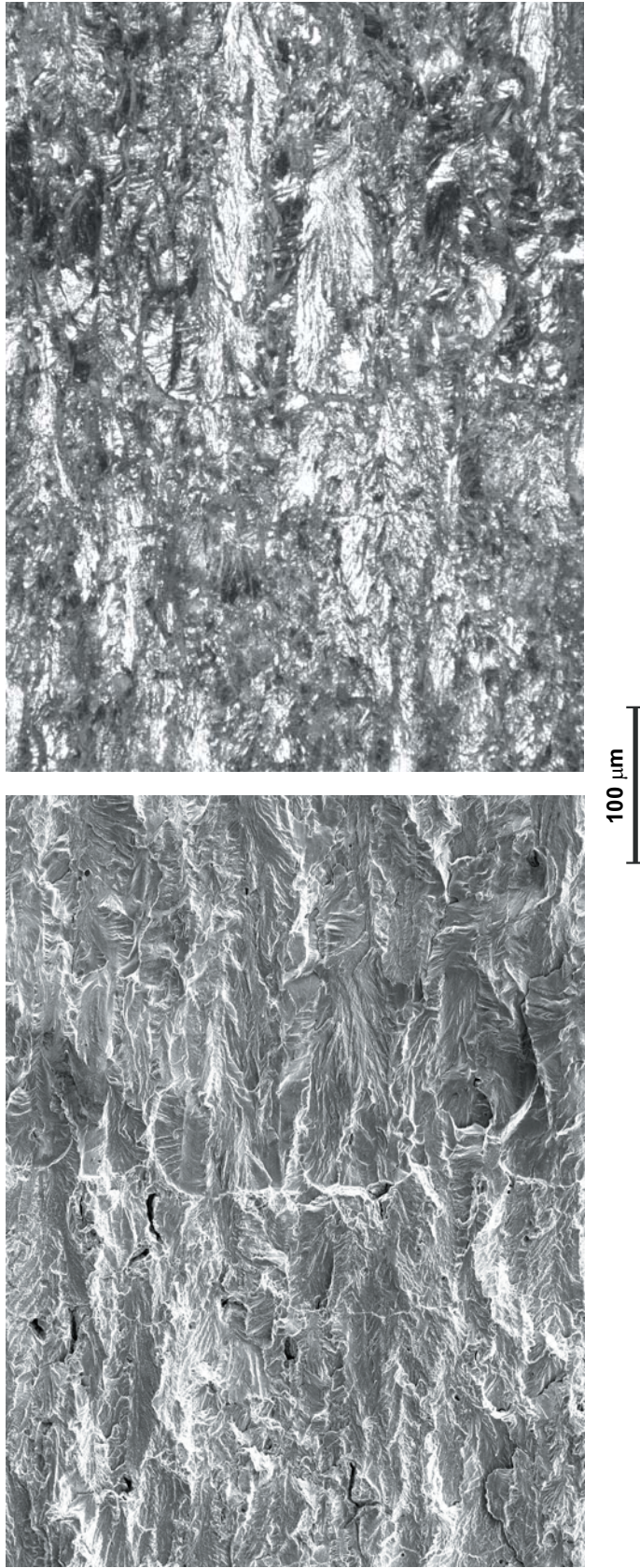


Fig. 36 Comparison of FEG-SEM and DFOM overviews of second threshold for specimen 6-3,  $R = 0.8$ : mainly wide rough ridges

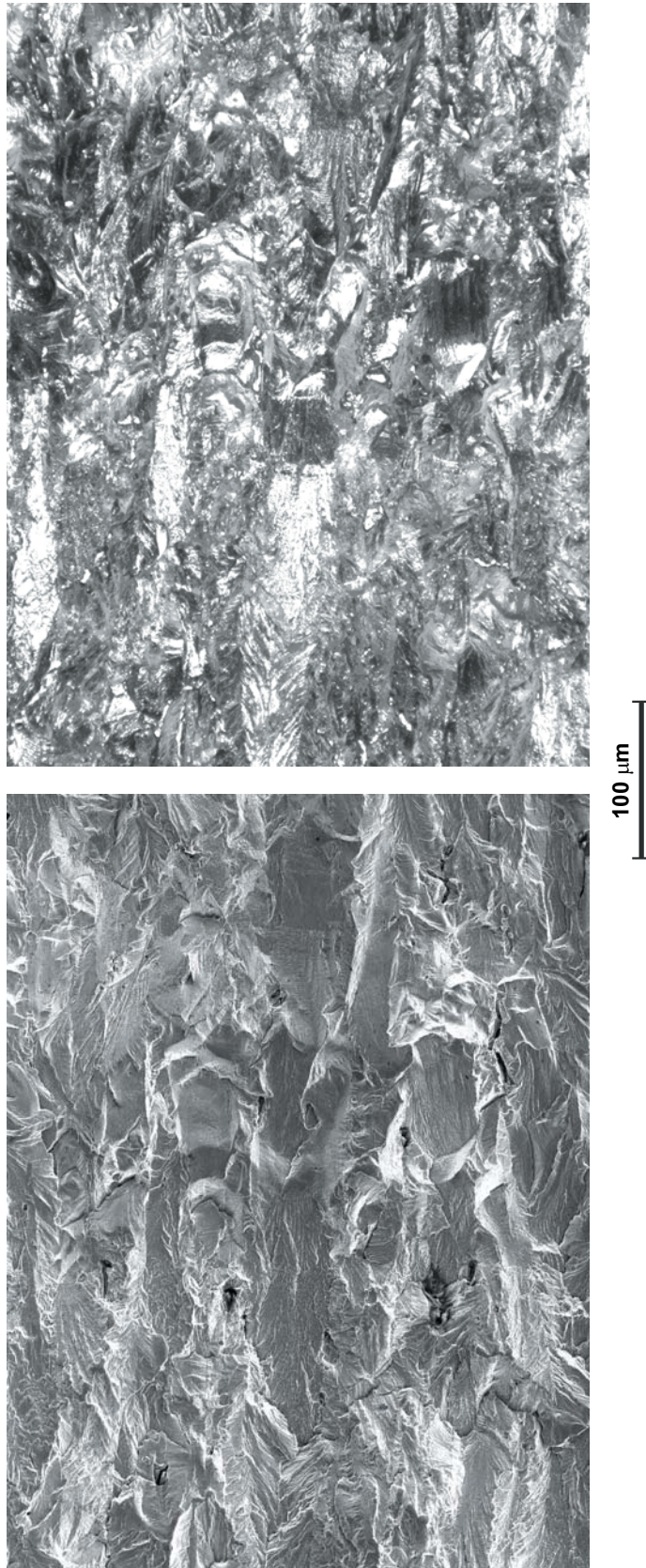


Fig. 37 Comparison of FEG-SEM and DFOM overviews of first threshold for specimen 6-2,  $R = 0.92$ : flat facets and rough ridges

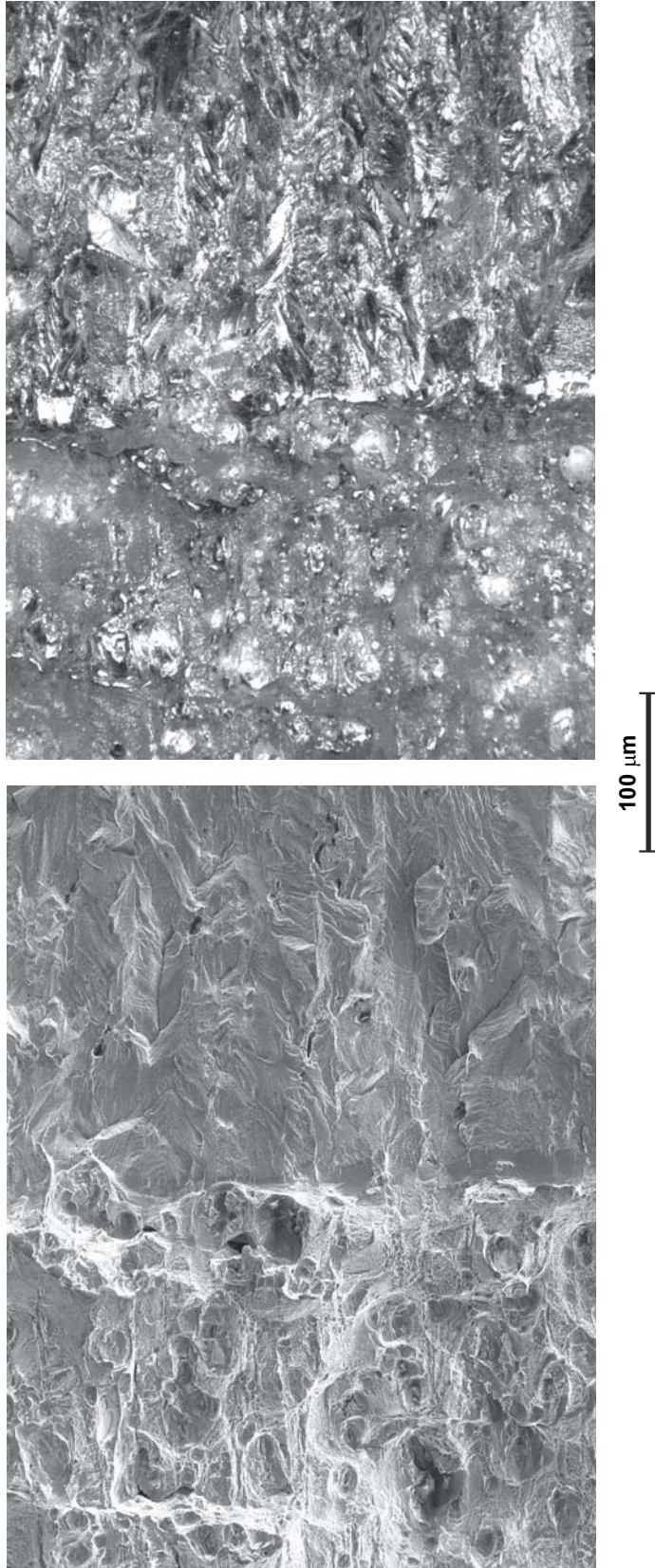
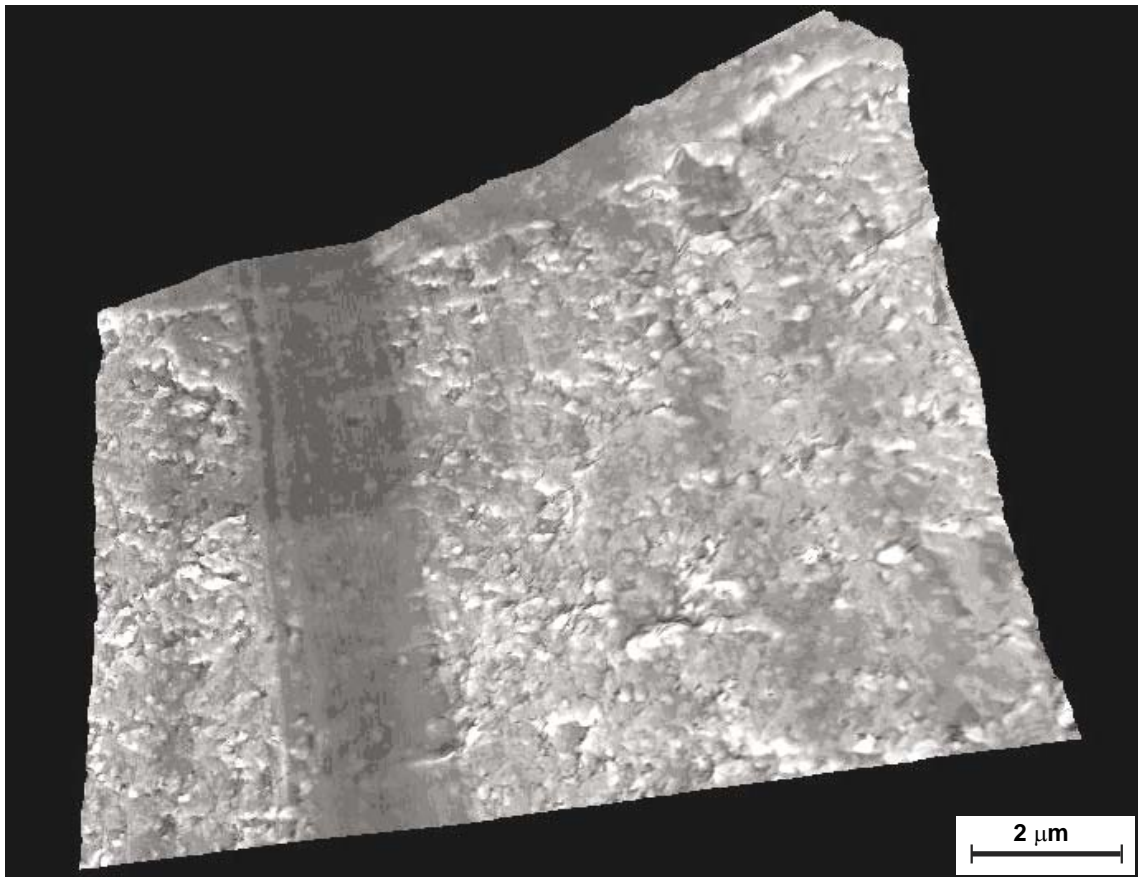
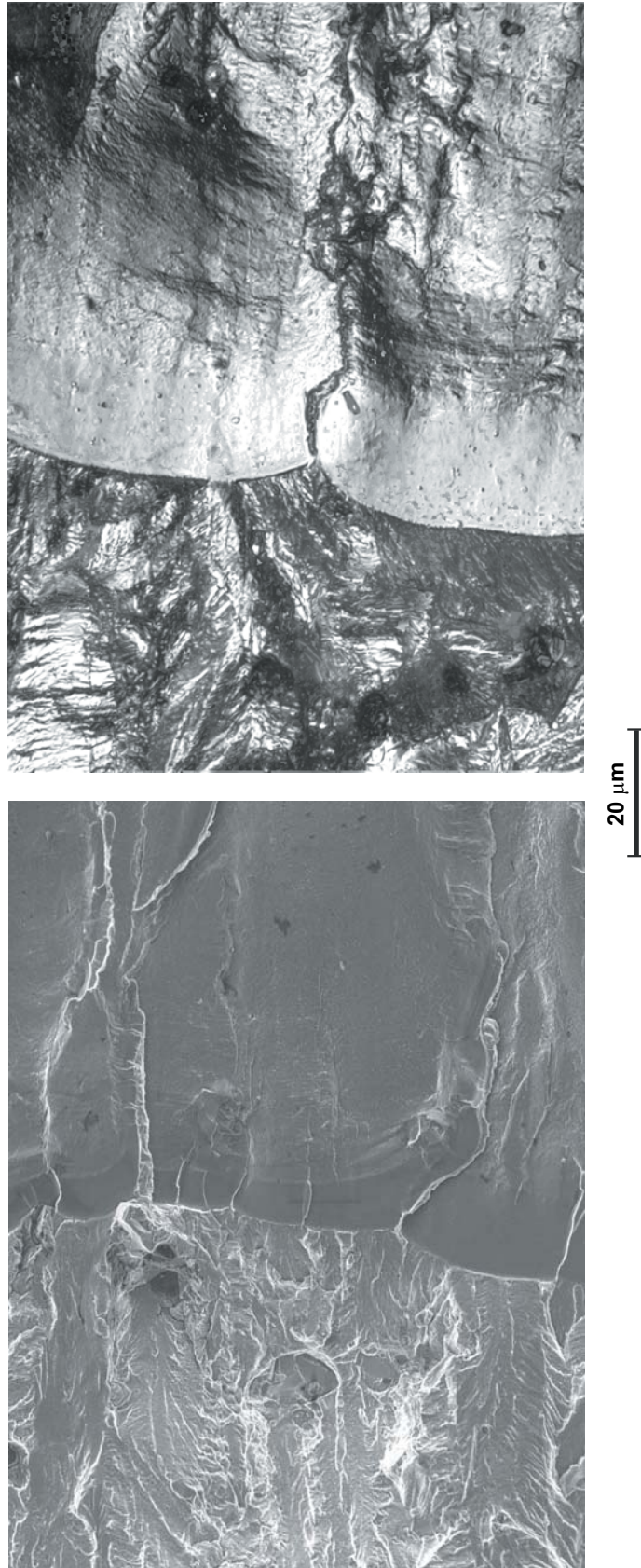


Fig. 38 Comparison of FEG-SEM and DFOM overviews of third threshold for specimen 6-2,  $R = 0.92$ : flat facets and rough ridges



*Fig. 39 Perspective view, constructed from a FEG-SEM stereopair, of a typical dark band between two light ones on a flat scallop: specimen 1-3,  $R = 0.1$*





*Fig. 40 Comparison of FEG-SEM and DFOM details (not identical areas) of second threshold for specimen 3-1,  $R = 0.4$ , 38-39% R.H.  
The final crack front consisted entirely of almost featureless flat scallops*

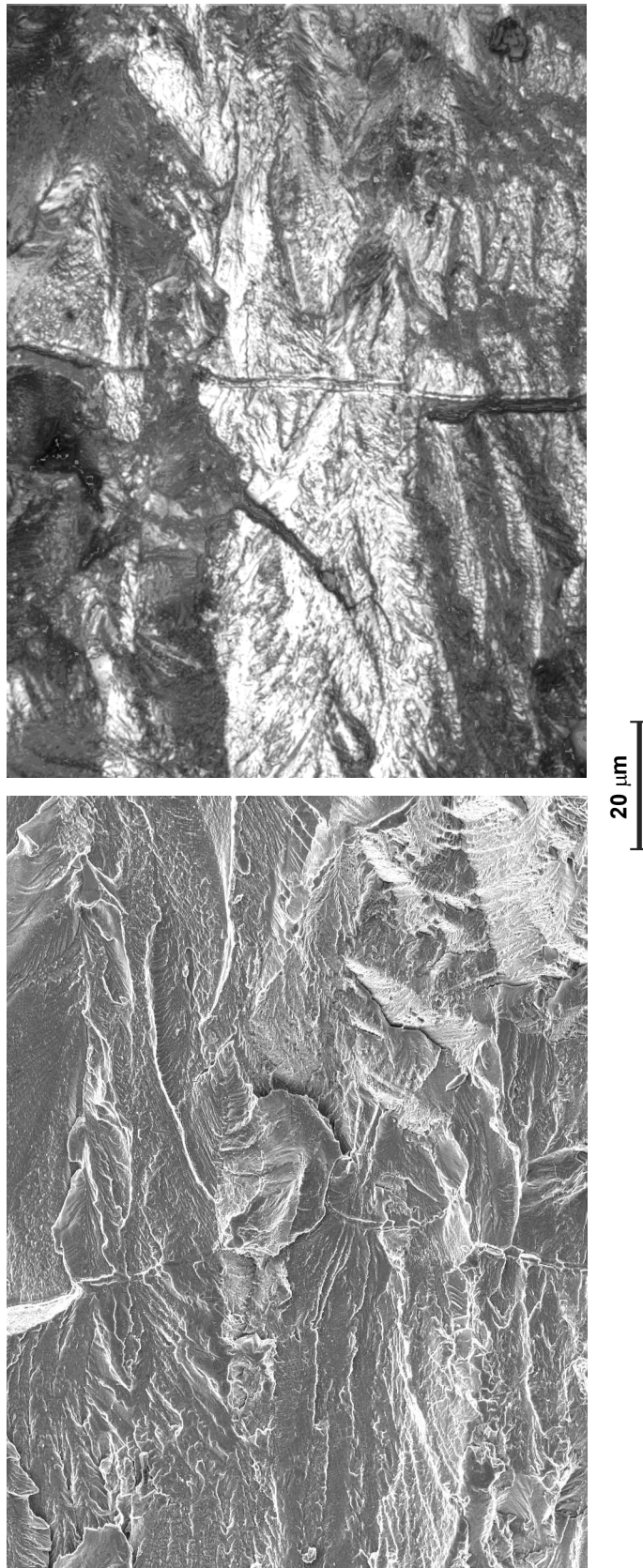


**Fig. 41** Comparison of FEG-SEM and DFOM details (not identical areas) of first threshold for specimen 2-2,  $R = 0.7$ , 29–30 % R.H.  
The final crack front preceding the narrow stretch zone between the first and second threshold determinations consisted almost entirely of wide rough ridges

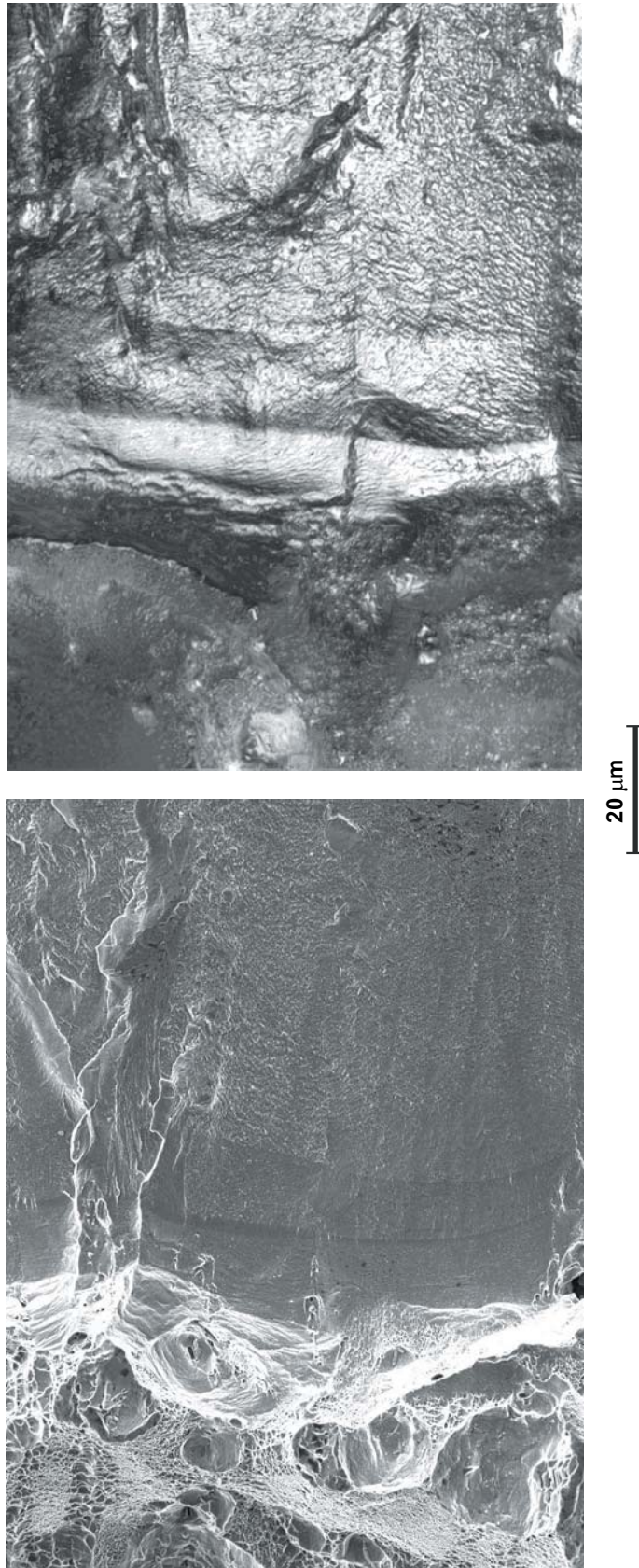


*Fig. 42 Comparison of FEG-SEM and DFOM details (not identical areas) of third threshold for specimen 2-2,  $R = 0.7$ , 38-39 % R.H.  
The final crack front consisted mainly of almost featureless flat scallops*

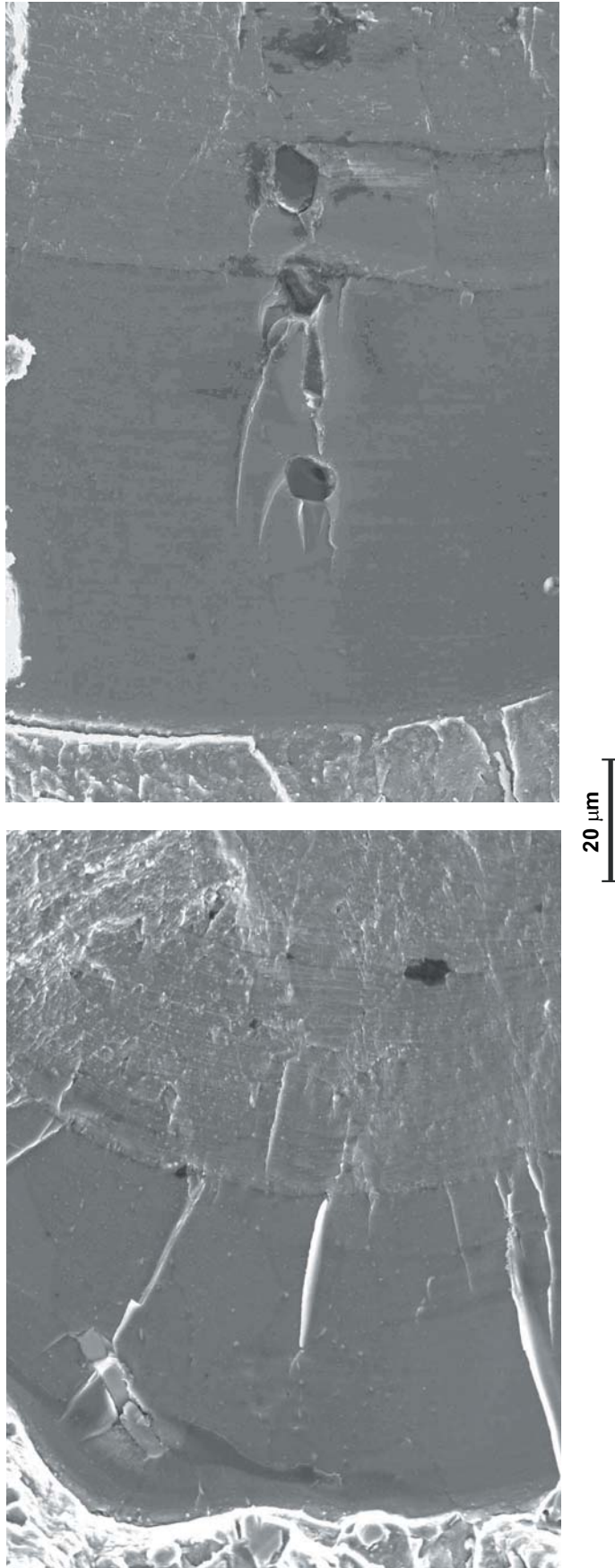


Fig. 43 FEG-SEM details of a brittle layer overlying the fatigue fracture surface at the second threshold for specimen 3-1,  $R = 0.4$ , 38-39 % R.H.

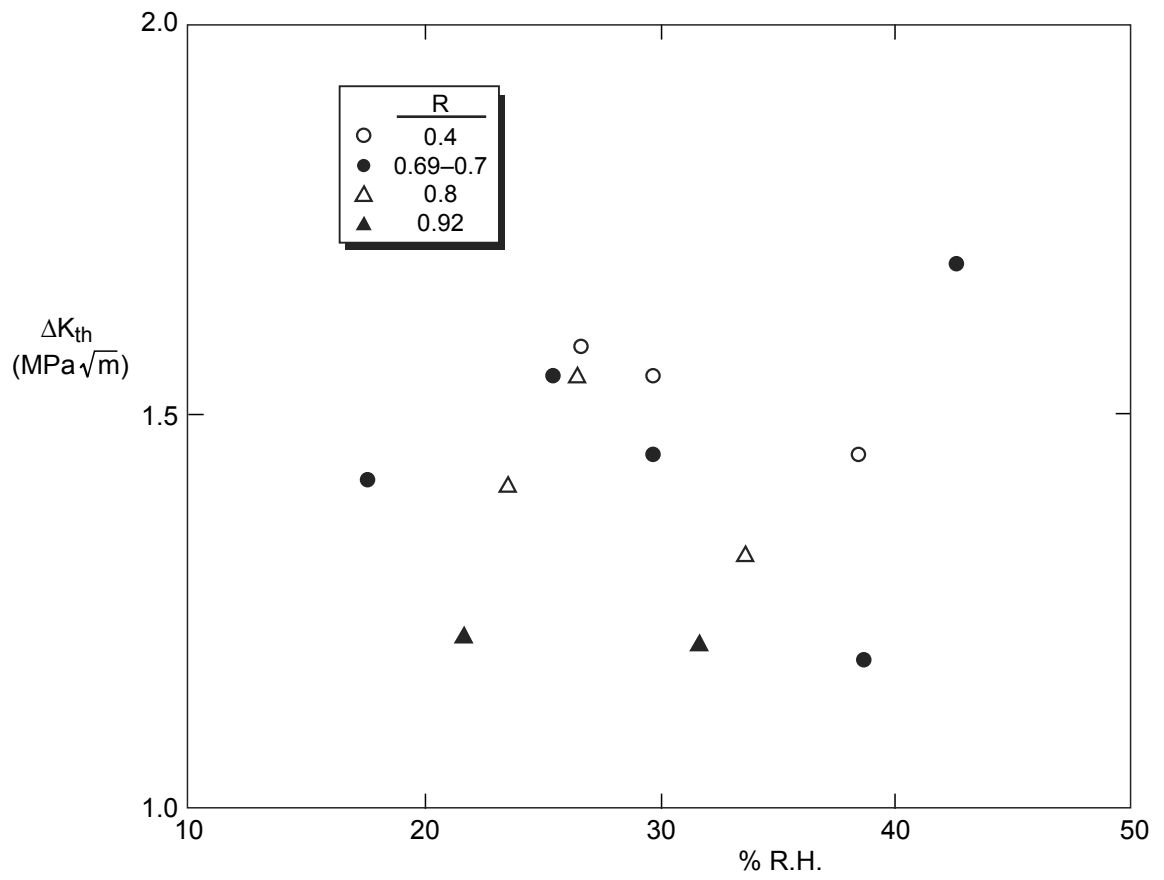
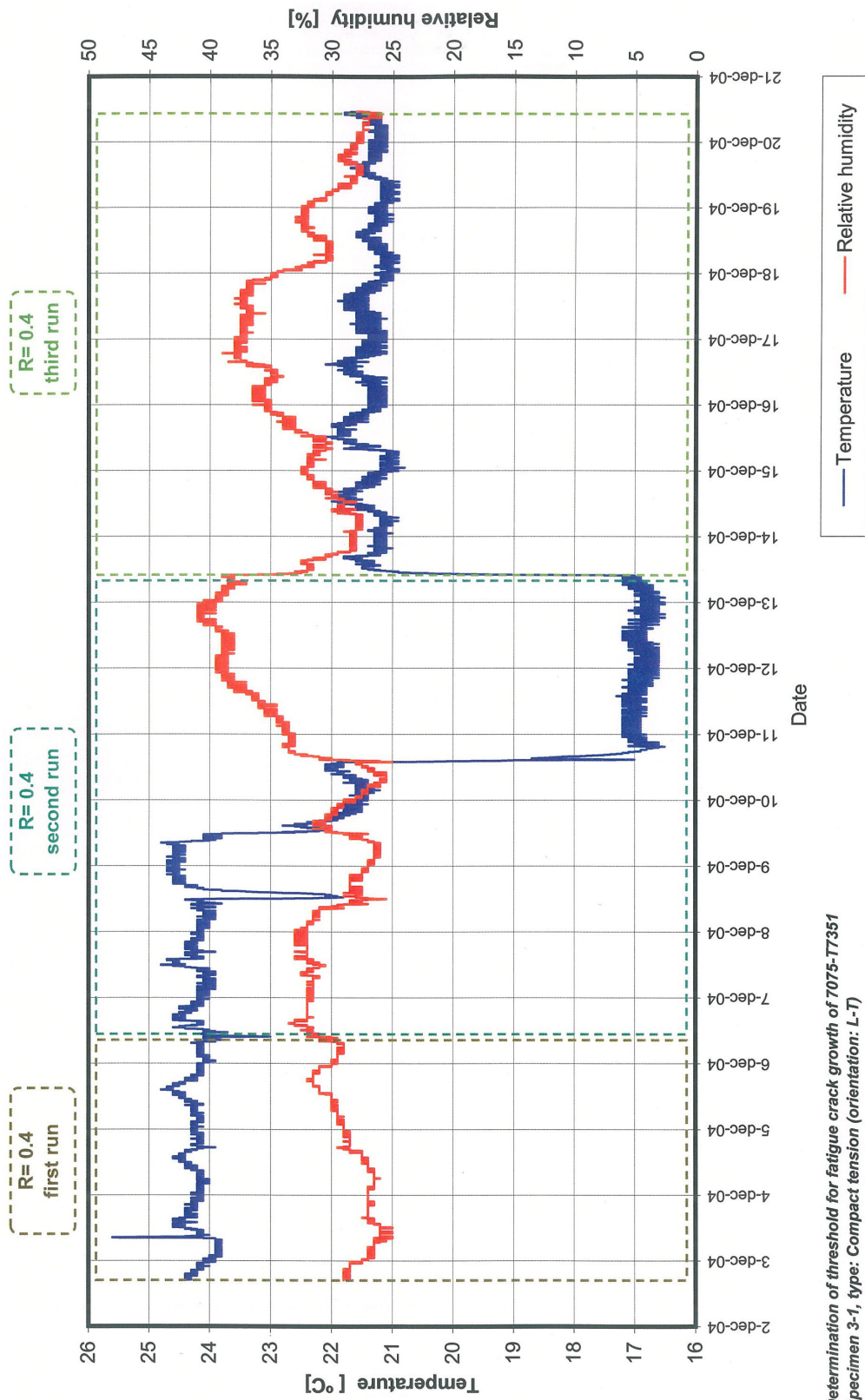


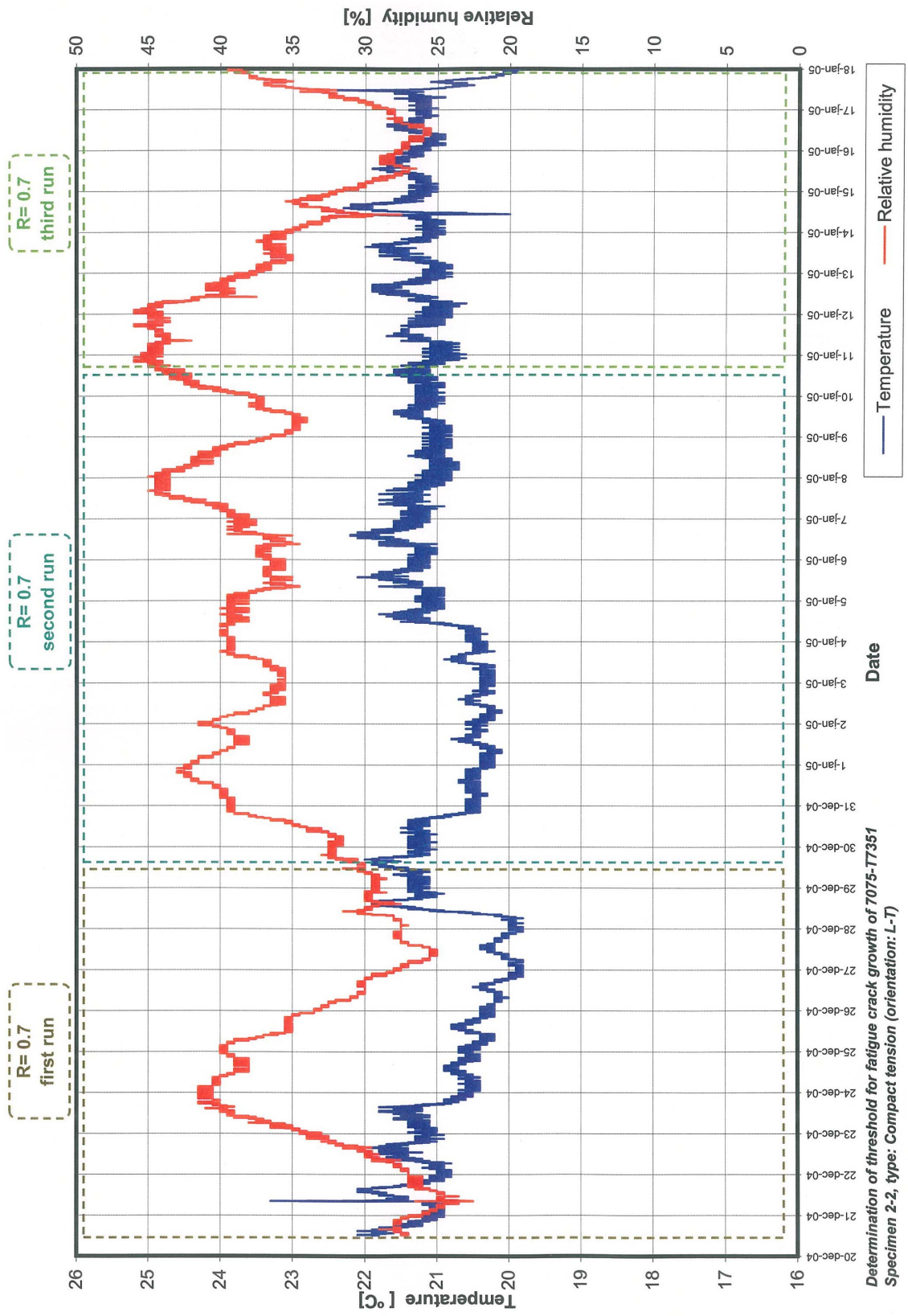
Fig. 44 Comparison of threshold atmospheric humidities (R.H.) and  $\Delta K_{th}$  values



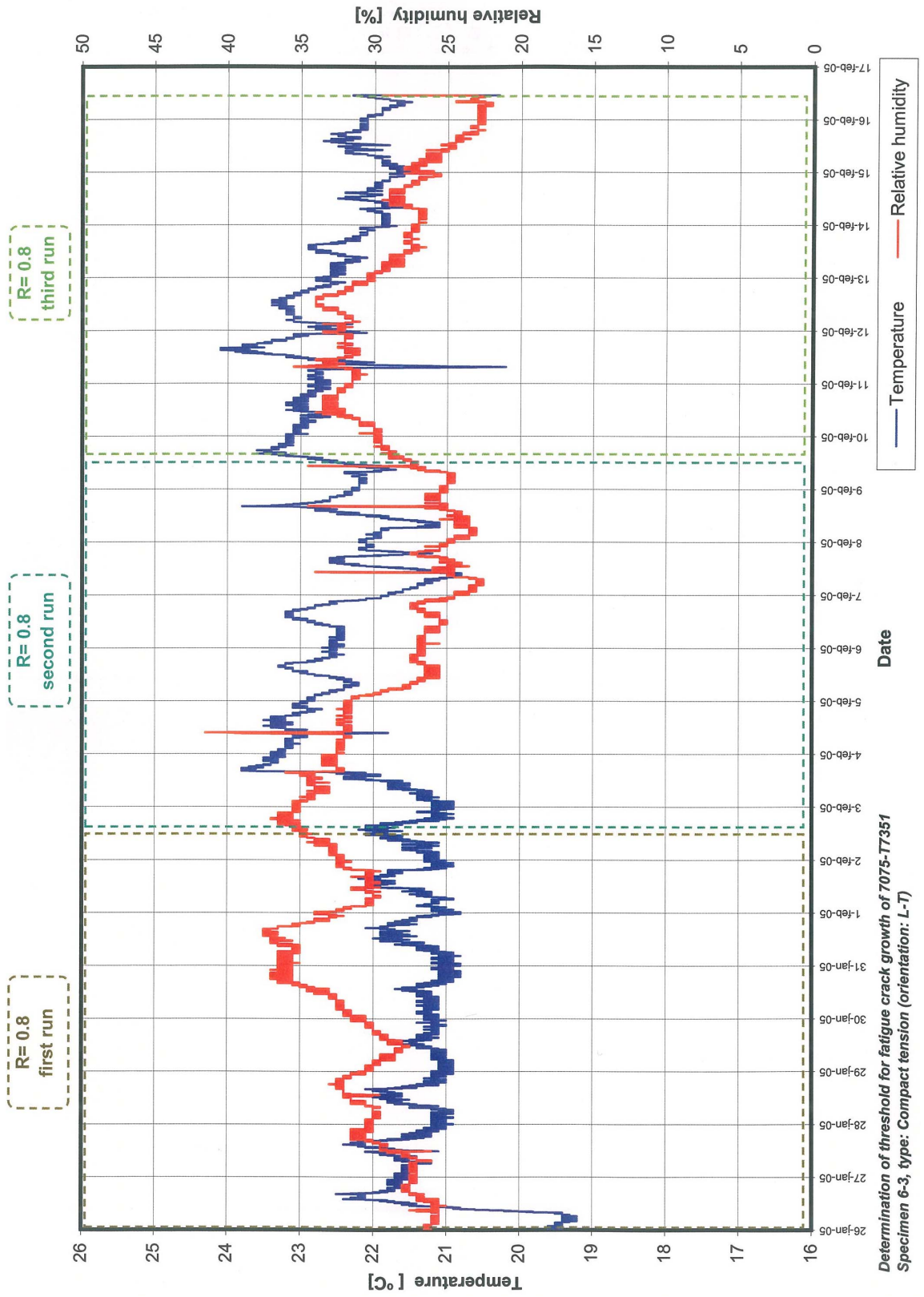
This page is intentionally left blank.

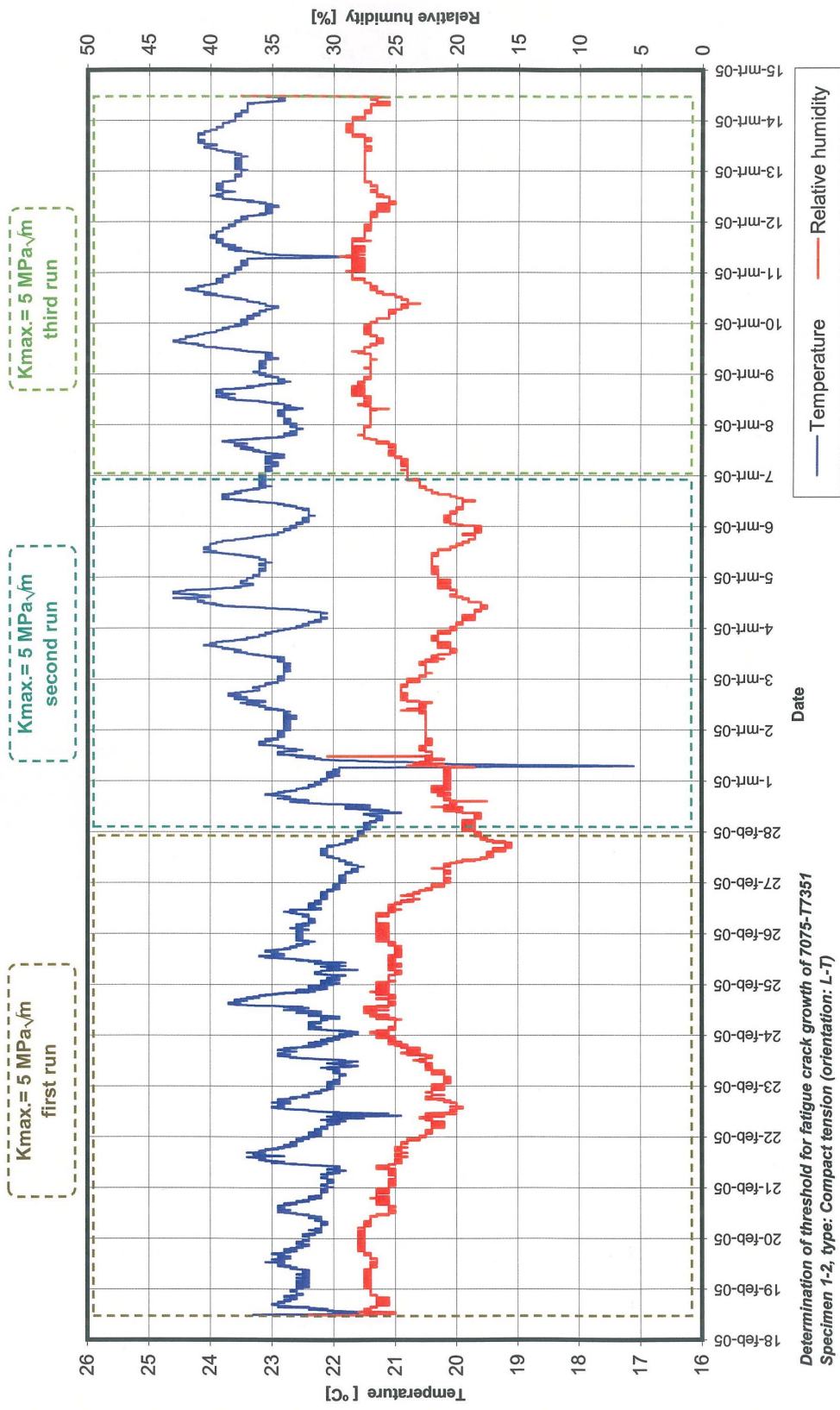
## Appendix A Temperature and humidity records during testing

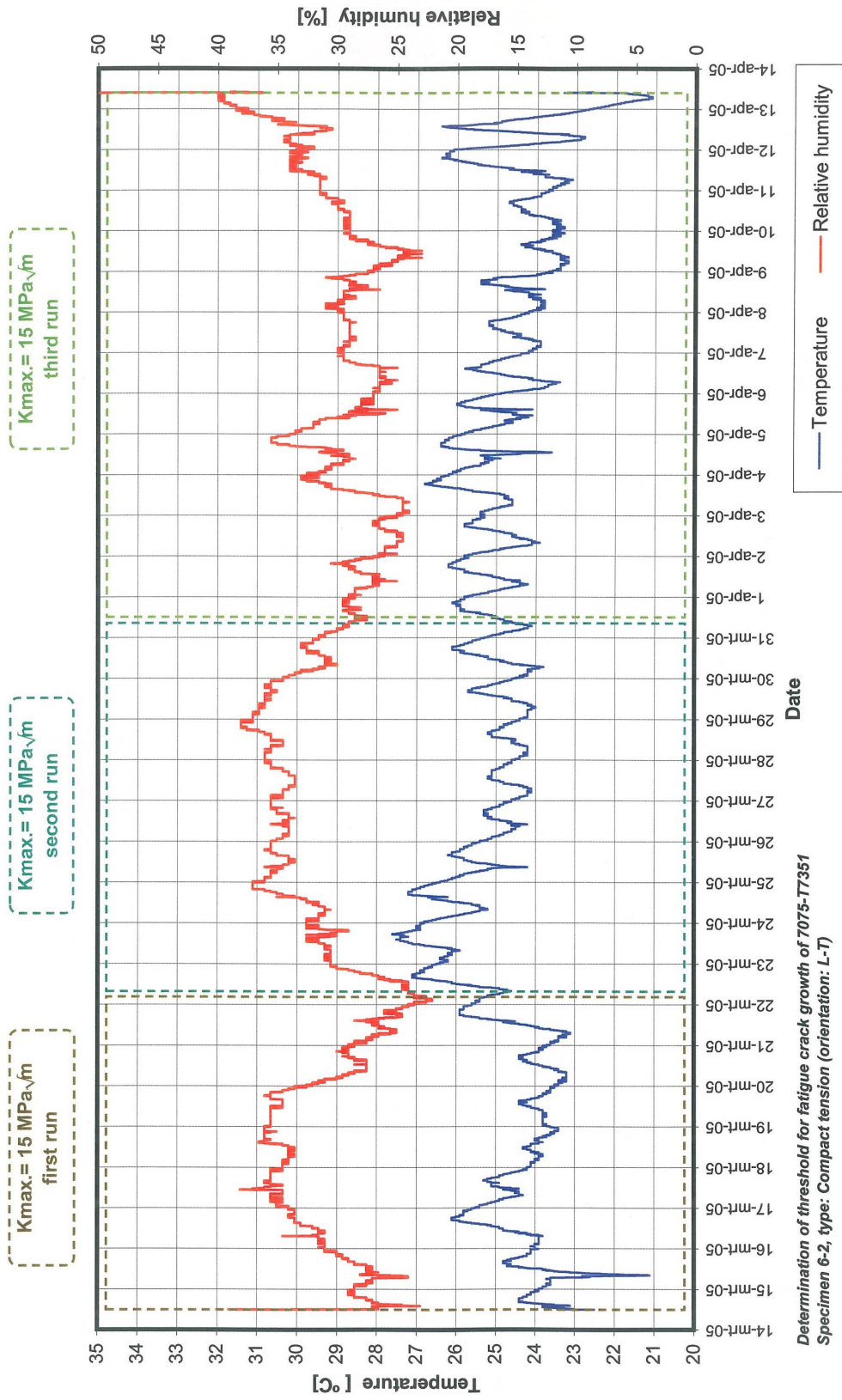


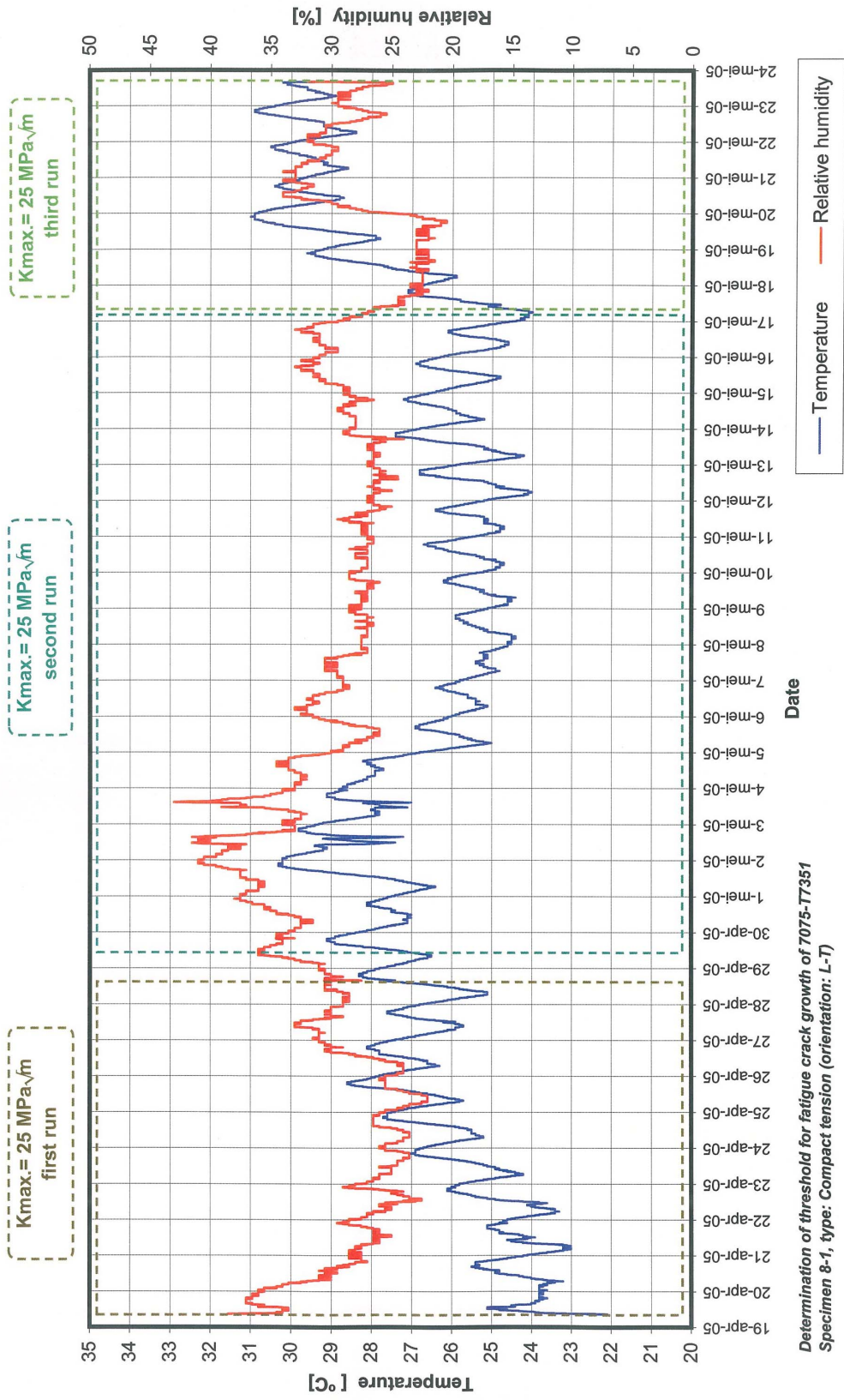












Determination of threshold for fatigue crack growth of 7075-T7351 Specimen 8-1, type: Compact tension (orientation: L-T)